1964

The effects of free-stream turbulence on heat transfer from a flat plate with a pressure gradient

George Hanbury Junkhan
Iowa State University

THE EFFECTS OF FREE-STREAM TURBULENCE ON HEAT TRANSFER FROM A FLAT PLATE WITH A PRESSURE GRADIENT

by

George Hanbury Junkhan

A Dissertation Submitted to the
Graduate Faculty in Partial Fulfillment of
The Requirements for the Degree of
DOCTOR OF PHILOSOPHY

Major Subjects: Mechanical Engineering
Theoretical and Applied Mechanics

Approved:

Signature was redacted for privacy.

In Charge of Major Work

Signature was redacted for privacy.

Heads of Major Departments

Signature was redacted for privacy.

Dean of Graduate College

Iowa State University
Of Science and Technology
Ames, Iowa

1964

TABLE OF CONTENTS

SYMBOLS

The following symbols are used in this dissertation and are defined as indicated:

A	Area of surface
B	Constant
C	Constant
c_f	Friction factor defined in Equation 34
D	Constant
d	Diameter
e_o	Average hot-wire bridge voltage without flow
$\bar{e}_w$	Average hot-wire bridge voltage with flow
$\sqrt{\overline{e'^2}}$	Root-mean-square value of fluctuating hot-wire voltage (see note at end of list)
g	Acceleration of gravity
H	Head
h	Convective heat transfer coefficient
i	Current
k_a	Thermal conductivity of air evaluated at at the mean boundary layer temperature
k_p	Thermal conductivity of plate material
L	Scale of turbulence
m	Exponent in Equation 33
N_{Nu_x}	Nusselt number based on distance from leading edge, x

N_{Re_x}	Reynolds number based on distance from leading edge, x
N_{Re_δ}	Reynolds number based on boundary layer thickness, δ
P	Power
p	Pressure
$\bar{p}$	Mean pressure
p'	Fluctuating pressure
Q	Heat transfer rate
Q_n	Net energy loss by convection
q_c	Energy loss by conduction
q_r	Energy loss by radiation
R	Resistance; result function in uncertainty analysis
R_a	Resistance at a reference condition a
$R_{xu'}$	Correlation coefficient
T	Turbulence intensity
T_a	Absolute ambient temperature
T_s	Absolute temperature of plate surface
t	Temperature
t_b	Temperature of plate back
t_f	Temperature of air stream or fluid
t_s	Temperature of plate surface, general surface in Equation 1
U	Free stream velocity
$\bar{U}$	Mean free stream velocity
U'	Fluctuating component of free stream velocity

$\sqrt{\overline{U'^2}}$	Root-mean-square value of fluctuating component of free stream velocity (see note at the end of list)
u	Velocity in x-direction in boundary layer
$\bar{u}$	Mean velocity in x-direction in boundary layer
u'	Fluctuating velocity in x-direction in boundary layer
u^+	Defined by Equation 35
v	Velocity in y-direction in boundary layer
$\bar{v}$	Mean velocity in y-direction in boundary layer
v'	Fluctuating velocity in y-direction in boundary layer
$v_1, v_2, v_3 \cdots v_n$	Variables in uncertainty analysis
w	Uncertainty in a quantity (for list of subscripts used with this symbol, see end of symbol list)
x	Distance measured parallel to surface of plate, distance from leading edge, coordinate direction
x_o	Unheated starting length
x_p	Plate thickness
y	Distance measured perpendicular to surface of plate, coordinate direction
y^+	Defined by Equation 36
α	Thermal diffusivity
δ	Boundary layer thickness
ϵ	Emissivity
$\overline{\Lambda}$	Mean value of Pohlhausen parameter defined in Equation 38

μ	Viscosity
ν	Kinematic viscosity
σ	Stefan-Boltzmann constant
ρ	Density
τ	Time
τ_o	Shearing stress at wall

Subscripts for Uncertainty Symbol w

1, 2, 3...n	Uncertainties in variables 1, 2, 3...n
A	Area
E	Voltage
e'	Root-mean-square bridge voltage
e_o	No-flow bridge voltage
e_w	Mean flow voltage
T	Turbulence
T_s	Absolute surface temperature
T_a	Absolute ambient temperature
t_b	$(t_s - t_b)$
t	$(t_s - t_f)$
Q	Q_n
N	Nusselt number
R	Reynolds number
U	Free stream velocity
x	Distance x
x_p	Plate thickness

ν	Kinematic viscosity
r	Calculated result
Ω	Resistance

NOTE: The symbols $\sqrt{\overline{e'^2}}$ and $\sqrt{\overline{U'^2}}$, as written in this thesis, imply that the time-averaging process is performed on the squared value of the fluctuating quantity.

INTRODUCTION

The investigation of heat transfer phenomena concerned with the convective mode of transfer is frequently resolved to the problem of determining the coefficient of heat transfer h defined by the equation

$$Q = hA(t_s - t_f) \tag{1}$$

Common practice for design purposes in engineering is the use of empirical formulas based on experimental data taken for geometries and flow conditions similar to the problem at hand, as, for example, in McAdams (24). This practice, however, does not eliminate the desirability of finding methods for calculating the heat transfer coefficient by analytical means. The analytical approach obviously requires a knowledge of the interaction of the variables affecting the value of the coefficient of heat transfer, and although a mass of data and experimental correlations have been compiled, the problem of analytical prediction of the heat transfer coefficient has not been solved for more than a few restricted cases. One reason for the difficulty in obtaining analytical solutions is the lack of information concerning the interaction of some variables with others, and the magnitude of these effects. Certainly the lack of a general mathematical flow model for expressing the conservation of energy and the equation of motion for a fluid in a readily solvable equation is another.

Analytical approaches are usually based on the solution of various forms of the equations of motion and of conservation of energy written for the boundary layer of fluid next to a solid wall. If enough simplifying assumptions are used, the equations may be solved. Examples are the boundary-layer approximations, or the assumption of fluid properties invariant with temperature or pressure and of zero turbulence intensity in many texts (34) (8) (22). Experimental investigations are frequently aimed at finding out how certain variables affect the boundary layer when heat is transferred through it. Those variables which do not have a large effect may then be neglected in an analytical approach, with a resulting simplification of equations. In general, the effect of variables such as fluid properties, velocities and wall geometry in the boundary layer have been investigated experimentally.

For many years it has been recognized that conditions in the free stream external to the boundary layer affect the heat transfer properties of the boundary layer. These free-stream conditions can cause a change from laminar to turbulent flow in the boundary layer and can cause the position of this transition to change. Moreover, changes have been found in heat transfer coefficients for certain wall geometries which have a static pressure distribution along the surface. This dissertation includes the results of an experimental investigation and a discussion of the interaction of a free-stream

condition, turbulence intensity, with pressure gradient and local Reynolds number in determining the rate of heat transfer from a flat plate. Emphasis has been placed on the collection of data which may serve as the basis for future analytical studies.

REVIEW OF PREVIOUS INVESTIGATIONS

Free-stream turbulence has been a parameter in several investigations concerning heat transfer. Perhaps the first to notice and appreciate its effects were investigators working on heat transfer from cylinders in crossflow. Investigations have also been carried on for other shapes. A review of those considered most pertinent to the current investigation is presented in the following paragraphs.

Definitions of the terms turbulence intensity and scale of turbulence used in this section are in Appendix A.

Cylindrical and Spherical Geometries

Giedt (15) presented data for an experimental investigation of the effect of free-stream turbulence intensity on local heat transfer and skin friction for a 4-inch diameter cylinder in crossflow. The two turbulence intensities used were estimated at less than one per cent and at about four per cent by methods suggested in work done on turbulence damping screens in wind tunnels (5). A single strip of nickel-chromium resistance alloy was wound in a helix around the circumference of the cylinder with thermocouples attached to the back side of the strip. Local coefficients were obtained from the circumferential temperature distribution, the electrical power input to the strip and calculated values of conduction and radiation losses.

The magnitude of the local heat transfer coefficient at the upstream stagnation point was found to increase about 25 per cent with the turbulence intensity increase noted above for approximate Reynolds numbers based on cylinder diameter of 95,000, 171,000 and 213,000. In addition, the average heat transfer coefficient for the whole cylinder was found to increase approximately 20 per cent.

Kestin and Maeder (18) performed experiments on a cylinder in which both the turbulence intensity and scale of turbulence were measured with a hot-wire anemometer. These tests were performed in an open-circuit wind tunnel on a cylinder which was heated internally by saturated steam at a pressure slightly above that of the atmosphere. The surface temperature for the cylinder was taken as the average of that recorded by five thermocouples located around a circumference of the cylinder. Measurements were made both with and without boundary layer trip wires on the surface of the cylinder in an effort to show that the effect of free-stream turbulence did not only change the position of transition from a laminar to a turbulent boundary layer, but had an independent effect of its own. The results confirmed that the free-stream turbulence intensity had an effect of its own. For example, at a Reynolds number based on cylinder diameter of 180,000, the Nusselt number at the upstream stagnation point showed a 30 per cent increase for a turbulence intensity rise from 1 per cent to 2.5 per cent. The overall mean Nusselt number was

found to increase by 26 per cent for a rise in free-stream turbulence intensity from 0.75 per cent to 2.66 per cent when the trip wires were in place. Without the trip wires in place, the mean Nusselt number increased 14 per cent under otherwise identical conditions. The scale of turbulence was measured over a small range, 0.162 cm to 0.574 cm and no effects were noticed. Kestin and Maeder speculated that free-stream oscillations may cause changes in the velocity and thermal boundary layers which in turn will cause departures from the Reynolds analogy between skin friction and heat transfer.

Van der Hegge Zijnen (40) measured heat transfer from a cylinder in crossflow for Reynolds numbers based on cylinder diameter from 60 to 25,800, for turbulence intensities ranging from 2 per cent to 13 per cent and for ratios of scale of turbulence to cylinder diameter varying from 0.31 to 240. He used a 0.01-cm diameter platinum wire, a 0.08-cm outside diameter nickel tube and brass tubes of eight outside diameters ranging from 0.306 cm to 4.19 cm. The wire and tubes were heated either by passing an electrical current through them, or by an electrical heater inside a tube. The conclusions reached were that for a constant Reynolds number the heat transfer increases continuously with the turbulence intensity and when the turbulence intensity is held constant, the Nusselt number increases with the Reynolds number. Moreover, when the Reynolds number and turbulence intensity are held

constant, the heat transfer either increases or decreases with increasing ratio of scale of turbulence to cylinder diameter, the maximum occurring when this ratio is around 1.5 to 1.6. Lastly, van der Hegge Zijnen noted that variations in both scale and turbulence intensity were more effective in changing the heat transfer than an increase in Reynolds number.

Seban (35), in studies of the effect of free-stream turbulence on heat transfer from cylinders in crossflow, found that the heat transfer coefficient increased, as found in previous work, but he also noted that the maximum increase was at the point of largest pressure gradient along the cylinder surface, and a minimum increase at the point of smallest pressure gradient, thus leading to speculation that the turbulence intensity has its greatest effect when a large pressure gradient is present. He also found that the transition from laminar to turbulent boundary layer flow took place at lower Reynolds numbers, but that once transition had taken place there was no effect of the turbulence on the heat transfer in the region of the turbulent boundary layer. His work was performed on circular cylinders of 1.25-inch and 1.87-inch diameters and on a cylinder of elliptical cross section with a 6-inch major axis and a 2-inch minor axis. The heat transfer elements were individual circumferential strips of nichrome. The range of air velocities used ranged from 150 to 350 ft per sec, with temperature differences between the cylinder and the air of from 15F to 20F. Turbulence

intensities were measured with a hot-wire anemometer. The scale of turbulence was small compared to the cylinder diameter, and thus non-contributory according to the previously noted work of van der Hegge Zijnen. Kestin, Maeder and Sogin (19) did further experimental work on a cylinder showing that the effect of free-stream turbulence is largest when the gradient of the free-stream velocity is greatest and when the free-stream velocity is at low turbulence intensity levels.

Work similar to that on cylinders has been performed on spheres. In general, similar conclusions have been found. An increase in the magnitude of the heat transfer coefficient at the upstream stagnation point and an increase in overall coefficient results as free-stream turbulence intensity increases. The most fruitful of the investigations involving spheres appear to be those by Sato and Sage (32) and by Short and Sage (36).

Flat Plate Geometries

Fage and Falkner (10), in experiments concerned with the analogy between skin friction and heat transfer from a flat plate and from cylinders in crossflow reported some of the first data on the effect of free-stream turbulence on heat transfer from a horizontal flat plate oriented with the flow parallel to the surface. The plate consisted of a platinum foil 0.70-cm long, 1.30-cm wide and 0.00127-cm thick. The foil was heated by passing an electric current through it,

and current and resistance measurements were used to compute the heat transfer. Thus, the entire plate was, in effect, a hot-film anemometer. Fage and Falkner concluded that changes in free stream turbulence did not affect the rate of heat transfer from the film. The conclusions for the cylinder were that changes in distributions of surface friction and heat transfer do take place, but no detailed investigation was made.

Sugawara, et al. (37) performed experiments on a flat plate for Reynolds numbers based on distance from the leading edge from about 3.9×10^3 to 3.5×10^5 with varying turbulence intensity in the free stream. Heat transfer was measured by heating the plate, placing it in the air stream, and measuring temperatures as the plate cooled. Values were calculated according to an equation previously developed for non-time-steady cooling. Turbulence intensity was measured by a hot-wire anemometer. The results showed a large increase in heat transfer coefficient with an increase in free-stream turbulence intensity.

Edwards and Furber (9) investigated the effect of free-stream turbulence on heat transfer from a flat plate with zero pressure gradient. The plate consisted of a plane surface about 3 feet long with a 6- by 4-inch heated copper plate imbedded in the surface 33 inches downstream from the leading edge. They were able to measure average coefficients over this area, which was electrically heated by nichrome strips in the interior of the model. The remainder of the model was

unheated. Three free-stream turbulence intensities were used, the magnitudes of which were estimated from the grid sizes used to generate the turbulence. The range of Reynolds numbers based on total plate length was from 200,000 to 2,500,000. The conclusions reached were that turbulence intensities up to an estimated 5 per cent did not influence the heat transfer, that turbulence intensity has little effect in the laminar boundary layer flow region, and that the position of transition from laminar to turbulent flow in the boundary layer is markedly affected by free-stream turbulence intensity. No effect of free-stream turbulence was found for heat transfer through a turbulent boundary layer.

A note to the paper of Edwards and Furber (9) by Whitefoot states that, using the same general methods, no effect of free-stream turbulence intensities up to about 11 per cent could be found.

Wang (43) investigated the effect of free-stream turbulence on the local heat transfer rates from two unit steam heaters mounted with their surfaces flush with the surface of a flat plate. The heaters were maintained at constant temperature by electric heating elements inside the units. The rest of the plate surface was maintained at very nearly the same temperature as the unit heaters by circulating steam from a small external boiler inside the plate. Free-stream turbulence intensity measurements were made with a hot-wire anemometer, and velocity profiles in the boundary layer were

obtained with a total-head probe. Wang conducted detailed experiments on the plate for a negligible pressure gradient, but some exploratory points for a favorable pressure gradient were also obtained. He found the local coefficient of heat transfer to be unaffected by turbulence intensity level in the laminar boundary layer region in the case of negligible pressure gradients. In the boundary layer transition region, local coefficients increased by as much as 220 per cent for a change in free-stream turbulence intensity from 0.80 to 2.50 per cent. In the turbulent boundary layer region, changes in the free-stream turbulence intensity produced no systematic effects on the local coefficient. For the case of a pressure gradient, the exploratory points indicated a sizeable increase in local coefficient for laminar boundary layers.

Wang also presented an analysis of the effect of free-stream oscillations on the laminar boundary layer. It assumed only one free stream oscillating velocity component, and shows that the degree to which the boundary layer is affected is dependent on the amplitude of the free stream oscillations only when the oscillations vary in the direction of the mean flow. Wang numerically calculated solutions for the equations of motion for a flat plate in a stream of constant mean velocity with a sinusoidally varying wave imposed on the free stream. His solution shows that at low frequency and amplitude, the effect on heat transfer coefficients will be small.

This analysis and its conclusions will be discussed in greater detail in subsequent sections.

Reynolds, Kays and Kline (30) performed heat transfer and thermal- and velocity-boundary layer experiments on an isothermal flat plate with a turbulent boundary layer. They did not directly determine the effect of free-stream turbulence on these variables, but the turbulence intensity of the free stream was reported. The results showed little difference from predictions for no free-stream turbulence. This work thus tends to confirm the work of Edwards and Furber (9).

Feiler and Yeager (12) reported on the effect of large amplitude oscillations on local heat transfer coefficients. The oscillations consisted of free-stream turbulence both with and without a sound field present. The sound field was generated by a siren installed upstream of the flat plate under test. The frequency of the sound field was varied from 34 to 680 cps and the root-mean-square flow amplitudes varied up to 65 per cent. The Nusselt number increased by as much as 65 per cent over a reference flow at the same Reynolds number. An empirical correlation for the Nusselt number as a function of the Reynolds number and the ratio of the root-mean-square amplitude of the fluctuating velocity to the mean flow velocity was developed. Schlieren photographs of the boundary-layer flow revealed a flow reversal in the layer that was correlated with the frequency of oscillations. The time-averaged value of the thermal boundary-layer thickness was

found to vary inversely as the Nusselt number. Heat transfer increases for turbulent flow were also reported. The increase in heat transfer for laminar and turbulent flows was ascribed to the same mechanism, as yet unknown, for both flows.

ANALYSIS OF THE EFFECTS OF FREE-STREAM TURBULENCE ON THE LAMINAR BOUNDARY LAYER EQUATIONS

The convective heat transfer from a body is controlled by the resistance to heat transfer through the boundary layer. The resistance of the boundary layer to heat transfer is determined by the nature of the flow in the boundary layer. In general, less resistance to heat transfer is encountered with a turbulent boundary layer than with a laminar one. The following analysis consists of a discussion of the effects of the free-stream turbulence on the equations of motion, continuity and energy for the laminar boundary layer, and is similar to the analysis in Schlichting (34) and Wang (43).

Effect on Fluid-Flow Characteristics

In flow over bodies immersed in a fluid, it is found that the boundary layer begins as a laminar type and may undergo a transition to the turbulent type as flow progresses over the body. The exact mechanism involved in the transition is not completely understood. It is known, however, that the transition of the boundary layer as well as the characteristics of the different boundary-layer types can be changed by conditions both internal and external to the boundary layer. This analysis is confined to the effects of free-stream turbulence on the boundary layer.

According to Schlichting (34), the free-stream turbulence intensity is a rough measure of the amplitude of the random

velocity fluctuations in the free stream. These fluctuations are not compatible with the usual assumptions of a steady-state free stream velocity as a boundary condition for the solution of the two-dimensional incompressible boundary layer equations, since they make the free stream velocity time-dependent. Of course, most solutions of the two-dimensional equations take the time-averaged free stream velocity as a boundary condition and thus disguise this problem. However, Kestin and Maeder (18) point out that due to the non-linear equations involved, it is necessary to employ the time-dependent boundary-layer equations together with the time-dependent boundary conditions and to perform the time averaging in the process of solving the equations.

For the case of a flat plate with zero pressure gradient, some experiments have shown little influence of free-stream turbulence on the boundary layer. When a pressure gradient is present, however, changes have occurred in the boundary layer. Thus, an analysis incorporating a pressure gradient is desirable.

In order to analyze the two-dimensional boundary layer with non-time-steady velocities, the simplifying assumption of only one varying free-stream component will be made. These variations will be assumed to occur in the direction of the mean velocity of the stream. The pressure and velocity components are assumed to consist of time-average values with

fluctuating values superimposed on them. Thus,

$$u = \bar{u}(x,y) + u'(x,y,\tau) \tag{2}$$

$$v = \bar{v}(x,y) + v'(x,y,\tau) \tag{3}$$

$$U = \bar{U}(x,y) + U'(x,\tau) \tag{4}$$

$$p = \bar{p}(x) + p'(x,\tau) \tag{5}$$

where u and v are boundary layer velocity components, τ is time, U is the free stream velocity which varies only in one direction and with time, p is pressure and the bar over a symbol denotes the temporal mean value and the prime represents the fluctuating part. Since this analysis is restricted to two dimensions in space, all components of velocity in the z-direction are assumed as zero. In addition, the assumption of a uniform pressure at any section across the boundary layer at any instant is considered in keeping with the order of magnitude analysis involved in obtaining the boundary layer equations.

Using the time-averaging techniques of Schlichting (34), it is found that

$$\overline{u'} = \overline{v'} = \overline{U'} = \overline{p'} = 0 \tag{6}$$

These functions for the velocities and the pressure are to be substituted in the two-dimensional non-time-steady

boundary layer equations of motion

$$\frac{\partial u}{\partial \tau} + u\frac{\partial u}{\partial x} + v\frac{\partial u}{\partial y} = -\frac{1}{\rho}\frac{\partial p}{\partial x} + \nu\frac{\partial^2 u}{\partial y^2} \tag{7}$$

the continuity equation for incompressible flow

$$\frac{\partial u}{\partial x} + \frac{\partial v}{\partial y} = 0 \tag{8}$$

and the non-time-steady equation for the free stream

$$\frac{\partial U}{\partial \tau} + U\frac{\partial U}{\partial x} = -\frac{1}{\rho}\frac{\partial p}{\partial x} \tag{9}$$

After substitution of the velocity functions, the equation of motion is

$$\frac{\partial(\bar{u} + u')}{\partial \tau} + (\bar{u} + u')\frac{\partial(\bar{u} + u')}{\partial x} + (\bar{v} + v')\frac{\partial(\bar{u} + u')}{\partial x} =$$

$$-\frac{1}{\rho}\frac{\partial(\bar{p} + p')}{\partial x} + \nu\frac{\partial^2(\bar{u} + u')}{\partial y^2} \tag{10}$$

the equation of continuity is

$$\frac{\partial(\bar{u} + u')}{\partial x} + \frac{\partial(\bar{v} + v')}{\partial y} = 0 \tag{11}$$

and the free stream equation is

$$(\bar{U} + U')\frac{\partial(\bar{U} + U')}{\partial x} + \frac{\partial(\bar{U} + U')}{\partial \tau} = -\frac{1}{\rho}\frac{\partial(\bar{p} + p')}{\partial x} \tag{12}$$

The free stream equation is then expanded and the pressure gradient term replaced with the left side of the free stream equation, giving

$$\frac{\partial \bar{u}}{\partial \tau} + \frac{\partial u'}{\partial \tau} + \bar{u}\frac{\partial \bar{u}}{\partial x} + \bar{u}\frac{\partial u'}{\partial x} + u'\frac{\partial \bar{u}}{\partial x} + u'\frac{\partial u'}{\partial x} + \bar{v}\frac{\partial u'}{\partial y} + v'\frac{\partial \bar{u}}{\partial y} +$$

$$v'\frac{\partial u'}{\partial y} + \bar{v}\frac{\partial \bar{u}}{\partial y} = \frac{\partial \bar{U}}{\partial \tau} + \frac{\partial U'}{\partial \tau} + \bar{U}\frac{\partial \bar{U}}{\partial x} + \bar{U}\frac{\partial U'}{\partial x} + U'\frac{\partial \bar{U}}{\partial x} + U'\frac{\partial U'}{\partial x} +$$

$$\nu\left[\frac{\partial^2 \bar{u}}{\partial y^2} + \frac{\partial^2 u'}{\partial y^2}\right] \qquad (13)$$

No boundary conditions can be placed on Equation 13 because of the random nature of the fluctuating parts of the dependent variables. In order to further analyze this equation, the time-average will be taken, keeping in mind that a loss of generality is involved. The time-averaged equation is

$$\bar{u}\frac{\partial \bar{u}}{\partial x} + \overline{u'\frac{\partial u'}{\partial x}} + \bar{v}\frac{\partial \bar{u}}{\partial y} + \overline{v'\frac{\partial u'}{\partial y}} = \bar{U}\frac{\partial \bar{U}}{\partial x} + \overline{U'\frac{\partial U'}{\partial x}} + \nu\frac{\partial^2 \bar{u}}{\partial y^2} \qquad (14)$$

This equation has been noted by others and may be found, for example, in Schlichting (34).

In a similar fashion, the continuity equation, when time-averaged is

$$\frac{\partial \bar{u}}{\partial x} + \frac{\partial \bar{v}}{\partial y} = 0 \qquad (15)$$

The only differences between the above equations of motion and the usual time-averaged boundary layer equations are the terms $\overline{u'\frac{\partial u'}{\partial x}}$, $\overline{v'\frac{\partial u'}{\partial y}}$ and $\overline{U'\frac{\partial U'}{\partial x}}$. It must be these terms that represent the effects of free-stream oscillations on the boundary layer.

Both of the terms $\overline{u'\frac{\partial u'}{\partial x}}$ and $\overline{U'\frac{\partial U'}{\partial x}}$ are dependent on x due to the partial derivative portions, therefore the values of these depend on a change on u' and/or U' with x. The term $v'\frac{\partial u'}{\partial y}$ can be shown to depend on x by noting that if u' were a function of y only, $\frac{\partial u'}{\partial x}$ would be zero. Thus, from the continuity equation, $\frac{\partial v'}{\partial y} = 0$, and, due to the continuum flow assumption of no slip at the wall, v' = 0 and the term $v'\frac{\partial u'}{\partial y}$ would vanish. Since v' is not zero, except at the wall, $v'\frac{\partial u'}{\partial x}$ must be dependent on x as well as y or the above hypothesis is valid.

In the event that U' is a constant not equal to zero, and $\frac{\partial U'}{\partial x} = 0$, it is possible that u' and v' may continue to depend on x and y, but if U' = 0, u' and v' will not exist.

Thus, one condition necessary for the free stream turbulence intensity to affect the boundary layer is that the

oscillations in the x-direction in the free stream and/or the boundary layer vary with x, i.e., that at least one of the components u', v', and U' vary with x.

A second effect necessary for the free-stream turbulence to affect the boundary layer is that u', v' and/or U' not be too small compared with $\bar{u}$, the mean velocity in the boundary layer.

To show this, consider Equation 14 in a rearranged form

$$\bar{u}\frac{\partial \bar{u}}{\partial x} + \bar{v}\frac{\partial \bar{u}}{\partial y} = \underline{\bar{U}\frac{\partial \bar{U}}{\partial x} + \overline{U'\frac{\partial U'}{\partial x}} - \overline{u'\frac{\partial u'}{\partial x}} - \overline{v'\frac{\partial u'}{\partial y}}} + \nu\frac{\partial^2 \bar{u}}{\partial y^2} \qquad (16)$$

All of the terms underlined by the bracket now appear in the same fashion as a pressure gradient term in the steady state boundary layer equation. Thus, if

$$\overline{u'\frac{\partial u'}{\partial x}}, \quad \overline{v'\frac{\partial u'}{\partial y}} \text{ and } \overline{U'\frac{\partial U'}{\partial x}}$$

are all small enough, no effect of oscillations in the free stream will be noticeable. Since all other non-pressure-gradient terms in the equation depend on u, it is necessary that at least one of the terms

$$\overline{u'\frac{\partial u'}{\partial x}}, \quad \overline{v'\frac{\partial u'}{\partial y}} \text{ or } \overline{U'\frac{\partial U'}{\partial x}}$$

be large enough compared to $\bar{u}$ to cause a change in the boundary layer. Looking at it another way, if these oscillations are small enough, the boundary layer velocity profile should remain unaltered from that of a mean velocity profile.

Effects on Heat Transfer

The above discussion of the effects of the free-stream oscillations on the boundary layer is based on the equations of motion and continuity. To show how the energy equation for two-dimensional flow, usually written as

$$\frac{\partial t}{\partial \tau} + u\frac{\partial t}{\partial x} + v\frac{\partial t}{\partial y} = \alpha \frac{\partial^2 t}{\partial y^2} \qquad (17)$$

is affected, it can be seen that if a constant temperature difference between the plate and the free stream is maintained, that is, an isothermal plate, the temperature profile will change only with changes in u and v (when the shape of the profile changes).

It may be noted from the above analysis that two conditions are necessary for free-stream turbulence to affect heat transfer. They are (1) the velocities u', v', and/or U' must change with x, and (2) the magnitude of u', v', and/or U' must not be too small compared to $\bar{u}$.

It is interesting to apply these two requirements to the flow about a cylinder and over a flat plate. For the cylinder, the first requirement is fulfilled by the slowing down of the stream as it approaches the stagnation point. It has been shown by Piercy and Richardson (27) that near the stagnation point of a cylinder, the amplitude of the oscillating portion of the flow increases. As the fluid moves over the forward part of the cylinder, the amplitude of the oscillations

decreases. Piercy and Richardson (26) made similar measurements near the stagnation point of a strut. They found an oscillation amplitude increase near the stagnation point (but not in the boundary layer) of about 4.5 times that of the free-stream oscillation amplitude value. As the stream approaches the stagnation point, and the mean velocity decreases, the increased amplitude of the oscillations is not small with respect to $\bar{u}$ and the second condition is then fulfilled.

In addition to the above, it should be noted that a negative pressure gradient will exist on the forward portion of the cylinder (accelerating flow). Taylor (38) has shown that for a contraction section (similar to that used in wind tunnels) the longitudinal component of the turbulent oscillations is reduced in the accelerating flow. The amount of reduction is dependent on the particular form of disturbance initially. There is also a strong deceleration ahead of the stagnation point, indicating an increase in relative magnitude of the fluctuating components.

The fixed flat plate at zero pressure gradient does not satisfy the above conditions. The turbulence intensity of the free-stream approaching the leading edge does not materially change provided the plate is situated far enough downstream from a turbulence-producing body for the intensity of turbulence in the stream to be approximately isotropic and of nearly constant magnitude, as, for example, the turbulence field

downstream of a grid (5). This has been the case for experimental observations by Wang (43) and Edwards and Furber (9).

For a fixed flat plate with negative pressure gradient along its surface, the resulting acceleration of the flow is consistent with the condition of change of oscillation amplitude with x. Thus, if the initial free-stream turbulence intensity approaching the plate is large enough to make the oscillation amplitude not small with respect to $\bar{u}$, an effect should be noticed because both conditions are fulfilled. The exploratory experimental work of Wang (43) has shown that this is true for a large favorable pressure gradient. Wang found a surprisingly uniform increase of about 65 per cent in the Nusselt number for an increase of free-stream turbulence intensity from 0.36 per cent to 1.71 per cent over the laminar boundary layer range of Reynolds numbers between 50,000 and 100,000.

EQUIPMENT USED FOR EXPERIMENTAL WORK

The analysis included in the previous section shows that some effect of free-stream turbulence may be expected on the temperature and velocity distributions in the boundary layer. It is not possible at present to solve the equations for a general set of boundary conditions. Thus, it was deemed appropriate to investigate the problem experimentally in order to obtain a clearer physical picture of the connection between free-stream turbulence and the boundary layer. The investigation was carried out on a flat plate, equipped with heated strips, which was placed in an air flow facility where measurements were taken. The equipment used is described in this section.

Air Flow Facility

The air-flow facility used was an open-circuit suction-type tunnel equipped with a constant-speed centifugal fan rated at 20 inches of water head and 13,000 cfm capacity. The tunnel configuration and some pertinent dimensions are shown in Figure 1.

The test section of the tunnel was 14 inches square and 66 inches long, and was constructed of Plexiglas plastic and aluminum. It was provided with a six-inch-long removable section at the upstream end for insertion of turbulence-promoting grids. Velocity profiles at the upstream end of the test section were uniform within one per cent over the range of

Figure 1. Air flow facility configuration

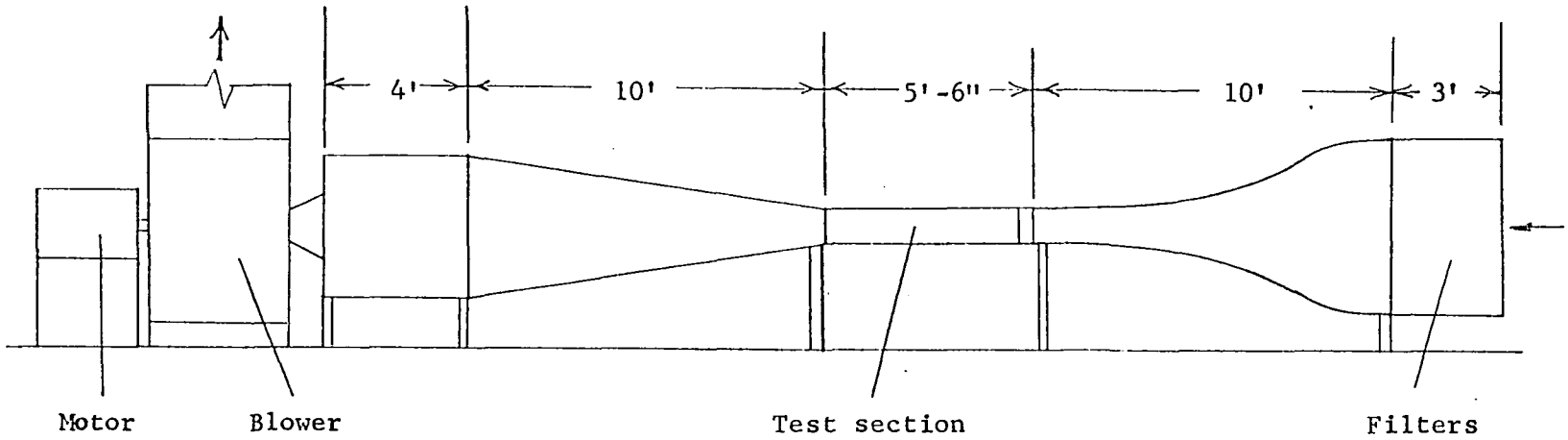
4'
10'
5'-6"
10'
3'
Motor
Blower
Test section
Filters

velocities involved in this work.

Turbulence intensities for the tunnel were measured using the hot-wire anemometer equipment described under the instrumentation heading in this chapter. The free tunnel had a measured minimum turbulence intensity of 0.4 per cent for the higher tunnel speeds, the turbulence intensity increasing to 0.8 per cent at the low tunnel speeds. Turbulence intensities higher than that for the free tunnel were obtained by using grids placed at the upstream end of the test section. Two grids were used, one of 0.090-inch diameter wire on one-inch centers, and the other of 0.250-inch diameter rod on one-inch centers. The mesh of both grids was square. The 0.090-inch grid produced turbulence levels from 1.8 per cent to 3.2 per cent during tests with the plate, while the 0.250-inch grid produced turbulence intensities of from 2.0 to 8.3 per cent during these tests. The 0.250-inch grid was used to check the test section behavior for turbulence downstream of a grid. Results of these data are shown in Figure 2. The recommended equation of Baines and Peterson (1) is represented by the line on the figure.

Flat Plate

The flat plate used was of the type used by Drake (4), Feiler and Yeager (12) and Scesa and Sauer (33) among others. The assembled plate was 14 inches wide, 42 inches long and about 5/8-inch thick. It was composed of five major parts--

Figure 2. Turbulence intensity downstream of a turbulence-promoting grid

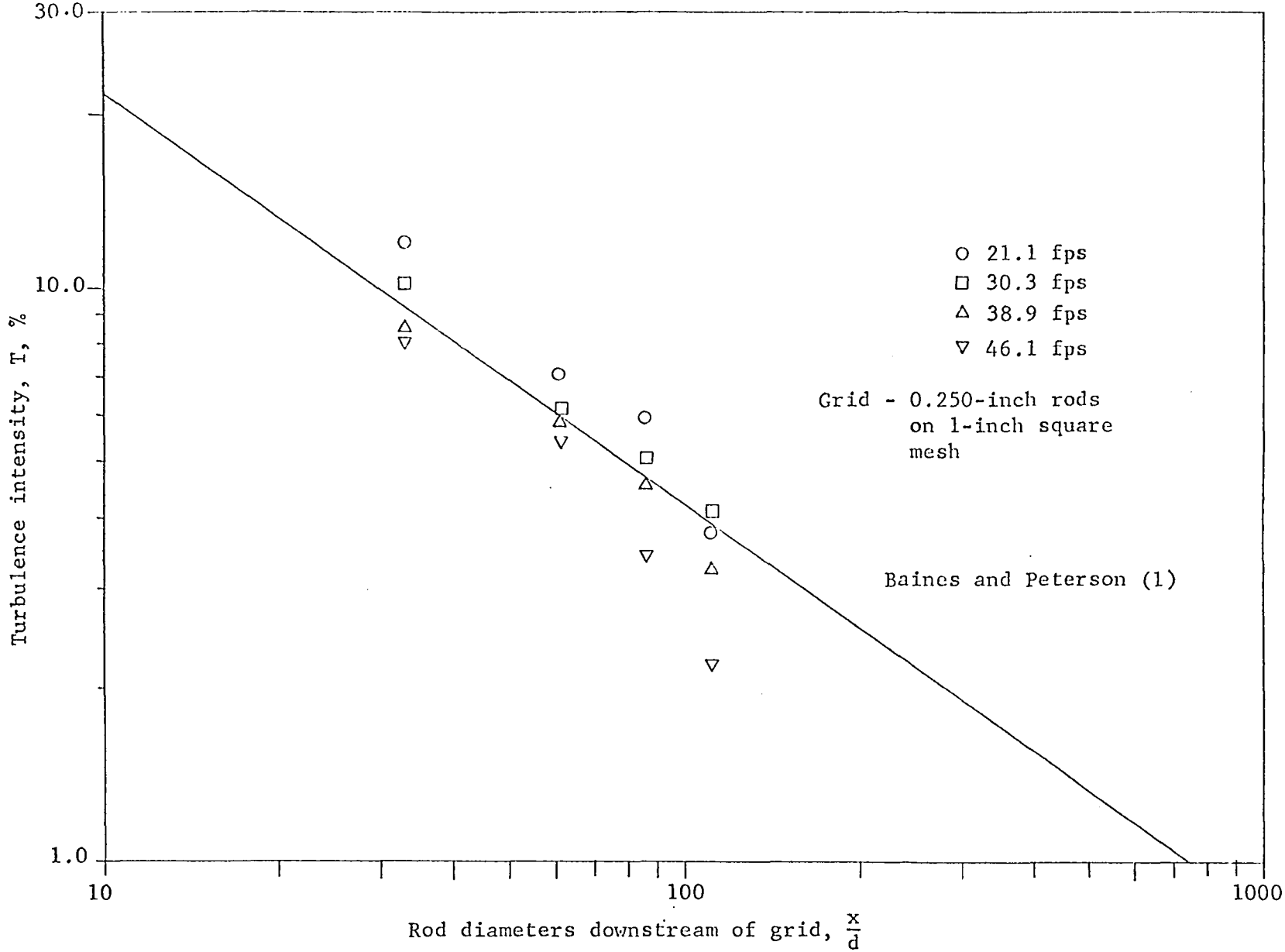
30.0
10.0
1.0
Turbulence intensity, T, %
10
100
1000
Rod diameters downstream of grid, x/d
○ 21.1 fps
□ 30.3 fps
△ 38.9 fps
▽ 46.1 fps
Grid - 0.250-inch rods on 1-inch square mesh
Baines and Peterson (1)

two side rails, a nosepiece, a plate back and a heat transfer surface. The arrangement of these parts is shown in Figure 3 in expanded form and in Appendix C as an assembly drawing.

Plate parts

The nosepiece was constructed of wood and provided with static pressure taps and a thermocouple for temperature measurement. The static pressure taps were used to help locate the stagnation point for the oncoming air flow so that a very slightly favorable angle of attack was maintained. The leading edge of the nosepiece was rounded with a small radius to aid in maintaining a stable stagnation point. This arrangement resulted in a negligible pressure gradient along the plate surface after some experimenting in positioning the plate in the test section. Pressure gradients along the plate surface were obtained by use of a false tunnel wall.

The side rails and plate back were primarily to add structural strength and insulation around the heat transfer surface. The plate back had grooves cut lengthwise in its interior surface to carry electrical wires and pressure tubing. These pieces were made of a paper-laminated phenolic insulating material known commercially as Insurok T-640.

The heat transfer surface was composed of 37 transverse strips of nickel-chromium resistance alloy, commercially known as Nichrome V, each one inch wide, 0.002 inches thick and 12 inches long on the working surface. These strips were mounted

Figure 3. Expanded view of major plate parts

Figure 4. Detail sketch of pressure tap installation

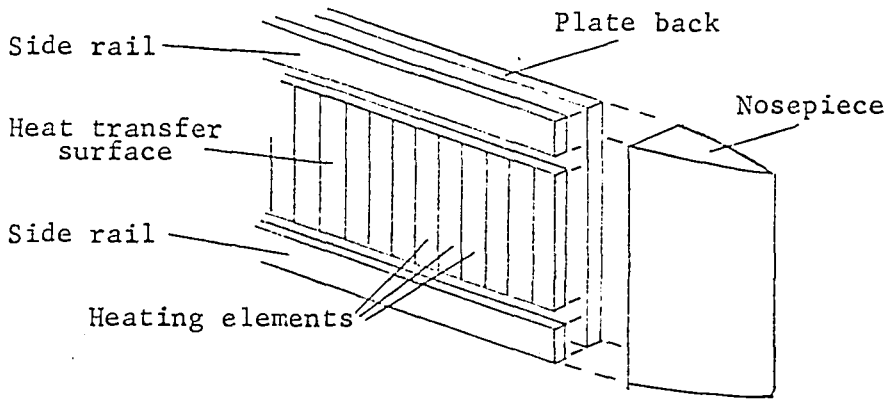
Plate back
Side rail
Nosepiece
Heat transfer surface
Side rail
Heating elements

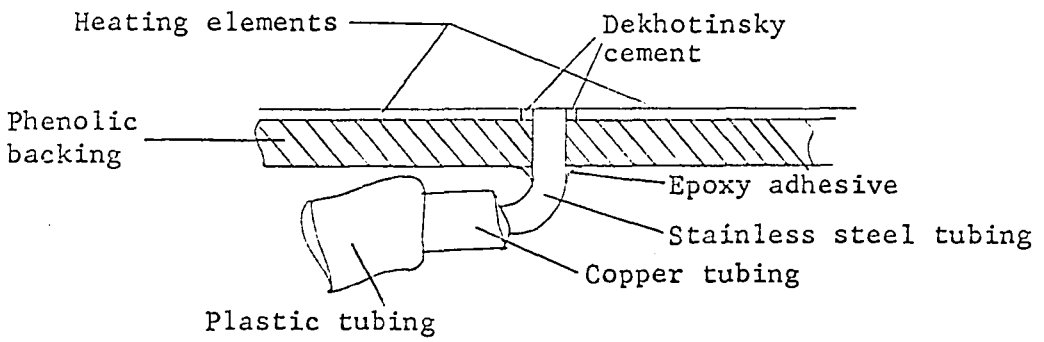
Heating elements
Dekhotinsky cement
Phenolic backing
Epoxy adhesive
Stainless steel tubing
Copper tubing
Plastic tubing

on a paper-laminated phenolic material identical to that used for the plate back and side rails by use of an epoxy-resin adhesive. The ends of the strips were bent 90 degrees over the edges of the phenolic material. Two holes were drilled through the resistance strip into the edge of the phenolic base and a small machine screw thread was tapped into this hole. A copper bus bar was held in position with screws in these holes at the end of the strip and electrical connections for power input and voltage measurement was made to the bus bar. The strips were spaced 1/16-inch apart on the heat transfer surface to allow stainless steel tubing static pressure taps to be installed between strips. The resulting 1/16-inch by 0.002-inch groove was filled with a high-temperature Dekhotinsky cement and each space was then smoothed by hand to assure a smooth working surface. A sketch of this portion of the plate is shown in Figure 4.

Pressure taps

Static pressures at the plate surface were measured by 0.020-inch inside diameter stainless steel tubing inserted between adjacent resistance strips. Care was taken to make sure the tubing did not cause an electrical short circuit between strips. The tubing was inserted through a hole drilled in the phenolic base and held in place with a spot of epoxy adhesive. Each tube was about 3/4-inch long and ended in a 1/8-inch outside diameter copper tube to which a plastic

tube leading to a manometer was attached. A detail of this portion of the plate is also shown in Figure 4.

Thermocouples

The temperature of each strip was measured with iron-constantan thermocouples of 30-gage (0.010-inch diameter) wire spot-welded to the back side of the nichrome strip. The thermocouples were made on a Weldmatic spot-welding machine with a butt-welding accessory device and then spot-welded to the back side of the 0.002-inch resistance strip. Care was taken to be sure the spot-welding operation did not leave a rough spot on the opposite surface of the strip over which the air flow would take place.

In order to check the lengthwise temperature distribution in the strips, several strips had an additional thermocouple attached one inch in from each end. The assembled heat transfer surface unit was checked for accuracy of temperature measurement over the range of temperatures for which it was to be used, by placing it, together with the necessary wiring and emf-measuring equipment in a room where the temperature was varied and allowed to come to equilibrium over a period of several hours.

The temperatures of the back side of the working surface were required when calculating the conduction losses from the resistance strips. These temperatures were obtained from measurements of emf on six thermocouples mounted on the back

side of the phenolic backing of the working surface. Placement of these thermocouples is shown in Appendix C.

Power wiring

After the central section of the plate was completed, the electrical power wiring was attached. The wiring diagram of the strips is shown in Figure 5. The power input to each strip was varied by changing the vernier resistance across each strip. The measurement of power input to each strip was accomplished by obtaining the strip resistance and voltage drop across each strip. In order to obtain the voltage drop of the resistance strip alone, separate potential wires were attached to each bus bar. The copper bus bars, each about two inches long, were of negligible resistance.

Instrumentation

Thermocouples

Thermocouple potentials were read with a Leeds and Northrup Model 8686 millivolt potentiometer. The manufacturer's stated limit of error for this instrument is $\pm$ 0.05 per cent + 3μv when used without reference junction compensation. All plate surface temperature measurements were made by two methods. The first was a differential reading between the free stream and the plate surface. The second was a potential measurement against an ice bath. Thermocouple potentials were checked by comparing the differential measurement against the difference found between the plate surface

Figure 5. Wiring diagram of plate heating elements

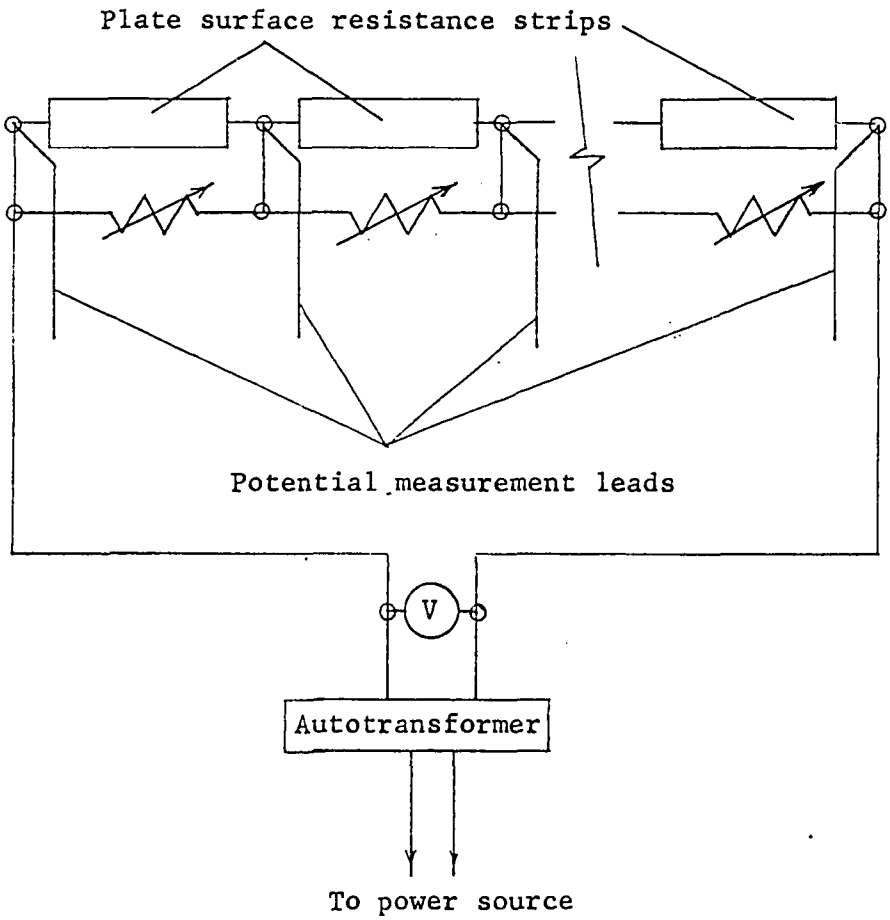
Plate surface resistance strips
Potential measurement leads
V
Autotransformer
To power source

potential measured against an ice bath. It was found that these measurements checked within 0.5 F.

The large number of thermocouples in the plate were connected to Leeds and Northrup thermocouple switches which were used to connect the potentiometer to the desired thermocouple. A circuit was designed so that each thermocouple in the entire system could be measured either differentially with the free-stream temperature or against an ice bath. Free stream temperature measurements were obtained with a shielded iron-constantan thermocouple located just upstream of the leading edge of the plate and about four inches away from the plate surface.

Velocity-profile instruments

The boundary-layer velocity-profile measurements were made with a total-head probe constructed from stainless steel hypodermic tubing with a flattened end section to reduce the velocity gradient across the opening facing into the flow. A sketch of this tube is shown in Figure 6. The opening of the tube was large enough to give a time constant of the measuring system of the order of two minutes when the pressure measurements were made with a Meriam Model 34FB2 micromanometer. The position of the boundary-layer probe in relation to the plate surface was found by use of the micrometer-adjustment probe positioner shown in Figure 7. The zero adjustment of the probe against the plate surface was made by

Figure 6. Sketch of probe used for boundary layer profiles

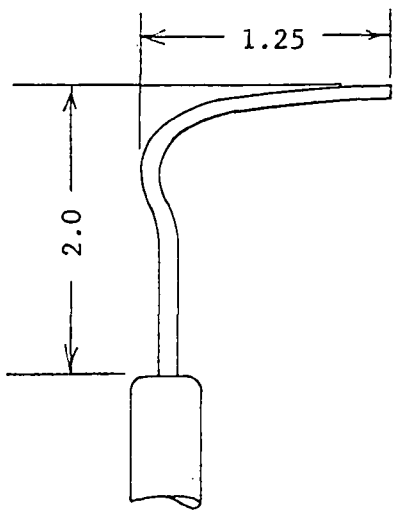

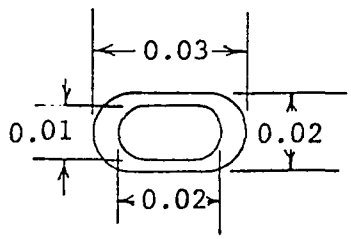

Enlarged view of probe tip

Figure 7. Micrometer probe positioner

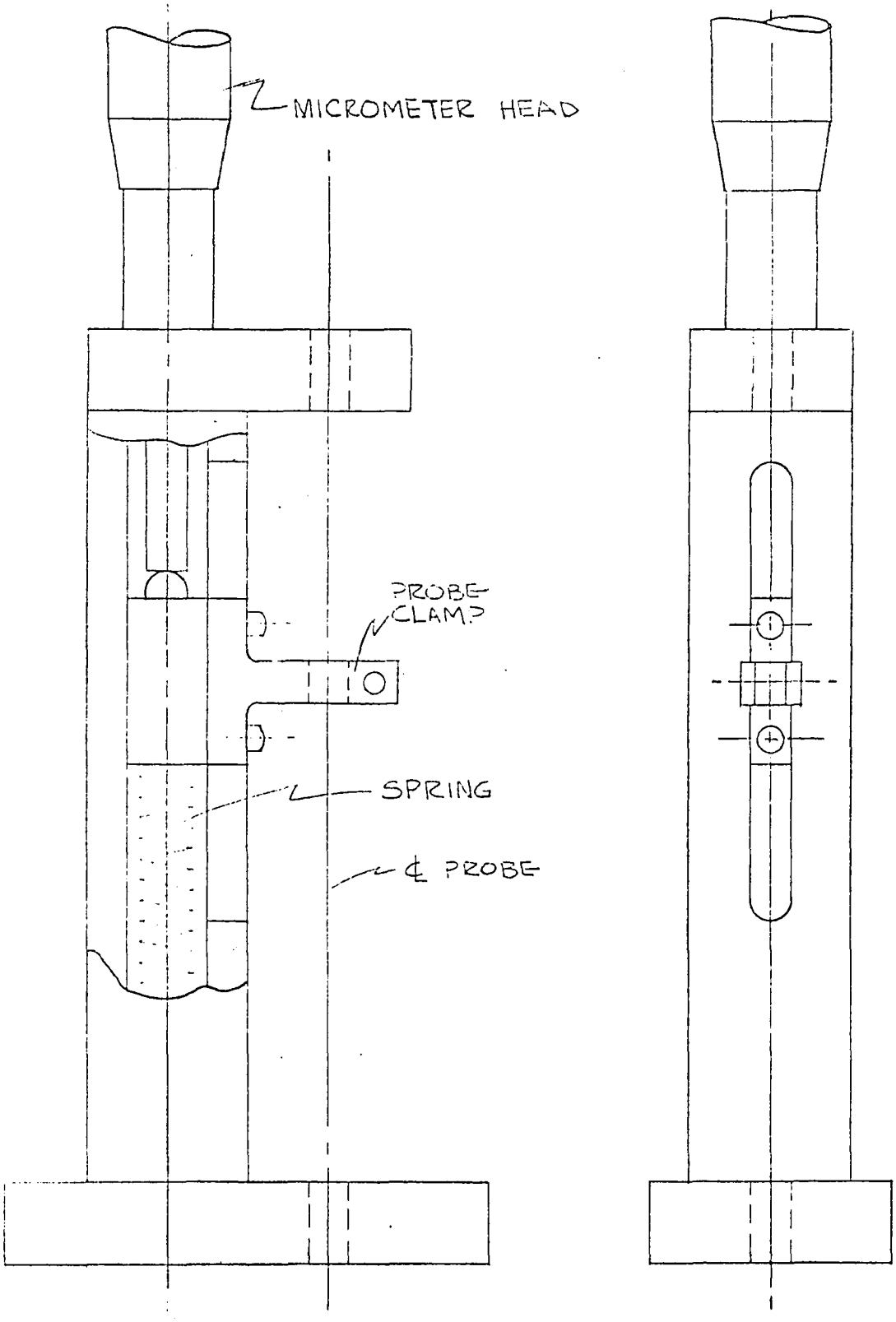
MICROMETER HEAD
PROBE CLAMP
SPRING
℄ PROBE

advancing the probe from a position some distance away from the plate until the tip of the probe and its image, reflected in the plate surface, just touched. It was found that repeatability of the zero position was within one part in one thousand by this method.

A standard pitot tube was used to determine the mean free-stream velocity of the tunnel.

Electrical instruments

A constant-temperature hot-wire anemometer system was used for determination of the turbulence intensities. The wire was 0.00015-inch diameter, approximately 0.050-inch long and made of a platinum-iridium alloy. The hot-wire amplifier used was an improved model of that described by Laurence and Landes (23) which has a frequency response of the probe, bridge, amplifier and cables that is essentially flat between 5 and 20,000 cycles per second.

The values of the magnitude of the fluctuating bridge voltage were determined with a modified average-square computer similar to that described by Laurence and Landes (23). A wiring diagram of the computer used is shown in Figure 8.

Values of $\bar{e}_w$, the average bridge voltage when the wire is in the air stream, and e_o, the average voltage when the wire is in still air, were made using a Tektronix Model 502 oscilloscope to measure the D.C. level. These voltages were of the order of 6 volts and the difference between $\bar{e}_w$ and e_o

Figure 8. Wiring diagram of average-square computer

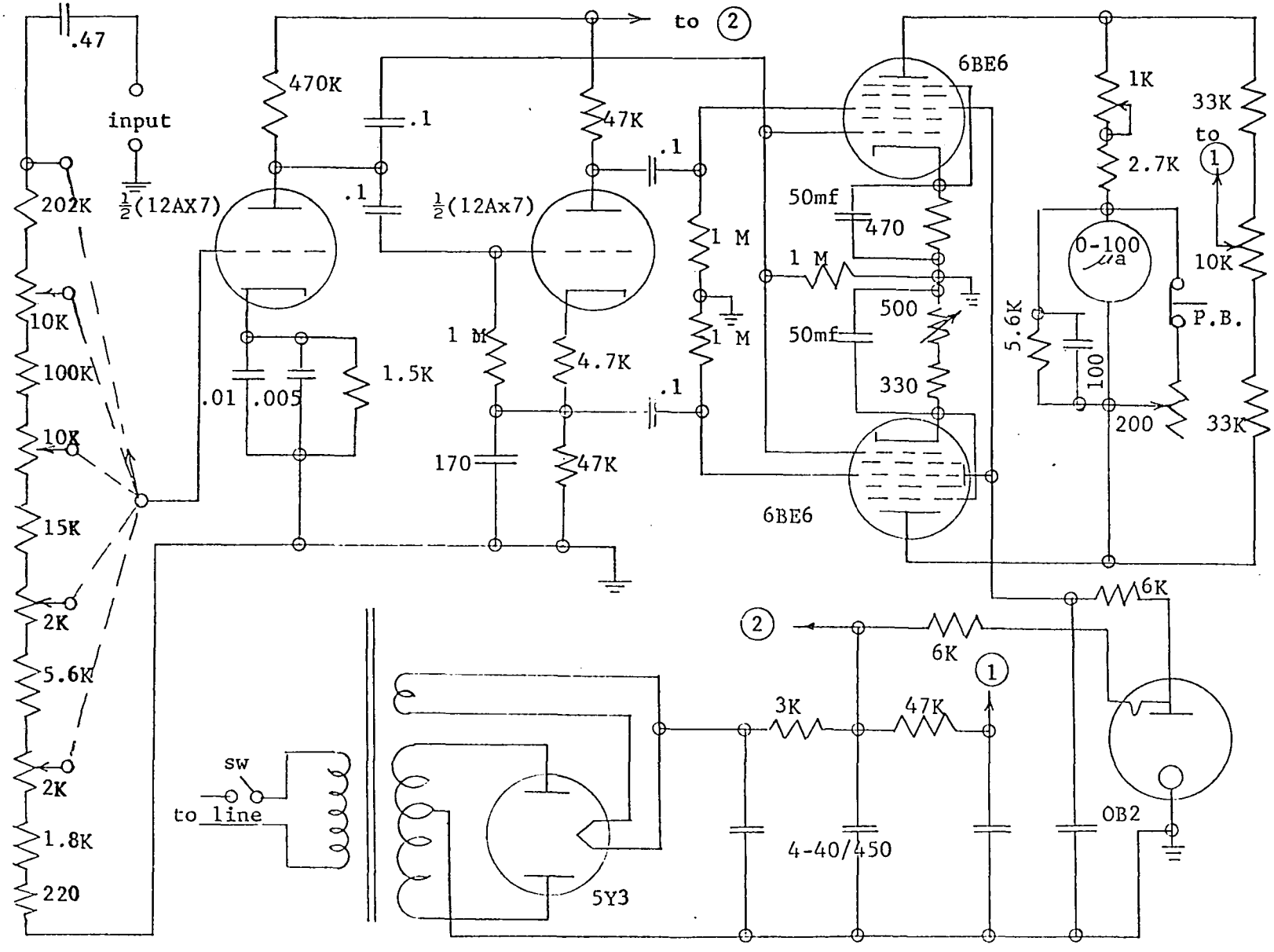
.47
input
202K
10K
100K
10K
15K
2K
5.6K
2K
1.8K
220
470K
.1
.1
½(12AX7)
½(12Ax7)
.01
.005
1.5K
1 M
4.7K
170
47K
.1
1 M
1 M
to ②
6BE6
6BE6
50mf
470
1 M
500
50mf
330
1K
2.7K
0-100 ua
5.6K
100
200
33K
to ①
10K
P.B.
33K
6K
② 6K ①
3K
47K
4-40/450
OB2
sw
to line
5Y3

was less than 1 volt. In order to measure this difference accurately, a constant bucking voltage consisting of calibrated mercury cells was used to reduce the voltage input to the oscilloscope to values which were readily measurable on the higher ranges of vertical amplifier gain, thus affording a larger movement of the trace for a small voltage change. Values of e_o were measured with the hot wire in still air at the same temperature as the tunnel air and values of $\bar{e}_w$ were measured with the hot wire in position in the wind tunnel. The hot-wire bridge was operated with a constant slight unbalance of 2 microamperes to prevent the amplifier from oscillating. The small systematic error thus introduced is considered negligible (25).

Power input to the resistance heaters was measured by obtaining the resistance of the heating elements and determining the voltage drop across the individual heater strips by means of the potential-measurement wires connected to each bus bar inside the plate. The resistance of each heater was measured on an Electro-Scientific Instruments impedance bridge after installation in the working surface of the plate. Capacitive and inductive effects of the heater system were found to be negligible. Line voltage to the heaters was reduced to a suitable value by use of an autotransformer, and the output of the autotransformer to the plate was continuously monitored during the testing time to maintain a constant voltage supply.

Procedure for Taking Data

The chronology for a run began when the tunnel fan was started and the dampers and vane-inlet control adjusted for the velocity required.

The plate-heater voltage was adjusted until the desired difference between the free stream temperature and the plate surface was obtained. The vernier resistors across each heater were adjusted until the plate surface was at a uniform temperature. Monitoring of the temperatures and readjustment of the voltages was required until steady-state conditions were reached. After steady-state conditions prevailed, the heat transfer information was recorded six times over a period of about fifteen minutes. On some runs, most frequently when operating when the boundary layer was in the transition range and somewhat unstable, additional heat transfer data were taken in order to be sure a true steady-state average could be obtained.

Immediately after the heat transfer information was obtained, a boundary layer search was made with the total head tube, using the plate surface static pressure to obtain the velocity head. It was assumed that the static pressure across the boundary layer was constant. This was verified within the limits of measurement of the manometer system by checking the static pressure distributions along the plate surface and in the free stream just above the plate surface outside the boundary layer at a distance sufficient to assure there was no

error in the reading due to the proximity of the wall.

After the boundary layer information had been obtained, the probe was removed and a hot-wire anemometer probe inserted in the test section so that the wire portion was parallel to the plate surface and perpendicular to the flow direction. The wire was kept at a distance of approximately one inch from the plate surface. Hot-wire data was then recorded.

Methods of Calculation

The methods used to calculate the experimental results are discussed in this section. A set of sample calculations for one run is in Appendix D.

Calculation of Nusselt number

In the presentation of the results of this investigation the Nusselt number,

$$N_{Nu_x} = \frac{hx}{k_a} \tag{17}$$

was found from values of h obtained from power and temperature measurements on the plate, the distance downstream from the leading edge, x, and the thermal conductivity of air taken from reference (16).

From the definition of the convective heat transfer coefficient h,

$$h = \frac{Q_n}{A(t_s - t_f)} \tag{18}$$

where A is the strip surface area, Q_n is the net rate of energy loss from the plate surface by convection, and $(t_s - t_f)$ is the temperature difference between the plate surface and the free stream.

The net rate of energy loss Q_n was found by measuring the electrical power input to the resistance strip and deducting the losses by radiation and conduction. Thus,

$$Q_n = P - q_r - q_c \tag{19}$$

where P is the total power input to the strip, q_r is the radiation loss and q_c is the convection loss.

The total power input was obtained from voltage and resistance measurements of each strip.

The temperature difference between the plate surface and the free stream was taken as the average of the readings measured by both differential measurements and against an ice bath.

In order to obtain the conduction loss, it was necessary to find the temperature distribution on the back side of the working surface, to know the thermal conductivity of the phenolic backing material and to estimate any end effects due to the finite length of the resistance strips. The temperature distribution on the back side of the working surface was obtained from the thermocouples mounted on the phenolic material. The temperature difference was read by a differential reading with the plate working surface thermocouples. Since the working surface of the plate was large with relation to

the thickness of the phenolic material, a one-dimensional flow of energy by conduction was assumed. The loss was calculated from

$$q_c = k_p A \frac{(t_s - t_b)}{x_p} \qquad (20)$$

where x_p is the thickness of the phenolic backing, $(t_s - t_b)$ is the difference between the plate surface temperature and the back side of the working surface, k_p is the thermal conductivity of the material and A is the area of the resistance strip. The thermal conductivity was found from values given in reference (13). The temperature variation along the length of a resistance strip (i.e. spanwise on the plate surface) for this type of construction was shown to be negligible by Drake (4). However, several strips had additional thermocouples attached one inch in from each end of the strip. These were checked and found to have less than one degree F difference from the centerline temperature of the same strip for most values of free stream temperature and velocity, although some of the higher velocity runs had variations of about 1.5 degrees F. It was not felt that conduction along the strip was a significant factor since the temperature difference between the working surface and the back side of the working surface remained constant. Radiation losses were calculated from

$$q_r = \epsilon \sigma A(T_s^4 - T_a^4) \qquad (21)$$

where ϵ is the emissivity of the strip material, A is the strip area, σ is the Stefan-Boltzmann constant, T_s is the absolute temperature of the strip surface and T_a is the temperature of the surroundings. The value of emmissivity was taken from Scesa and Sauer (33) for Nichrome V resistance alloy. The temperature of the surroundings was taken as the room wall surface temperature. Corrections for absorption in the room atmosphere and in the plastic tunnel wall were assumed to be negligible. The radiation geometric "view factor" was assumed to be unity as implied in Equation 21.

The Nusselt numbers presented in the results section have been corrected for the unheated starting length of the nose-piece according to the equation of Eckert (7) for the laminar range,

$$N_{Nu_x,\ corrected} = N_{Nu_x} \left[1 - \left(\frac{x_o}{x} \right)^{3/4} \right]^{-1/3} \qquad (22)$$

and the Nusselt numbers in the turbulent range have been corrected according to the equation of Rubesin (31)

$$N_{Nu_x,\ corrected} = N_{Nu_x} \left[1 - \left(\frac{x_o}{x} \right)^{39/40} \right]^{-7/39} \qquad (23)$$

Calculation of Reynolds number

The Reynolds number for an experimental point for flows where the pressure gradient along the plate surface was negligible was formed from

$$N_{Re_x} = \frac{\overline{U}x}{\nu} \tag{24}$$

where $\overline{U}$ is the mean free stream velocity, x is the distance from the leading edge of the plate and ν is the kinematic viscosity of air at low pressures taken from reference (16).

The free stream velocity was determined from the velocity head, density and temperature of the free stream according to the expression

$$\overline{U} = \sqrt{2gH} \tag{25}$$

where H is the velocity head. The density was calculated from the perfect gas law using the static pressure in the test section and the average of the plate surface and free stream temperatures.

Boundary-layer measurements

The boundary layer data as taken during the experimental runs involved an inherent error due to the height of the total head probe. A correction to the measured distance above the plate surface was made according to the findings of Young and Maas (44). This correction involved adding a correction

factor based on the ratio of the probe height to the measured distance of the probe from the surface.

When the boundary layer thickness was required in calculations, it was taken as the distance above the surface where the boundary layer velocity was 0.993 of the free stream velocity. Since some investigators assume the position of the boundary layer thickness to be at 0.99 of the free stream velocity and others use 0.995, an intermediate value was chosen. The selection of the velocity where the free stream and the boundary layer are considered to merge is an arbitrary choice.

Turbulence intensity measurements

Data taken with the hot-wire anemometer were reduced using equations based on the relation

$$\frac{i^2R}{R - Ra} = B + D\sqrt{U} \qquad (26)$$

King (20) developed the original form of Equation 24 for incompressible flow, assuming that heat transfer from the wire did not change the flow field. The viscous effects of the flow about the wire were not taken into account. These limitations have not been proved to be serious for low-speed continuum flows, and a large amount of data in the technical literature indicates the equation may be used with little error for applications such as the present study.

Equation 26 gives a relationship between fluid velocity and current through the wire. For a wire of constant resistance (i.e., constant temperature), R is constant and the turbulence intensity may be found from the relation

$$T = \frac{\sqrt{\overline{u'^2}}}{\bar{U}} = \frac{4\sqrt{\overline{e'^2}}}{\bar{e}_w \left[1 - \left(\frac{e_o}{e_w}\right)^2\right]} \qquad (27)$$

which was originally developed by Laurence and Landes (23) and in which $\bar{e}_w$ is the average bridge voltage measured when the wire is in the air stream, e_o is the average bridge voltage when the wire is in still air and $\sqrt{\overline{e'^2}}$ is the root-mean-square of the fluctuating voltage about the average bridge voltage when the wire is in the airstream.

Uncertainties in Experimental Results

It would be of value to have sufficient replication of data for each flow condition to treat it statistically. In engineering experiments, however, it is difficult to obtain more than one or two data points for a given run or operating condition. This fact precludes statistical treatment of data. Nevertheless, some estimate of error is desirable. The estimates of error for this experiment are based on the "single sample" procedures of Kline and McClintock (21) and the examples of Thrasher and Binder (39).

The method of Kline and McClintock (21) requires that each variable used in the computation of a quantity be assigned an uncertainty interval together with odds that the value of a given variable lies within this interval. Were it possible to treat the data for any variable statistically, the uncertainty interval would correspond to some precision index, such as a standard deviation. Lacking enough data for such treatment, the investigator must use his familiarity with the experimental equipment, his knowledge of the phenomena involved, and his assessment of the care used in gathering data to state an interval of uncertainty for the values of these data and give odds that the values are within that interval.

Uncertainty in the Nusselt number

From Kline and McClintock (21), the uncertainty in a calculated result which is found from a linear function of variables is

$$w_r = \left[\left(\frac{\partial R}{\partial v_1} w_1\right)^2 + \left(\frac{\partial R}{\partial v_2} w_2\right)^2 + \ldots + \left(\frac{\partial R}{\partial v_n} w_n\right)^2\right]^{1/2} \quad (28)$$

where w_r is the uncertainty interval in the calculated result, R is the function, v_1, v_2, ... v_n are variables in the function R and the w_1, w_2, ... w_n are the uncertainty limits placed on the several variables by the experimenter.

Applying the above to the calculation for the Nusselt number, from Equations 18 and 19, the Nusselt number is

$$N_{Nu_x} = \frac{Q_n x}{A k_a (t_s - t_f)} \tag{29}$$

Thus Equation 28 becomes, for the Nusselt number

$$w_N = \left[\left(\frac{\partial N_{Nu_x}}{\partial Q_n} w_Q \right)^2 + \left(\frac{\partial N_{Nu_x}}{\partial x} w_x \right)^2 + \left(\frac{\partial N_{Nu_x}}{\partial A} w_A \right)^2 + \left(\frac{\partial N_{Nu_x}}{\partial (t_s - t_f)} w_t \right)^2 \right]^{1/2} \tag{30}$$

It should be noted that the uncertainty in Q_n in Equation 30 is dependent on the uncertainties of several other variables. These have been treated in a manner similar to the Nusselt number to obtain the uncertainty in Q_n. Values of the uncertainties used in Equation 30 are tabulated in Appendix B.

When uncertainty intervals were calculated, it was readily apparent that two experimental data readings were responsible for the major portion of the uncertainty in the Nusselt number. These were the voltage reading for the power input and the temperature difference used for calculating the conduction loss through the plate back. These readings were known to be critical when testing started and every effort was

made to secure accurate data. The maximum predicted uncertainty in the Nusselt number found for the experiment was 7.51 per cent. A listing of the maximum uncertainties for various runs is in Appendix B.

Uncertainties in the Reynolds number

The equation for the Reynolds number uncertainty is

$$w_R = \left[\left(\frac{\partial N_{Re_x}}{\partial \bar{U}} w_U\right)^2 + \left(\frac{\partial N_{Re_x}}{\partial x} w_x\right)^2 + \left(\frac{\partial N_{Re_x}}{\partial \nu} w_\nu\right)^2\right]^{1/2} \quad (31)$$

The uncertainties for the individual variables may be found in Appendix B. The maximum uncertainty in the Reynolds number for all runs was found to be 2.53 per cent. It should be noted that the measurements here were much less critical than those for the Nusselt number, and little variation from run to run was encountered.

Uncertainties in the pressure gradient

The only measurement made for this parameter was the static pressure, which has an estimated uncertainty of $\pm$ 0.001 inch of water (odds of 20 to 1).

Uncertainties in turbulence intensity measurement

The turbulence intensity was measured with a hot-wire anemometer of the constant temperature type, which, for lower levels of turbulence, say less than 2 per cent, is not as precise as other types. The uncertainty interval for the

turbulence intensity is expressed as

$$w_T = \left[\left(\frac{\partial T}{\partial \sqrt{\bar{e}'^2}} w_{e'} \right)^2 + \left(\frac{\partial T}{\partial e_o} w_{e_o} \right)^2 + \left(\frac{\partial T}{\partial e_w} w_{e_w} \right)^2 \right]^{1/2} \quad (32)$$

and values of the calculated uncertainty for all runs are in Appendix B. The maximum value of uncertainty in all runs was 17.5 per cent of the turbulence intensity reported. It is important to recognize that in this work the relative values of turbulence intensity are more of value than the absolute magnitude. In addition, only a very low turbulence intensities, where the fluctuating components are small and therefore hard to measure, was the uncertainty this large.

RESULTS OF THE EXPERIMENTAL INVESTIGATION

The results of the experimental investigation are presented and discussed in the following section classified according to the variables of primary interest in each series of tests. Comparisons to published works of others are made where possible.

Zero Pressure Gradient

The first series of tests was carried out with no pressure gradient along the plate surface. The objective of these tests was to check the wind tunnel and plate equipment against earlier analytical and experimental work that had been done on this configuration, and to observe the effects of an increased free-stream turbulence intensity to check the results of other investigators. The pressure distribution for this series of tests is shown in Figure 9 as the ratio of the static pressure to the stagnation pressure of the free stream measured opposite the first heat transfer measuring station back from the leading edge. All other pressure distributions are presented in the same way.

The heat transfer results are shown in Figure 10, where the two sets of points correspond to different ranges of free stream turbulence intensities, one for the free tunnel with no grid, where the range was from 0.40 to 0.80 per cent, and the other for the range from 1.30 to 1.80 per cent. The higher

Figure 9. Static pressure distribution for zero pressure gradient

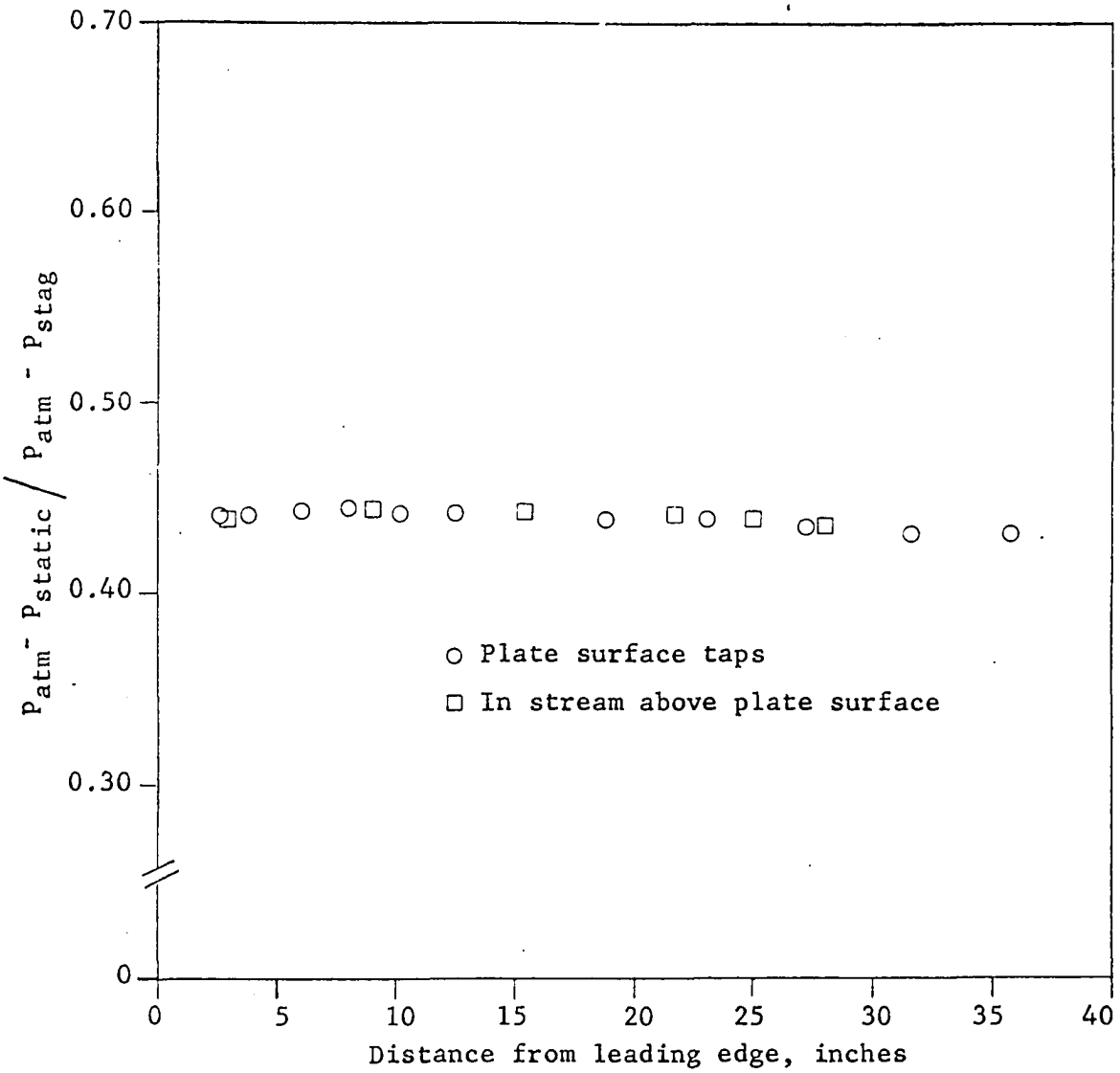
0.70
0.60
0.50
0.40
0.30
0
$P_{atm} - P_{static} / P_{atm} - P_{stag}$
Plate surface taps
In stream above plate surface
0
5
10
15
20
25
30
35
40
Distance from leading edge, inches

Figure 10. Heat transfer results for zero pressure gradient

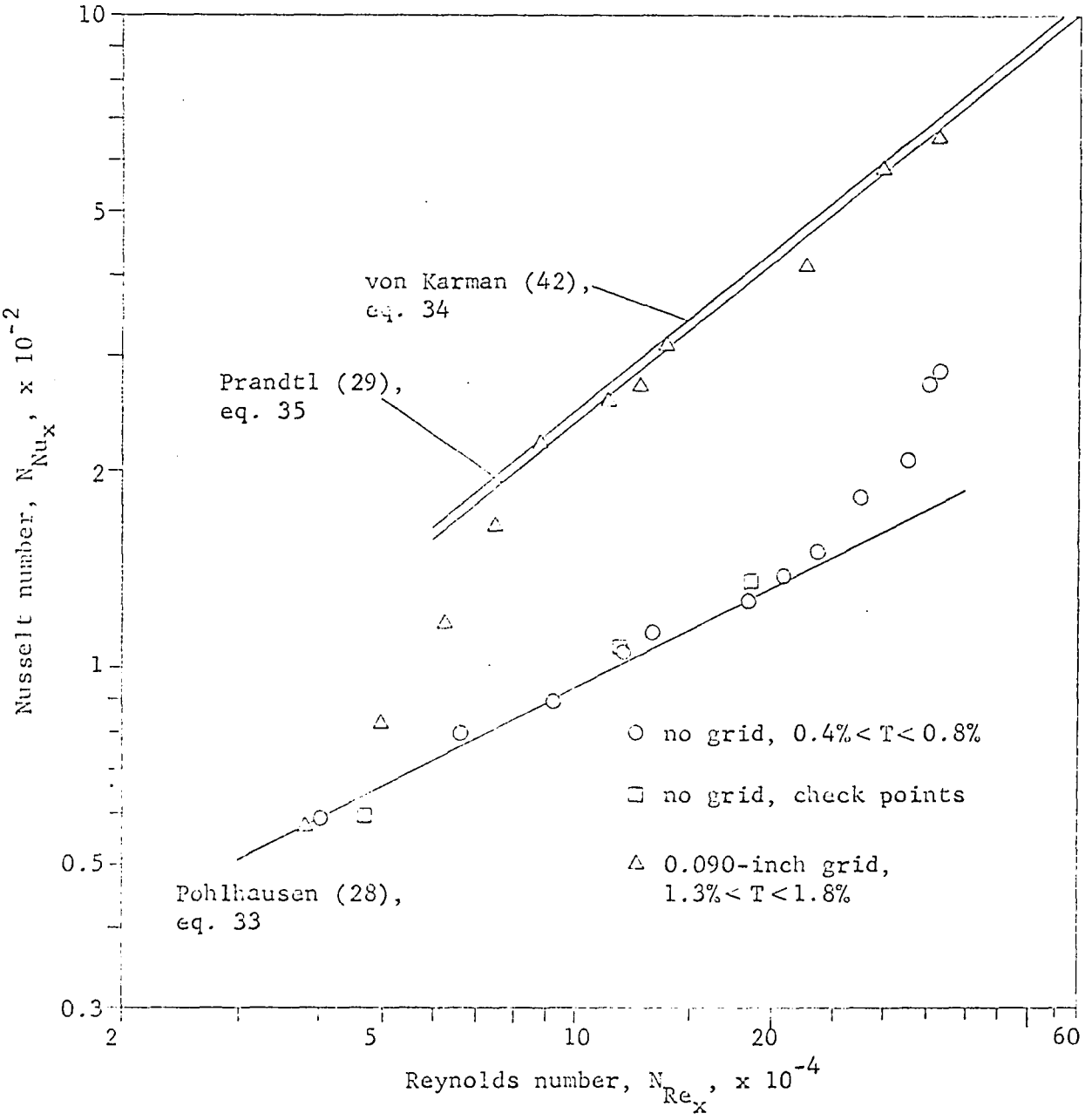
10
5
2
1
0.5
0.3
2
5
10
20
60
Nusselt number, N_{Nu_x}, x 10^{-2}
Reynolds number, N_{Re_x}, x 10^{-4}
von Karman (42), eq. 34
Prandtl (29), eq. 35
Pohlhausen (28), eq. 33
○ no grid, 0.4% < T < 0.8%
□ no grid, check points
△ 0.090-inch grid, 1.3% < T < 1.8%

range is due to the insertion of the 0.090-inch grid upstream of the plate.

The results for the laminar range of Reynolds numbers with no grid in place agree within $\pm$ 5 per cent of the line representing the equation of Pohlhausen (28) for the laminar boundary layer. For the higher Reynolds numbers, the points are above the line and indicate that they are deviating further from the line as the Reynolds number increases. This is to be expected as the transition from laminar to turbulent flow in the boundary layer occurs near these Reynolds numbers.

The results obtained with the 0.090-inch grid in place indicate that the position of transition moved toward the leading edge and that the flow over the plate surface was primarily turbulent. The points in the turbulent Reynolds number range agree with the equations from the literature as shown in Figure 10. The equations represented by lines on the figure, all calculated for a Prandtl number of 0.7, are that of Pohlhausen (28) for a laminar boundary layer,

$$N_{Nu_x} = 0.295 \left(N_{Re_x} \right)^{0.5} \tag{33}$$

the equation of von Karman (42) for a turbulent boundary layer

$$N_{Nu_x} = 0.241 \left(N_{Re_x} \right)^{0.8} \tag{34}$$

and the equation originally due to Prandtl (29) for a turbulent boundary layer

$$N_{Nu_x} = 0.236\left(N_{Re_x}\right)^{0.8} \tag{35}$$

In order to check the behavior of the boundary layer as indicated by the heat transfer results, velocity profiles of the boundary layer were taken at several positions along the plate surface. Typical profiles for Reynolds numbers in the laminar range are shown in Figure 11 where they agree well with the line representing the Blasius solution to the two-dimensional boundary layer equations. Note that points are presented for flow with and without heat transfer. Velocity profiles for the turbulent boundary layer are shown in Figure 12 where the agreement with the universal turbulent velocity profile is good.

These profiles were plotted on the universal turbulent boundary layer coordinates suggested by Clauser (3). Plotting the data to these coordinates involves knowledge of the coefficient of friction, c_f, defined as

$$c_f = \frac{2\tau_o}{\rho\bar{U}^2} \tag{36}$$

Determination of values of c_f for each run was made according to a procedure proposed by Clauser (2). These values of c_f were then used to compute values of u^+ and y^+ which are

Figure 11. Laminar boundary layer profiles for zero pressure gradient

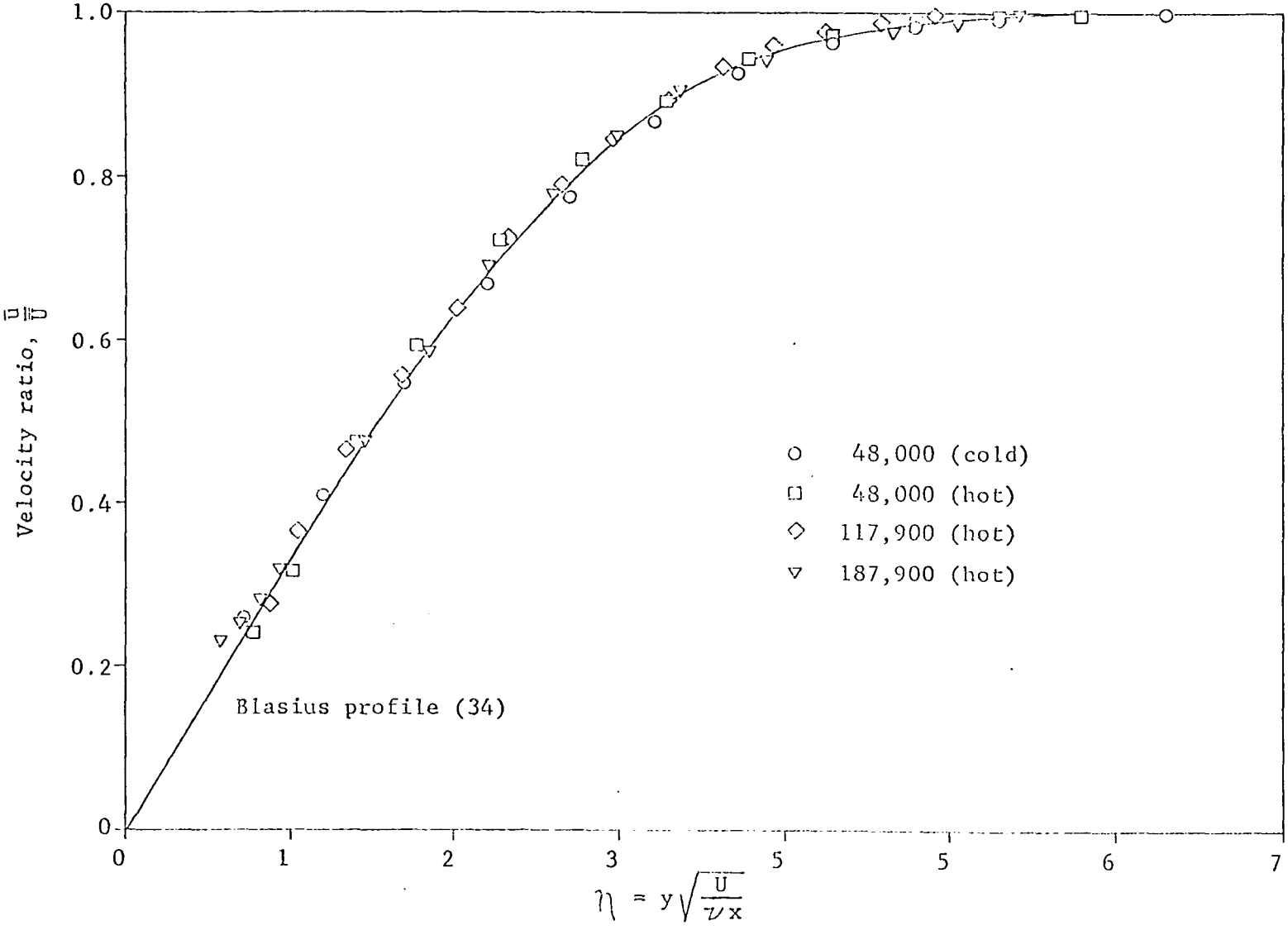
1.0
0.8
0.6
0.4
0.2
0
Velocity ratio, $\frac{\bar{u}}{U}$
0
1
2
3
5
5
6
7
$\eta = y\sqrt{\frac{U}{\nu x}}$
48,000 (cold)
48,000 (hot)
117,900 (hot)
187,900 (hot)
Blasius profile (34)

Figure 12. Turbulent boundary layer profiles for zero pressure gradient

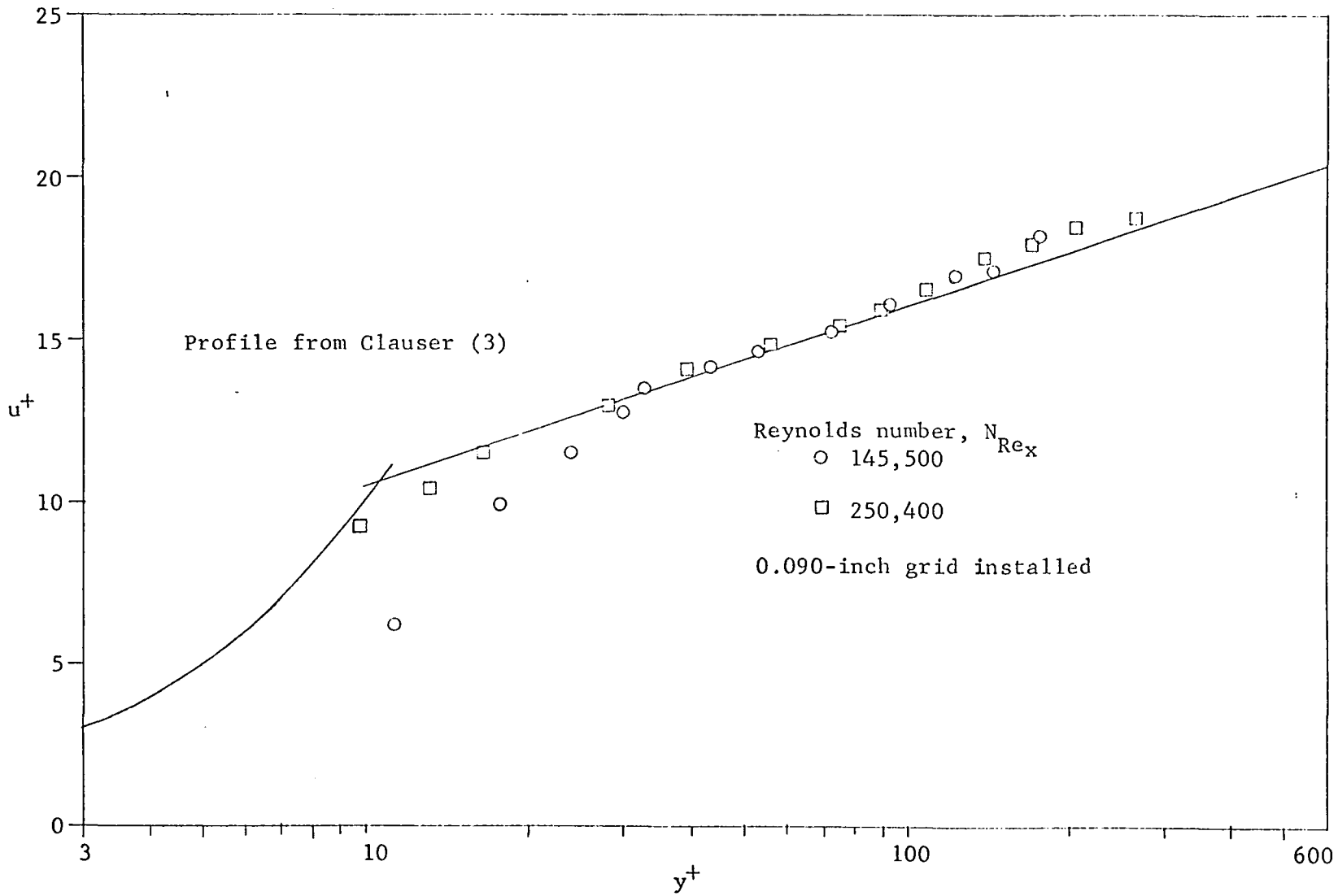
25
20
15
10
5
0
u^+
3
10
100
600
y^+
Profile from Clauser (3)
Reynolds number, N_{Re_x}
145,500
250,400
0.090-inch grid installed

defined as

$$u^+ = \sqrt{\frac{2}{c_f}} \frac{u}{\bar{U}} \tag{37}$$

$$y^+ = \sqrt{\frac{c_f}{2}} \frac{\bar{U}y}{\nu} \tag{38}$$

It should be noted that the temperature difference between the plate surface and the free stream was maintained at approximately 30F for the data shown, with the exception of the check points which were at temperature differences of 15 and 20 F. Little effect of heat transfer on the boundary layer could be expected at these temperature differences since the variation in fluid properties across the boundary layer is small.

The results of this series show that, for the Reynolds number range investigated, the analytical solution of Pohlhausen and the semi-empirical equations of von Karman and Prandtl agree with the experimental data. The points also agree with the experimental data of Edwards and Furber (9) and Wang (43), who showed that the effect of increased free stream turbulence intensity only serves to advance the position of transition of the boundary layer and has no effect on the heat transfer in the laminar range.

Since the free stream turbulence generated by the .090-inch wire grid was sufficient to cause transition to be complete at a Reynolds number of about 100,000, and, since the

results indicate only a further change in the position of transition, a higher free stream turbulence intensity would show only turbulent boundary layer flow over the Reynolds number range. For this reason, no higher free stream turbulence intensities were run.

A further comparison of the data with published results can be made by using the heat transfer data to determine the Reynolds numbers of transition and comparing them with the work of Gazley (14) on transition of the laminar boundary layer. This is done in Figure 13 where it appears that the experimental plate used had somewhat lower transition Reynolds numbers than Gazley predicts.

Low Favorable Pressure Gradient

This series of tests was run with the lower of two pressure gradients used. The pressure distribution for this series is shown in Figure 14.

Low favorable pressure gradient, no grid

The heat transfer results for the low pressure gradient without a grid are shown in Figure 15 in the form of the local Nusselt number N_{Nu_x} as a function of the local Reynolds number, N_{Re_x}. The Nusselt numbers shown have been corrected for the unheated starting length of the nosepiece by the same procedure used for the zero pressure gradient data.

Figure 13. Transition Reynolds numbers for zero pressure gradient

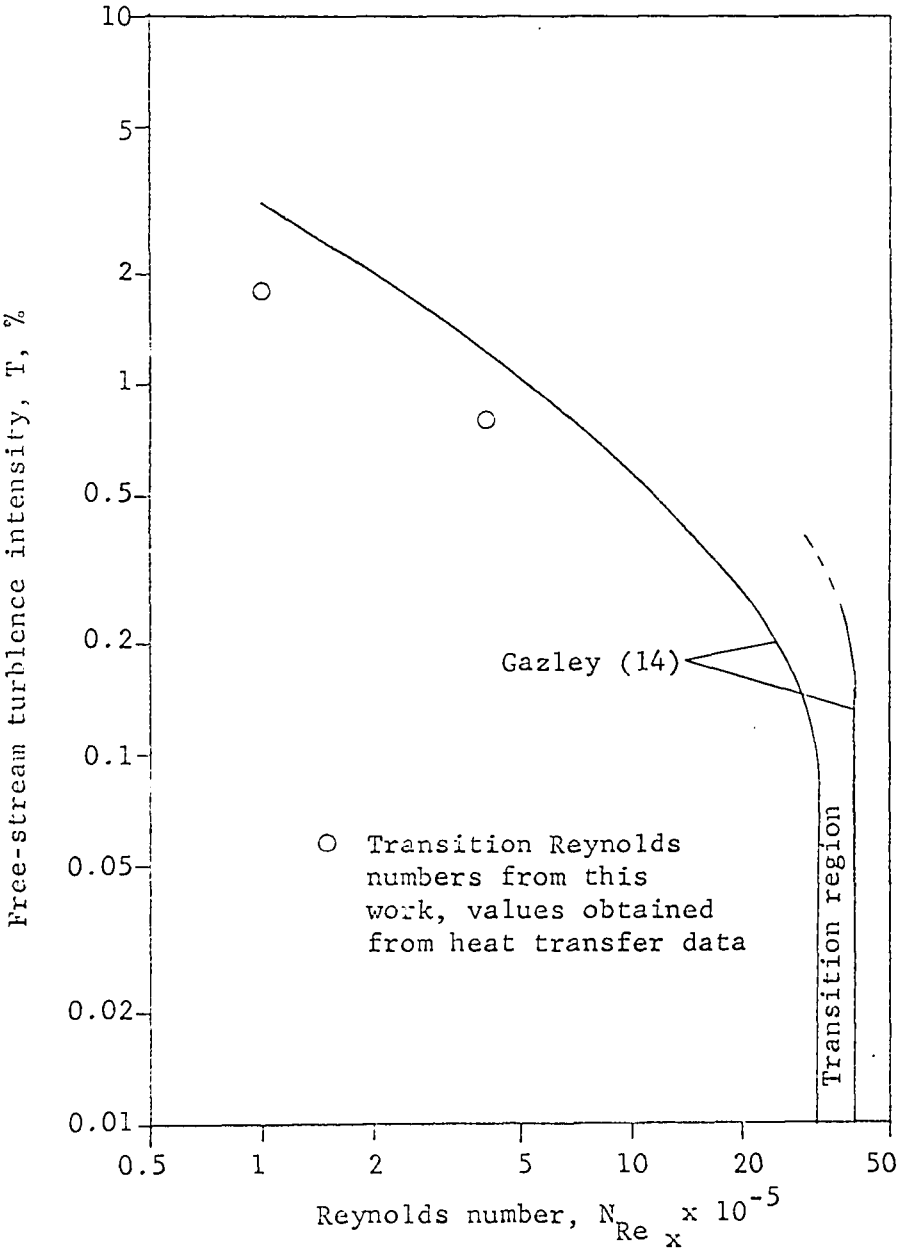
10
5
2
1
0.5
0.2
0.1
0.05
0.02
0.01
0.5
1
2
5
10
20
50
Free-stream turblence intensity, T, %
Reynolds number, $N_{Re_x} \times 10^{-5}$
Gazley (14)
Transition Reynolds numbers from this work, values obtained from heat transfer data
Transition region

Figure 14. Static pressure distribution for low favorable pressure gradient

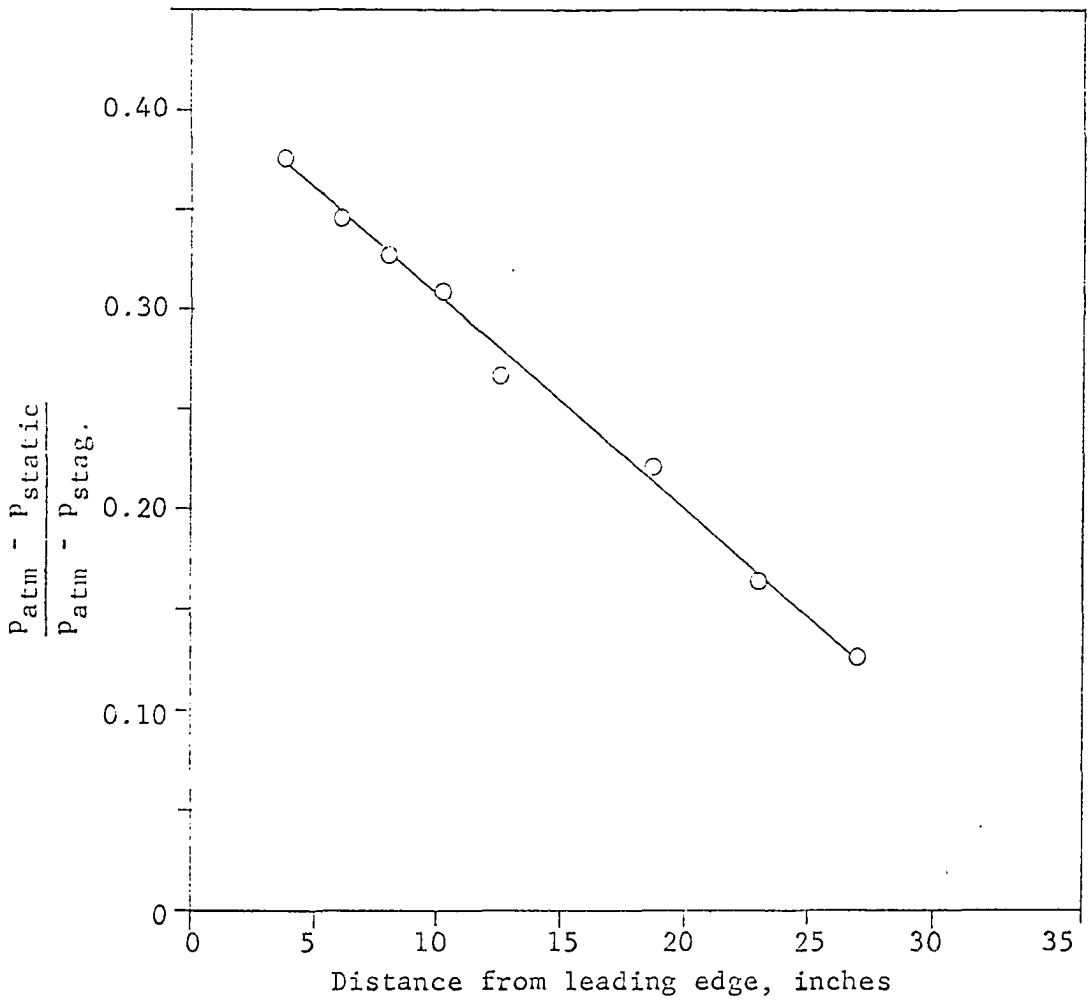
0.40
0.30
0.20
0.10
0
0
5
10
15
20
25
30
35
$\frac{P_{atm} - P_{static}}{P_{atm} - P_{stag.}}$
Distance from leading edge, inches

Figure 15. Heat transfer results for low favorable pressure gradient with no grid

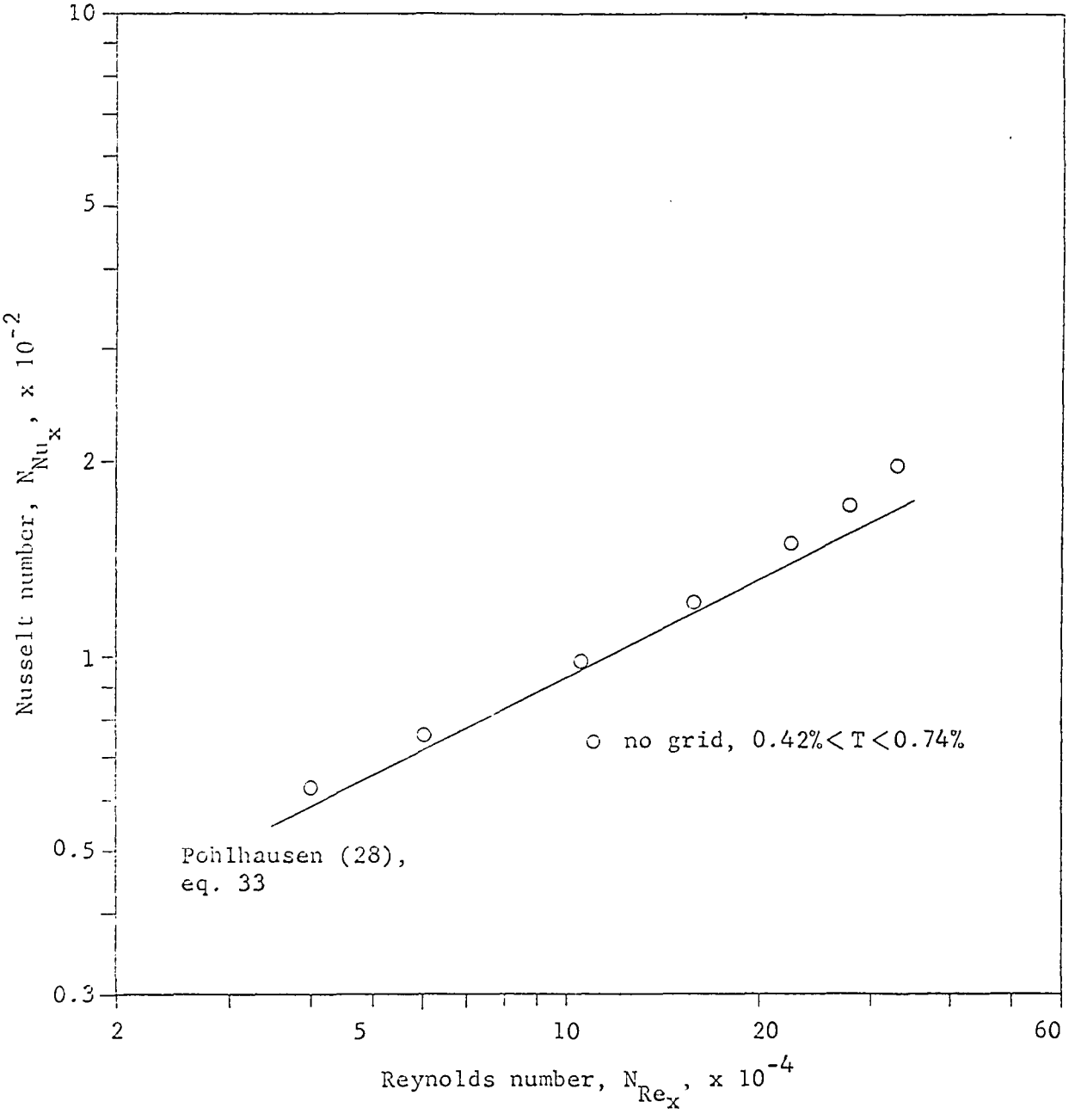
10
5
2
1
0.5
0.3
Nusselt number, N_{Nu_x}, x 10^{-2}
2
5
10
20
60
Reynolds number, N_{Re_x}, x 10^{-4}
o no grid, 0.42% < T < 0.74%
Pohlhausen (28),
eq. 33

The points obtained by experiment lie only slightly above the Pohlhausen relation for the laminar boundary layer and no significant increase in heat transfer is apparent. No indication of boundary layer transition is evident from these data.

The absence of a transition region in the heat transfer data is confirmed by boundary layer profiles taken at several stations along the plate surface. Since there was a pressure gradient along the plate surface, the free stream velocity could be expected to vary with distance back from the leading edge of the plate, and the boundary layer profiles could no longer be expected to conform to the shape of the Blasius profile. However, the fact that the heat transfer data correlate in a straight line on the coordinates used suggests a similarity in boundary layer profile shape. This can be explained by noting that there are some solutions of the laminar boundary layer equations which admit similar profiles and have a variation in free stream velocity. One solution of this type applies to the free-stream velocity variation

$$U(x) = Cx^m \tag{39}$$

where C and m are constants. This corresponds to a solution of Falkner and Skan's (11) equations of the two-dimensional boundary layer found by Hartree (17).

The present test conditions approximated this type of solution. The free stream velocity was plotted as a function of length on logarithmic coordinates and the slope found.

The exponent m as found by this method was 0.149 for the low pressure gradient, independent of the magnitude of the free stream velocity. The boundary layers were then plotted using Hartree's coordinates as shown in Figure 16 where coordinates for m = 0.149 were interpolated between the tabulated values for m = 0.10 and m = 0.20 given in Hartree's paper (17). It is seen that the data correlate well on these coordinates and that the analytical solution by Hartree is closely followed for the range of Reynolds numbers investigated. The difference between Hartree's definition of the parameter η and Blasius' definition is the factor $\sqrt{\frac{m+1}{2}}$.

The turbulence intensity range over which the data were obtained was from 0.42 to 0.74 per cent. No effect of this low level of turbulence is noticeable from either the heat transfer data or the boundary layer data.

The temperature difference between the plate and the free stream was a nominal 30 F. The actual temperature difference varied by less than 1 F from strip to strip along the plate surface while the deviation from the nominal terperature difference for the whole plate was about 1 F. Because of the small temperature difference between the plate surface and the free stream, little effect of heat transfer on the position of the transition point of the boundary layer could be expected.

Low favorable pressure gradient, 0.090 inch grid

The addition of the 0.090 inch grid upstream of the plate

Figure 16. Boundary layer profiles for low pressure gradient with no grid

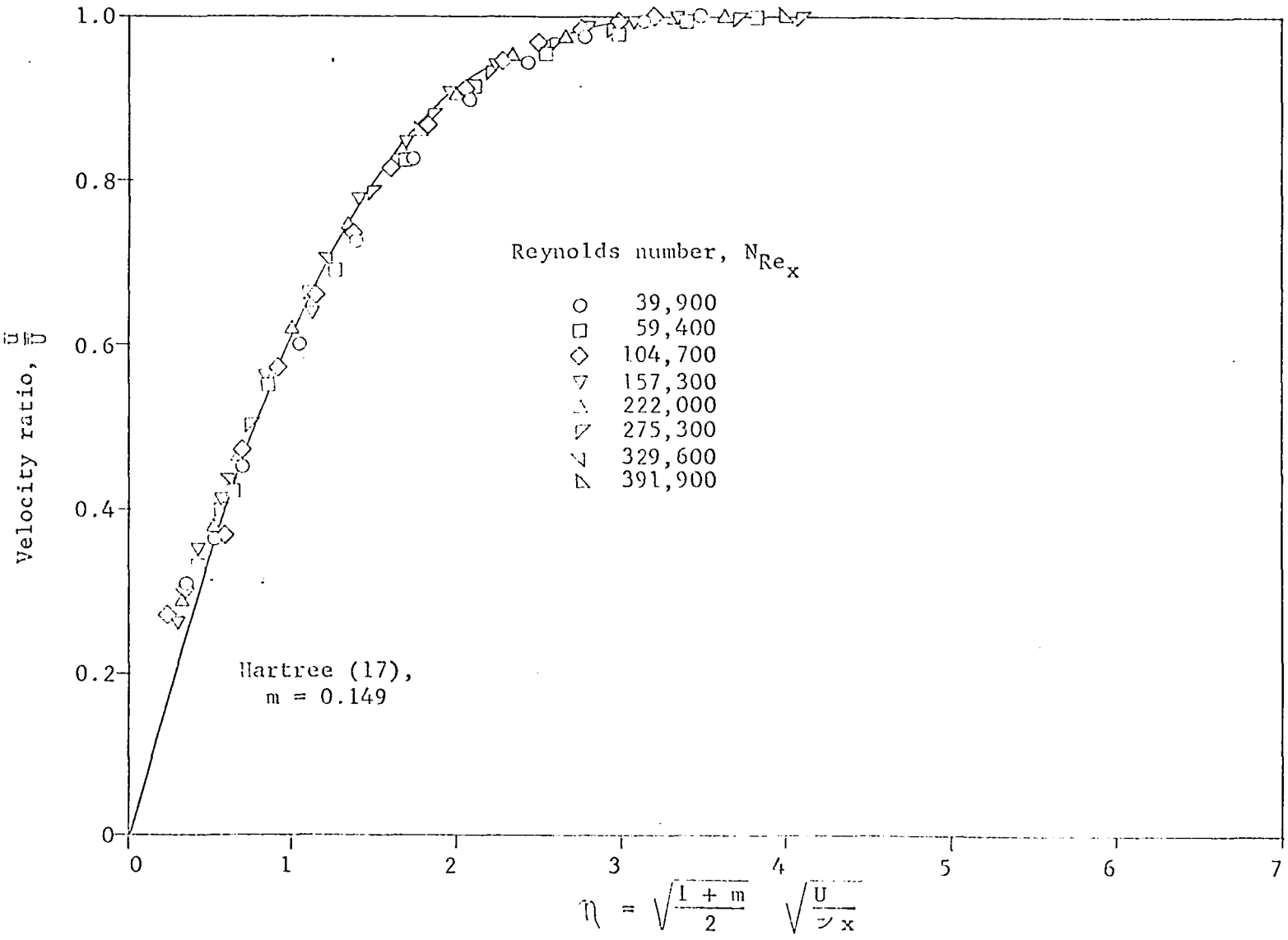
1.0
0.8
0.6
0.4
0.2
0
Velocity ratio, $\frac{\bar{u}}{U}$
Reynolds number, N_{Re_x}
39,900
59,400
104,700
157,300
222,000
275,300
329,600
391,900
Hartree (17),
m = 0.149
0
1
2
3
4
5
6
7
$\eta = \sqrt{\frac{1+m}{2}} \sqrt{\frac{U}{\nu x}}$

resulted in an increase in Nusselt number from the values found for data taken with no grid, the plate being undisturbed from the position it occupied for the runs with no grid. The variation in local Nusselt number corrected for unheated starting length with Reynolds number is shown in Figure 17.

The heat transfer data points lie from 15 to 35 per cent above the Pohlhausen relation line at the low Reynolds numbers. A transition from laminar to turbulent flow in the boundary layer is indicated in the Reynolds number range from 200,000 to 250,000. The data points for flows with Reynolds numbers higher than 250,000 lie close to the lines representing Equations 34 and 35 for turbulent flow.

Boundary layer profiles for the data are plotted in Figures 18 and 19. The profiles in Figure 18 are shown compared with Hartree's solution as was done for the boundary layer profiles taken when no grid was present. The experimental points in this figure are for Reynolds numbers up to 244,900, which is in the region of transition indicated by the heat transfer data. It is clear from this figure that the velocity distributions for different Reynolds numbers are more scattered than those taken with no grid. Since Hartree's solution results in profiles which are similar in profile for a given value of m, but different Reynolds numbers, and, since the data obtained with no grid behaved in this manner, the increase in free-stream turbulence intensity seems to have at least partially destroyed the similarity of the profiles.

Figure 17. Heat transfer results for low favorable pressure gradient with 0.090-inch grid

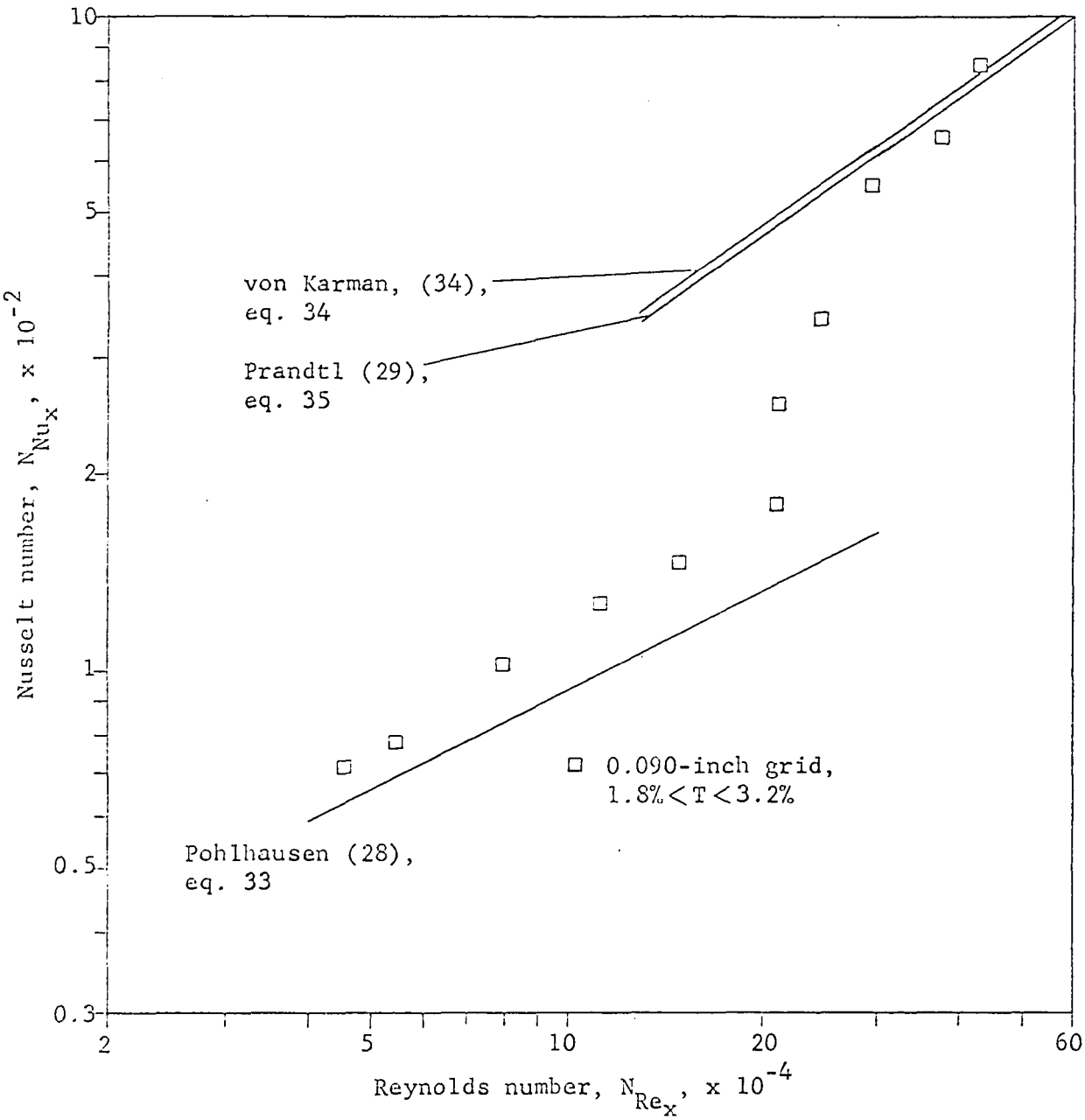
10
5
2
1
0.5
0.3
2
5
10
20
60
Nusselt number, N_{Nu_x}, x 10^{-2}
Reynolds number, N_{Re_x}, x 10^{-4}
von Karman, (34), eq. 34
Prandtl (29), eq. 35
Pohlhausen (28), eq. 33
0.090-inch grid, 1.8% < T < 3.2%

Figure 18. Boundary layer profiles for low favorable pressure gradient with 0.090-inch grid

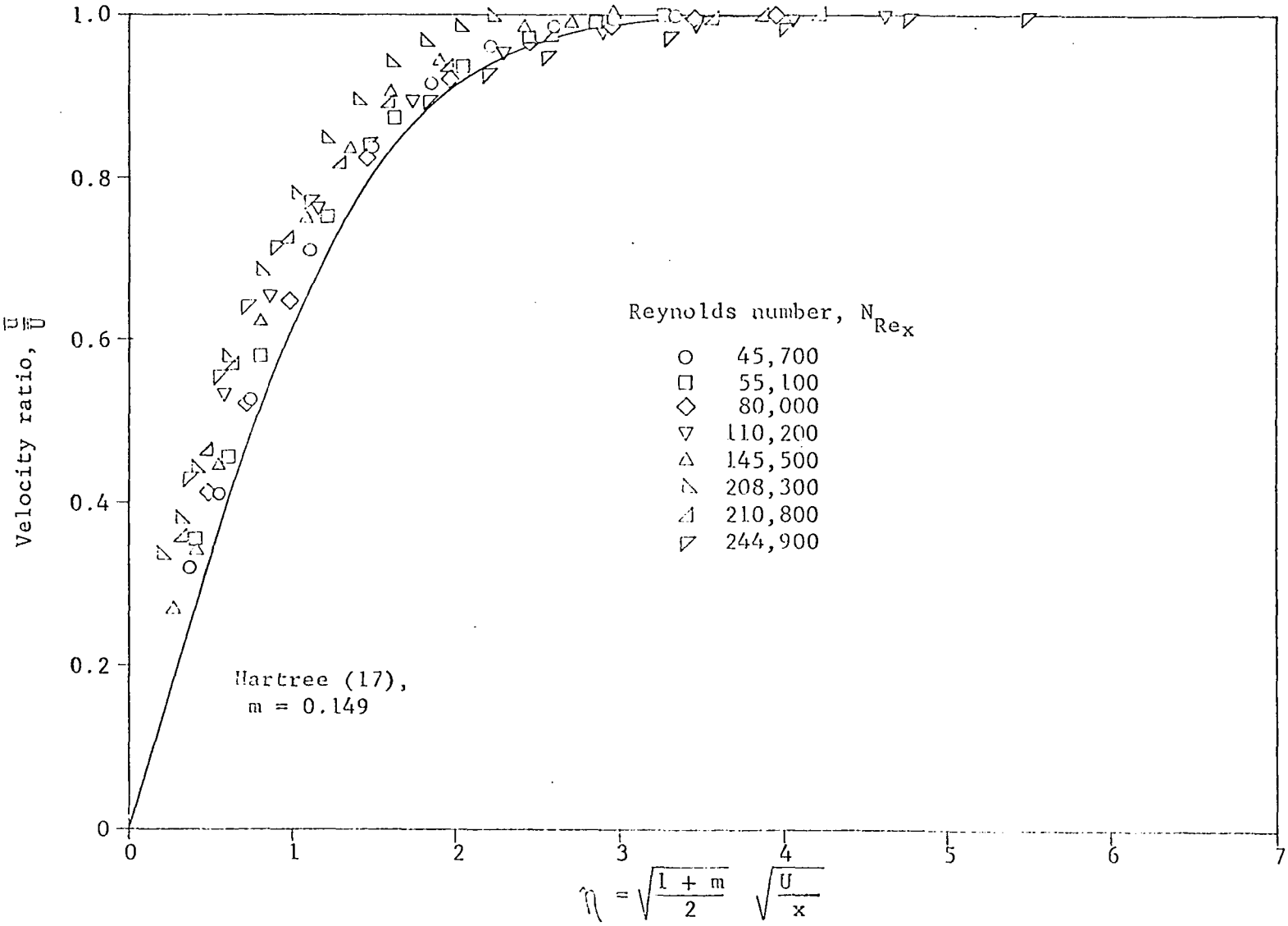
1.0
0.8
0.6
0.4
0.2
0
Velocity ratio, $\frac{u}{U}$
0
1
2
3
4
5
6
7
$\eta = \sqrt{\frac{1+m}{2}} \sqrt{\frac{U}{x}}$
Reynolds number, N_{Re_x}
45,700
55,100
80,000
110,200
145,500
208,300
210,800
244,900
Hartree (17),
m = 0.149

Figure 19. Turbulent boundary layer profiles for low favorable gradient with 0.090-inch grid

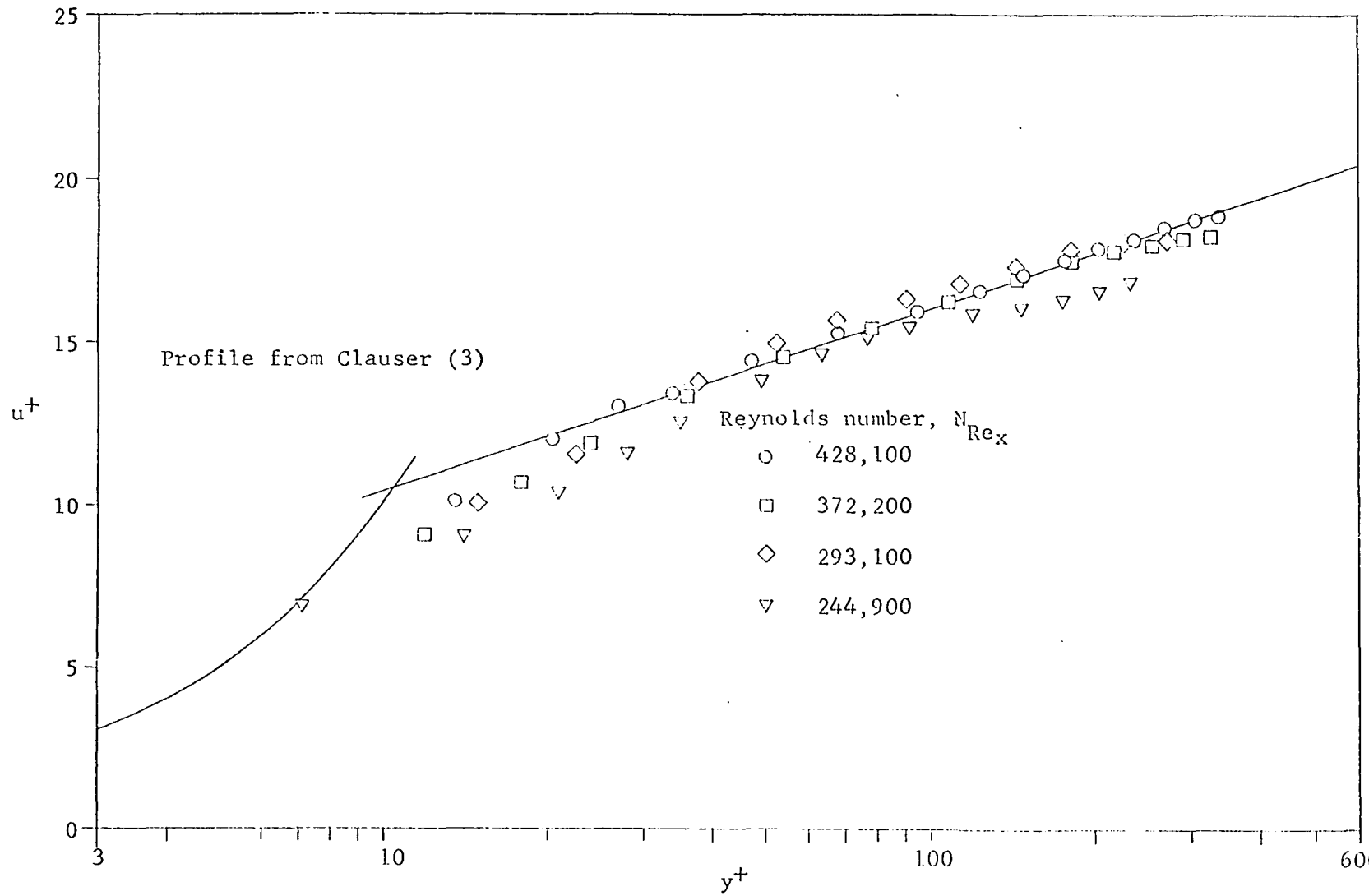
25
20
15
10
5
0
u+
3
10
100
600
y+
Profile from Clauser (3)
Reynolds number, N_{Re_x}
428,100
372,200
293,100
244,900

It is also interesting to note that the profile data taken with the 0.090-inch grid present are generally to the left of the analytical line, whereas the profile data taken with no grid present lie on the line. Thus, it also appears that the shape of the profile has been changed slightly with the addition of the grid.

A further examination of the boundary layer profiles indicates that the distributions for Reynolds numbers of 208,300, 210,800 and 244,900 deviate most from the rest of the data. These profiles are all in the transition region as determined by the heat transfer data and might therefore exhibit erratic behavior.

The boundary layer profiles for Reynolds numbers of 244,900 and higher were apparently turbulent on the heat transfer plot. To confirm this, these profiles are plotted on the universal turbulent boundary layer coordinates in Figure 19, where the profile for the transition Reynolds number of 244,900 deviates most from the other profile data. It may thus be concluded that the transition indicated by the boundary layer profiles and that shown in the heat transfer correlation are in agreement, and that this particular profile was indeed in the transition region.

The turbulence intensities for these data ranged from 1.84 to 3.20 per cent. The effects of raising the free stream turbulence seem to have been an increase in the Nusselt number for the laminar boundary layer range and a lowering of the

transition Reynolds number range to approximately 200,000 to 250,000. In addition, similarity of the boundary layer profiles has been somewhat destroyed and the general shape of these profiles has been affected.

Low favorable pressure gradient, 0.250-inch grid

The turbulence produced by the 0.250 inch grid raised the Nusselt numbers for low Reynolds numbers approximately the same amount found for the 0.090 inch grid. A value for the increase at a higher Reynolds number is hard to estimate since it is not possible to tell where the transition from laminar to turbulent flow occurs.

The heat transfer data shown in Figure 20 do not indicate any transition of the boundary layer, and it appears that the points fall on a line of the turbulent heat transfer correlation equations extended to the lower Reynolds numbers. Investigation of the boundary layer profiles tends to support this idea. The boundary layer profile for the lowest Reynolds number in Figure 21 nearly matches the line for Hartree's solution for the plate without free stream turbulence. As the Reynolds numbers increase, the points fan out until poor agreement with the solution is apparent. The line on Figure 21 that deviates most from the Hartree solution is for a Reynolds number of 141,900. This same profile, when plotted on the universal turbulent boundary layer coordinates of Figure 22 agrees fairly well with the universal profile, and

Figure 20. Heat transfer results for low favorable pressure with 0.250-inch grid

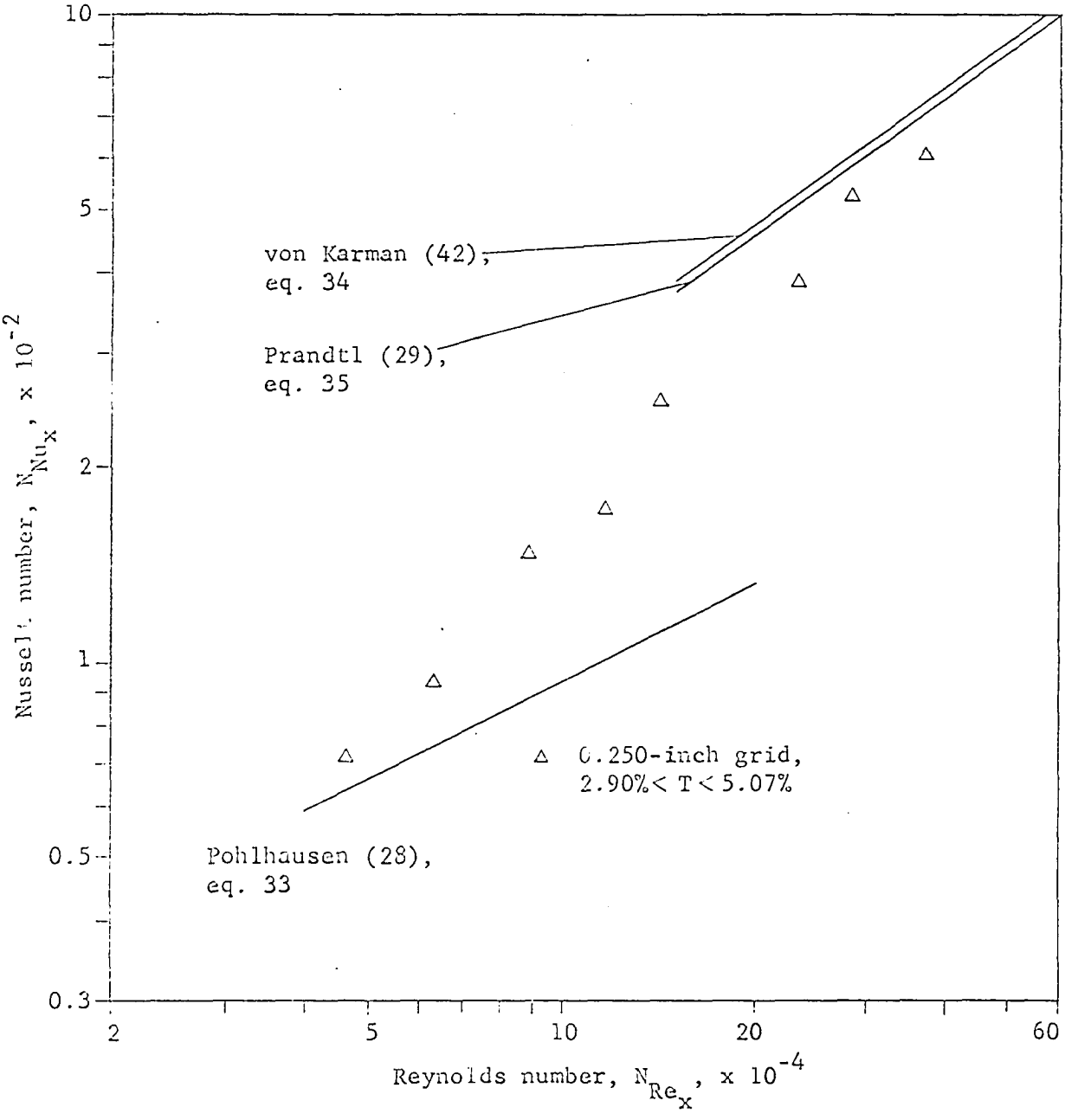
10
5
2
1
0.5
0.3
2
5
10
20
60
von Karman (42), eq. 34
Prandtl (29), eq. 35
Pohlhausen (28), eq. 33
0.250-inch grid, 2.90% < T < 5.07%
Nusselt number, N_{Nu_x}, x 10^{-2}
Reynolds number, N_{Re_x}, x 10^{-4}

Figure 21. Boundary layer profiles for low favorable pressure gradient with 0.250-inch grid

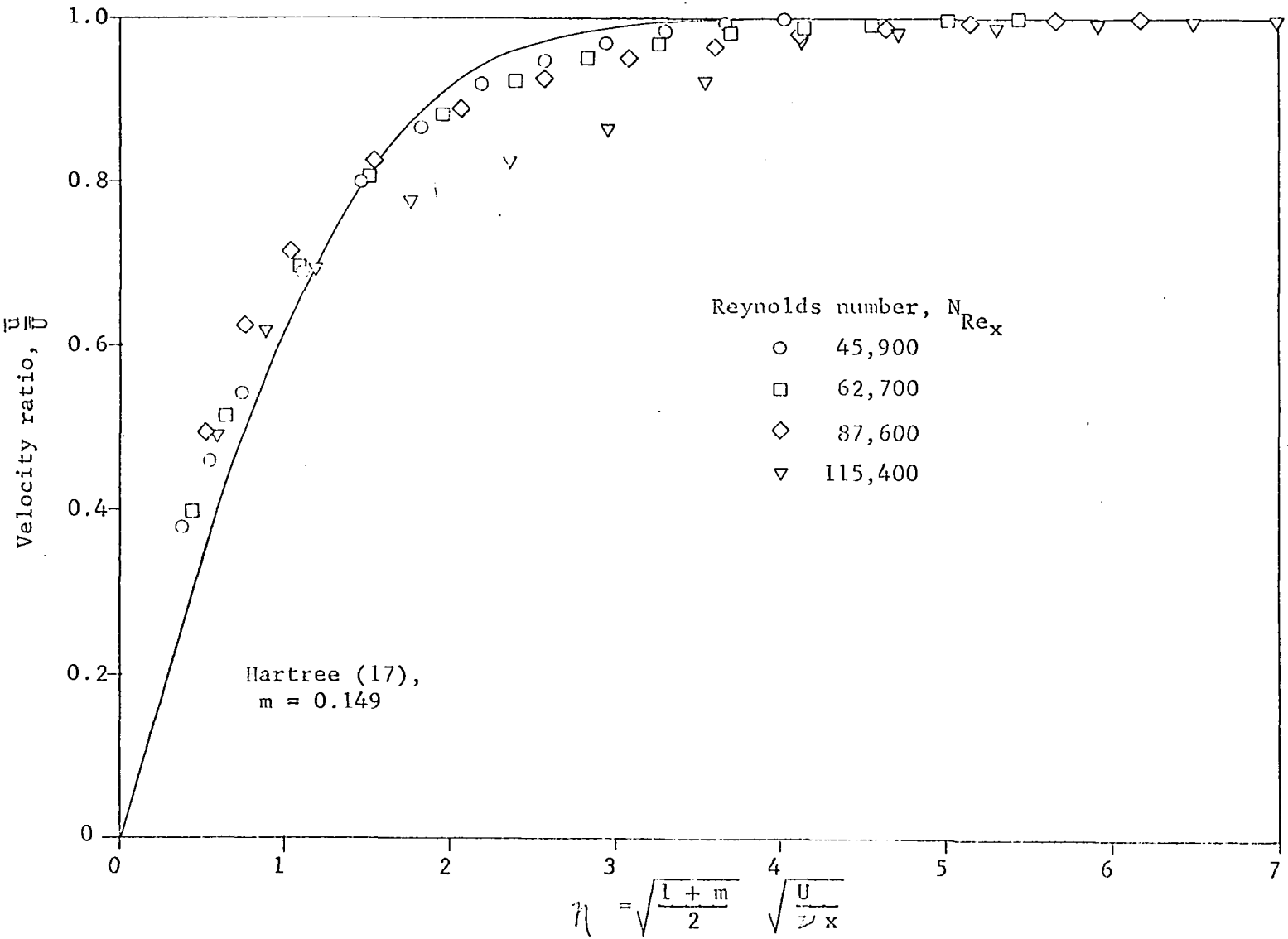
1.0
0.8
0.6
0.4
0.2
0
Velocity ratio, $\frac{\bar{u}}{\bar{U}}$
0
1
2
3
4
5
6
7
$\eta = \sqrt{\frac{l + m}{2}} \sqrt{\frac{U}{\nu x}}$
Reynolds number, N_{Re_x}
45,900
62,700
87,600
115,400
Hartree (17),
m = 0.149

Figure 22. Turbulent boundary layer profiles for low favorable pressure gradient with 0.250-inch grid

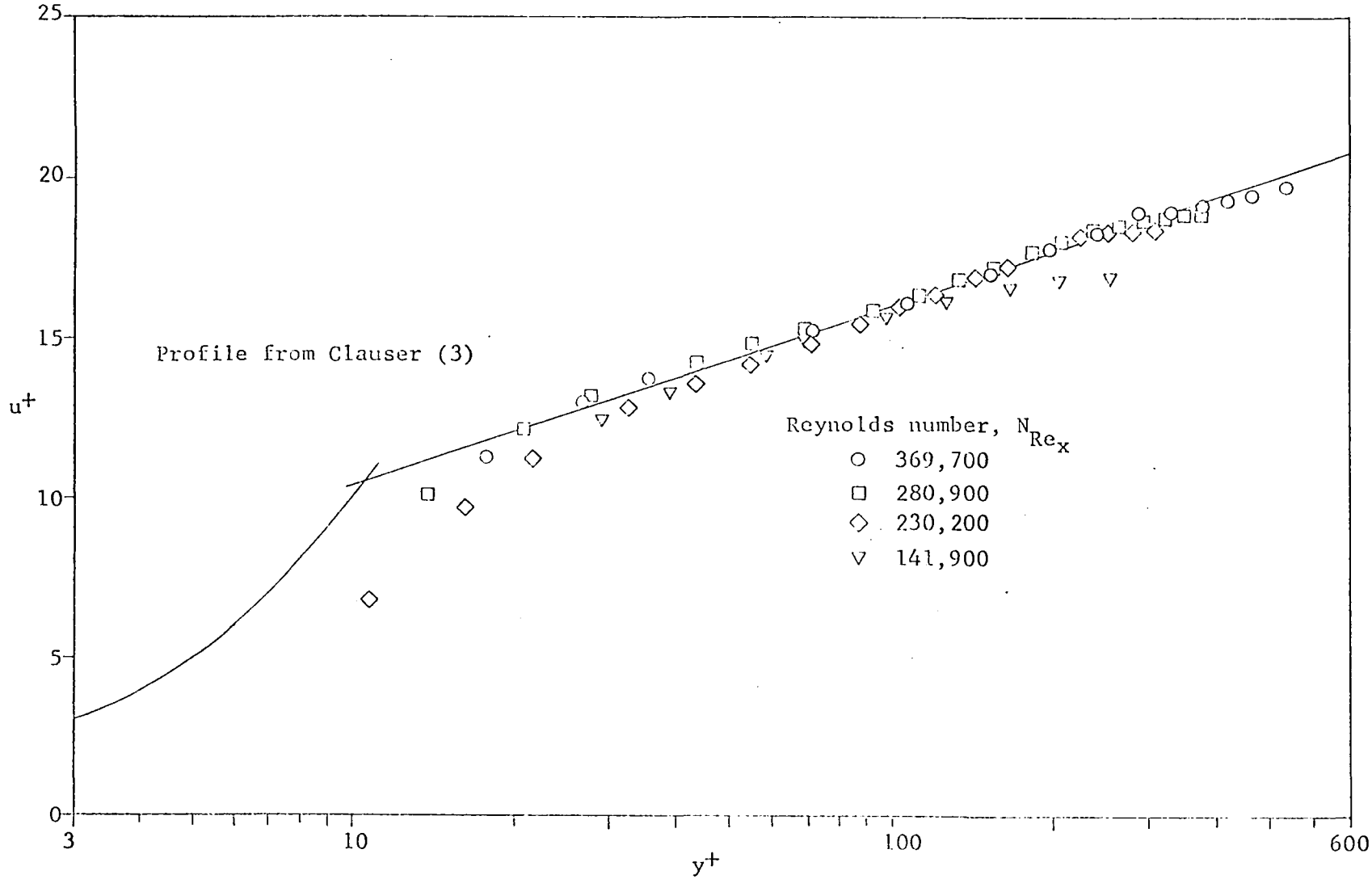
25
20
15
10
5
0
u+
3
10
100
600
y+
Profile from Clauser (3)
Reynolds number, N_{Re_x}
369,700
280,900
230,200
141,900

the points of profiles for higher Reynolds numbers agree even better. Thus the change from laminar to turbulent flow is not characterized by a distinct transition in this case, but in a gradual change which is apparently brought about by the increased free stream turbulence. The region of transition has thus been "stretched out" from a relatively small and easily identifiable location to one in which the "point" of transition is large and no longer discernable from the heat transfer data.

A comparison of the boundary layer profiles for the data taken at the low pressure gradient shows that the general profile shape has changed even more from the changes noted for the 0.090 inch grid. This change is evident from Figure 23 where the open points represent the intermediate free stream turbulence level of the 0.090 inch grid and the flagged points represent the turbulence level of the 0.250 inch grid. In general, the thickness of the boundary layers represented by the flagged points is greater than the thickness of those for the open points. It might then be hypothesized that the boundary layer is thickening with increasing free stream turbulence level, under the influence of a pressure gradient. It is recalled that the thickening of the boundary layer is a characteristic of transition from laminar to turbulent flow. Thus, one might expect that the heat transfer results for the higher free-stream turbulence intensities are justified in appearing as a continuation of the correlation for turbulent

Figure 23. Comparison of boundary layer profiles for low favorable pressure gradient with 0.090- and 0.250-inch grids

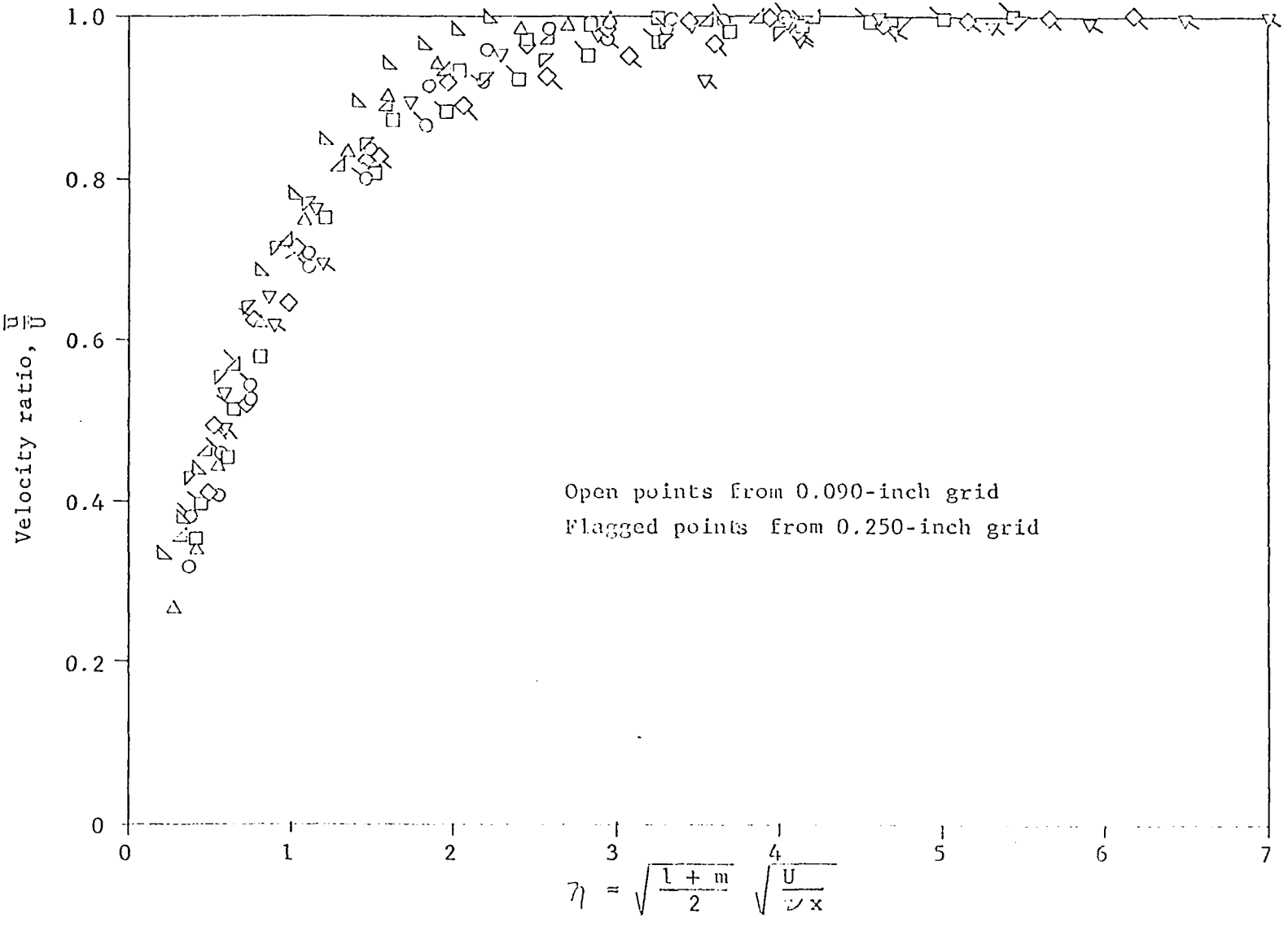
1.0
0.8
0.6
0.4
0.2
0
Velocity ratio, $\frac{\bar{u}}{\bar{U}}$
0
1
2
3
4
5
6
7
Open points from 0.090-inch grid
Flagged points from 0.250-inch grid
$\eta = \sqrt{\frac{l + m}{2}} \sqrt{\frac{U}{\nu x}}$

flow since the boundary layer is no longer purely laminar under these conditions.

High Favorable Pressure Gradient

The results of this section are for tests carried out with the highest of the pressure gradients used. The pressure distribution for this series is shown in Figure 24.

High favorable pressure gradient, no grid

The heat transfer data for an increased pressure gradient with no turbulence-producing grid shown in Figure 25 are similar to those obtained with the lower pressure gradient in that most of the points lie only slightly above the line for the Pohlhausen relation for a laminar boundary layer. In this case, however, the change of position of the false tunnel wall required an increased pressure drop through the test section, which in turn necessitated operation of the tunnel at pressure ratios for which the free stream turbulence intensity was somewhat higher than the range of turbulence intensities used with the lower pressure gradient. This operation resulted in a turbulence intensity range of from 0.74 to 0.92 per cent. The increased level of turbulence advanced the position of the boundary layer transition so that the data taken at higher Reynolds numbers entered the transition range. Thus, an increase in Nusselt number over the Pohlhausen relation is found at Reynolds numbers above 250,000 in Figure 25. The heat transfer data taken at a Reynolds number of 456,300

Figure 24. Static pressure distribution for high favorable pressure gradient

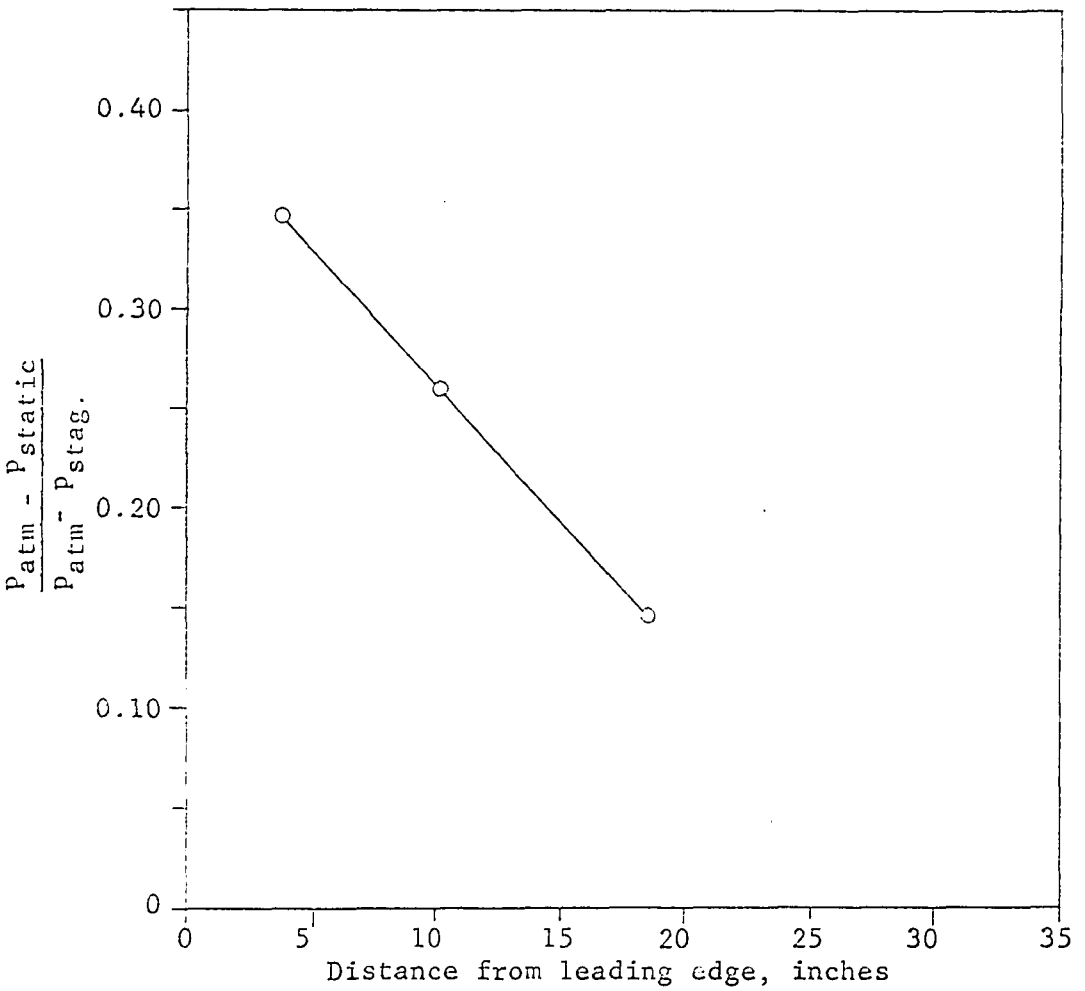
0.40
0.30
0.20
0.10
0
0
5
10
15
20
25
30
35
Distance from leading edge, inches
$\frac{p_{atm} - p_{static}}{p_{atm} - p_{stag.}}$

Figure 25. Heat transfer results for high favorable pressure gradient with no grid

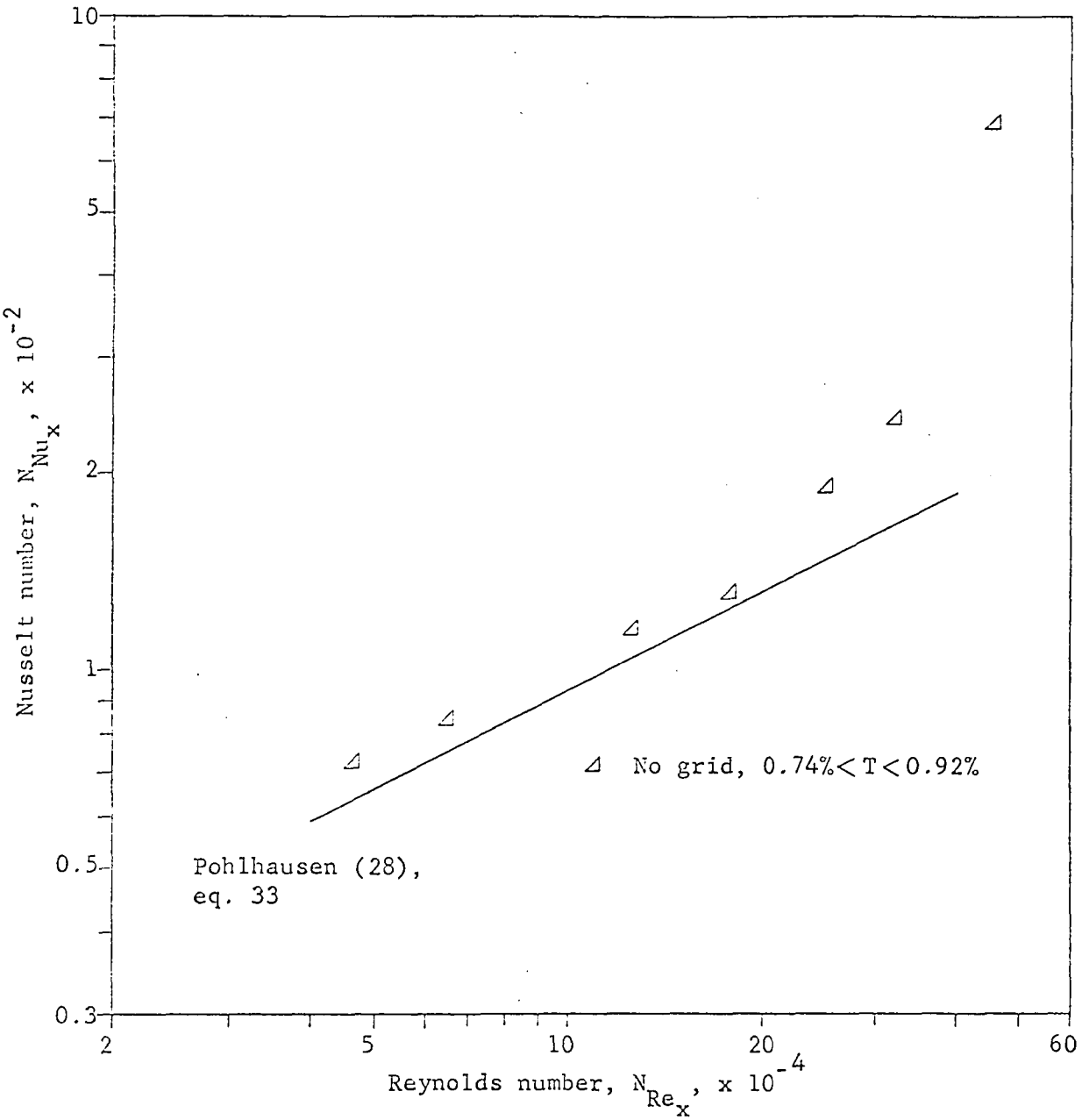
10
5
2
1
0.5
0.3
Nusselt number, N_{Nu_x}, x 10^{-2}
2
5
10
20
60
Reynolds number, N_{Re_x}, x 10^{-4}
No grid, 0.74%< T <0.92%
Pohlhausen (28),
eq. 33

appear to be in the turbulent range.

The value of the exponent m in the free stream was found to be 0.160, independent of the magnitude of the free stream velocity. The boundary layer profiles in Figure 26 are compared with the line representing Hartree's solution for this value of m. These profiles display the same similarity of profile shape found for the low pressure profiles taken without a grid for Reynolds numbers up to 322,000. One further profile was taken for the heat transfer point at a Reynolds number of 456,300. This profile was plotted on the universal turbulent boundary layer coordinates in Figure 27, where the agreement with the universal profile is only fair. It was concluded that this point was in the transition range.

High favorable pressure gradient, 0.090 inch grid

The heat transfer data for the higher pressure gradient with the 0.090 inch grid in place behaved similar to the data found for the corresponding turbulence level with the lower pressure gradient. The low Reynolds number points are from 15 to 35 per cent higher than the recommended equation, as shown in Figure 28. A transition from laminar to turbulent flow is found in the Reynolds number range from 200,000 to 250,000 as was found for the lower pressure gradient. The points in the turbulent Reynolds number range are in agreement with equations and the recommended equations of Prandtl and von Karman respectively.

Figure 26. Boundary layer profiles for high favorable pressure gradient with no grid

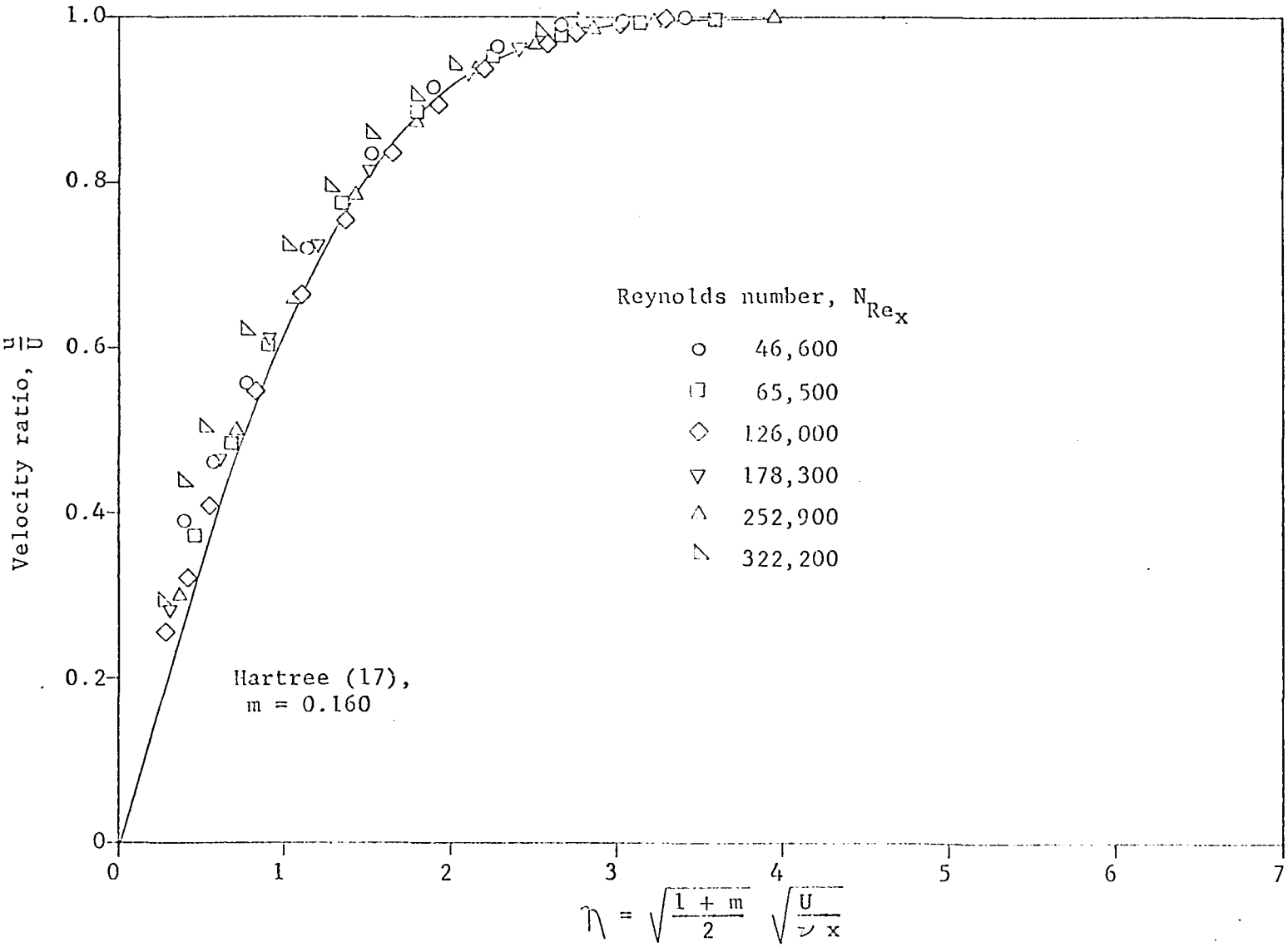
1.0
0.8
0.6
0.4
0.2
0
Velocity ratio, $\frac{u}{U}$
Reynolds number, N_{Re_x}
46,600
65,500
126,000
178,300
252,900
322,200
Hartree (17),
m = 0.160
0
1
2
3
4
5
6
7
$\eta = \sqrt{\frac{1+m}{2}} \sqrt{\frac{U}{\nu x}}$

Figure 27. Turbulent boundary layer profiles for high favorable pressure gradient with no grid

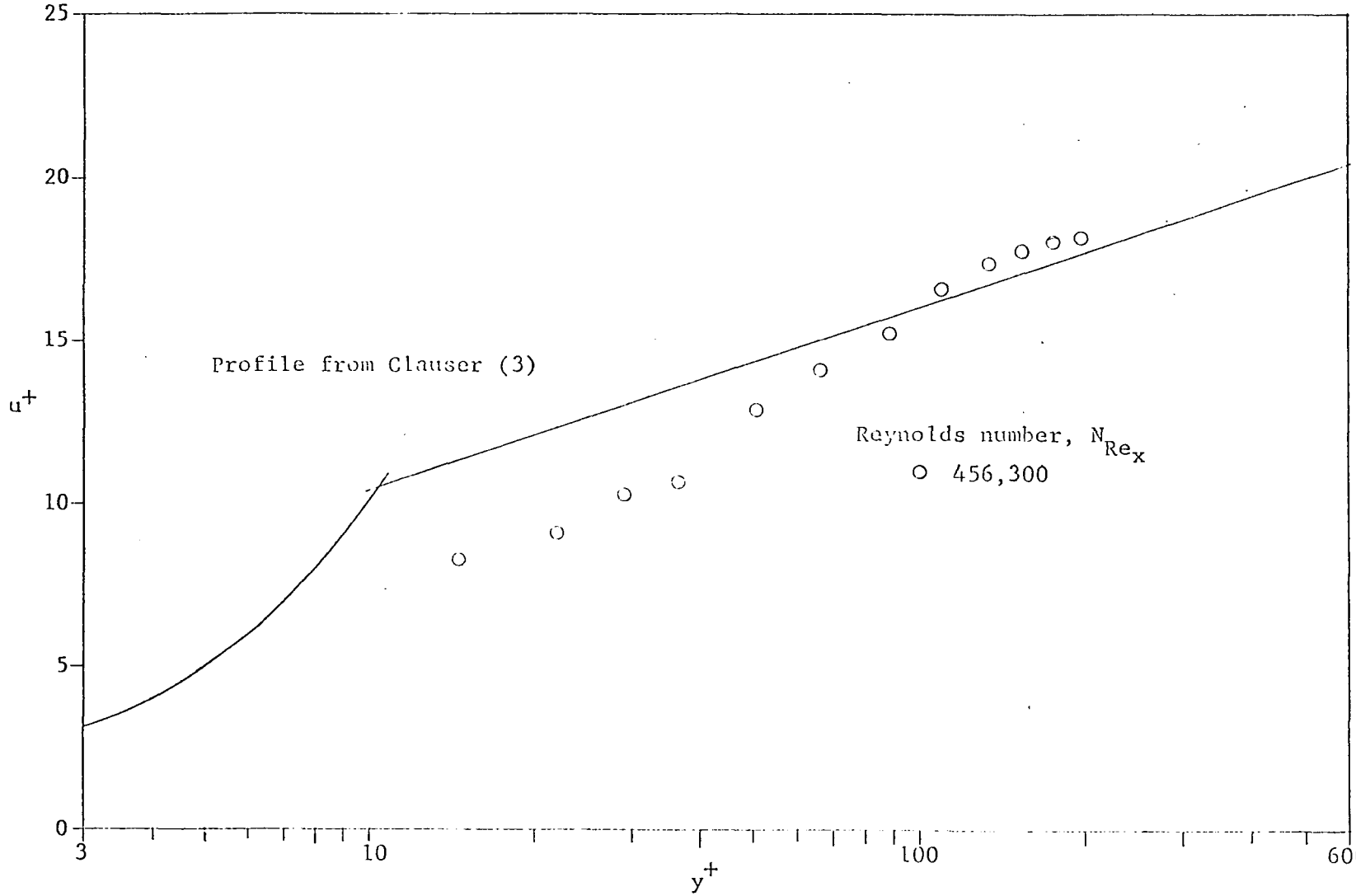
25
20
15
10
5
0
u^+
3
10
100
600
y^+
Profile from Clauser (3)
Reynolds number, N_{Re_x}
456,300

Figure 28. Heat transfer results for high favorable pressure gradient with 0.090-inch grid

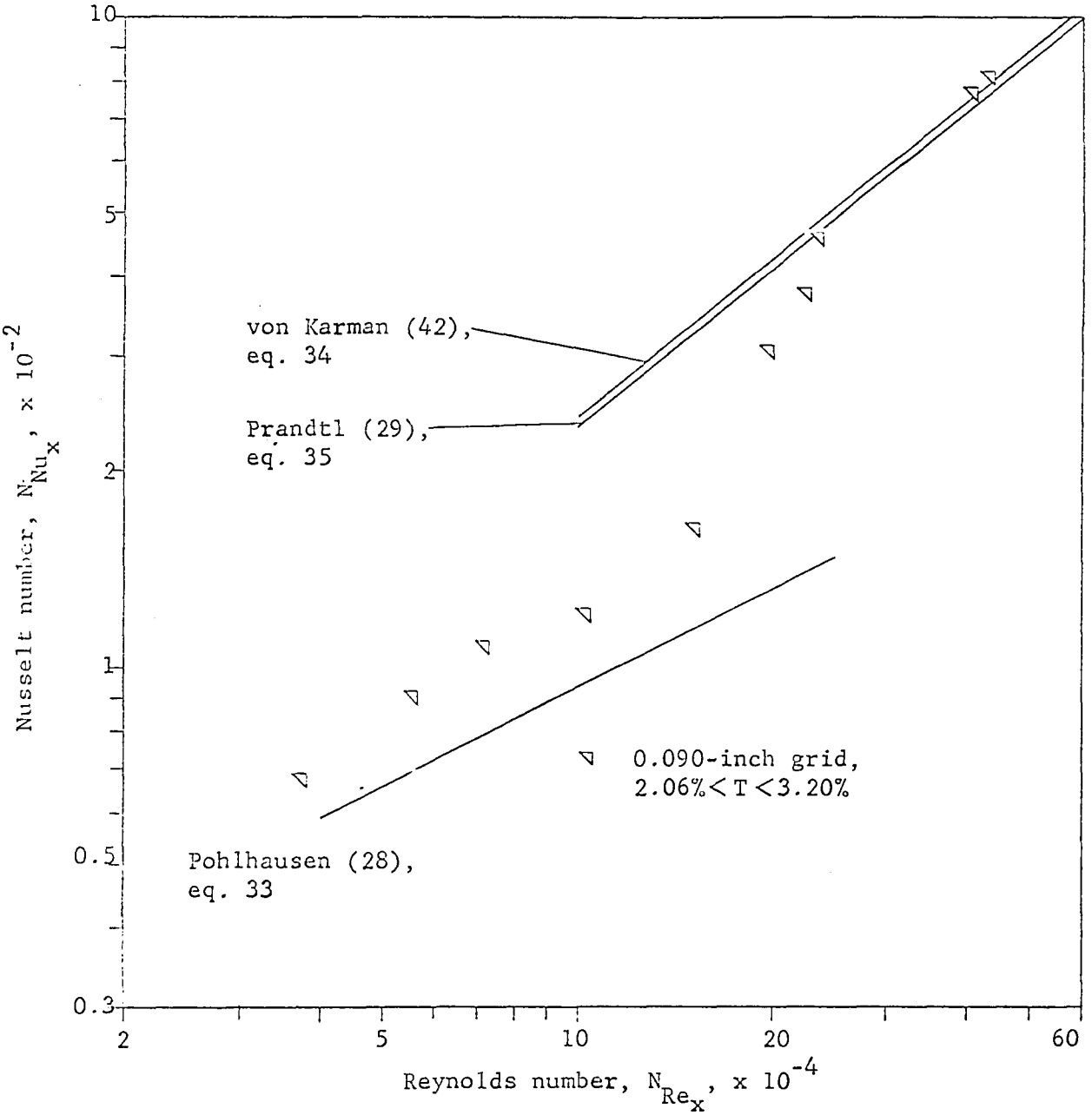
10
5
2
1
0.5
0.3
2
5
10
20
60
Nusselt number, N_{Nu_x}, x 10^{-2}
Reynolds number, N_{Re_x}, x 10^{-4}
von Karman (42), eq. 34
Prandtl (29), eq. 35
Pohlhausen (28), eq. 33
0.090-inch grid, 2.06% < T < 3.20%

The boundary layer profiles in Figures 29 and 30 with the heat transfer data show that the position of transition and the character of the boundary layer is much the same as predicted above from the heat transfer data and might be predicted from the behavior at the lower pressure gradient. The profiles tend toward non-similarity for the laminar range and differ from the Hartree solution, especially for the Reynolds numbers approaching the transition region. The profiles for the turbulent region agree with the universal profile.

The range of turbulence intensity for these data was from 2.06 to 3.20 per cent.

High favorable pressure gradient, 0.250 inch grid

An effect of increase of Nusselt number with free stream turbulence intensity is found in Figure 31 for the 0.250 inch grid which is similar to that found for the 0.090 inch grid. At the low Reynolds numbers, an increase of about 14 per cent was found, but estimation of further increases for the laminar boundary layer at higher Reynolds numbers was not possible due to the difficulty in establishing a Reynolds number region for transition. The data again appear to be an extension of the Prandtl and von Karman relations for turbulent flow.

The boundary layer profiles shown in Figure 32 exhibit tendencies similar to those found for the low pressure gradient. The profiles suggest that at a Reynolds number of about

Figure 29. Boundary layer profiles for high favorable pressure gradient with 0.090-inch grid

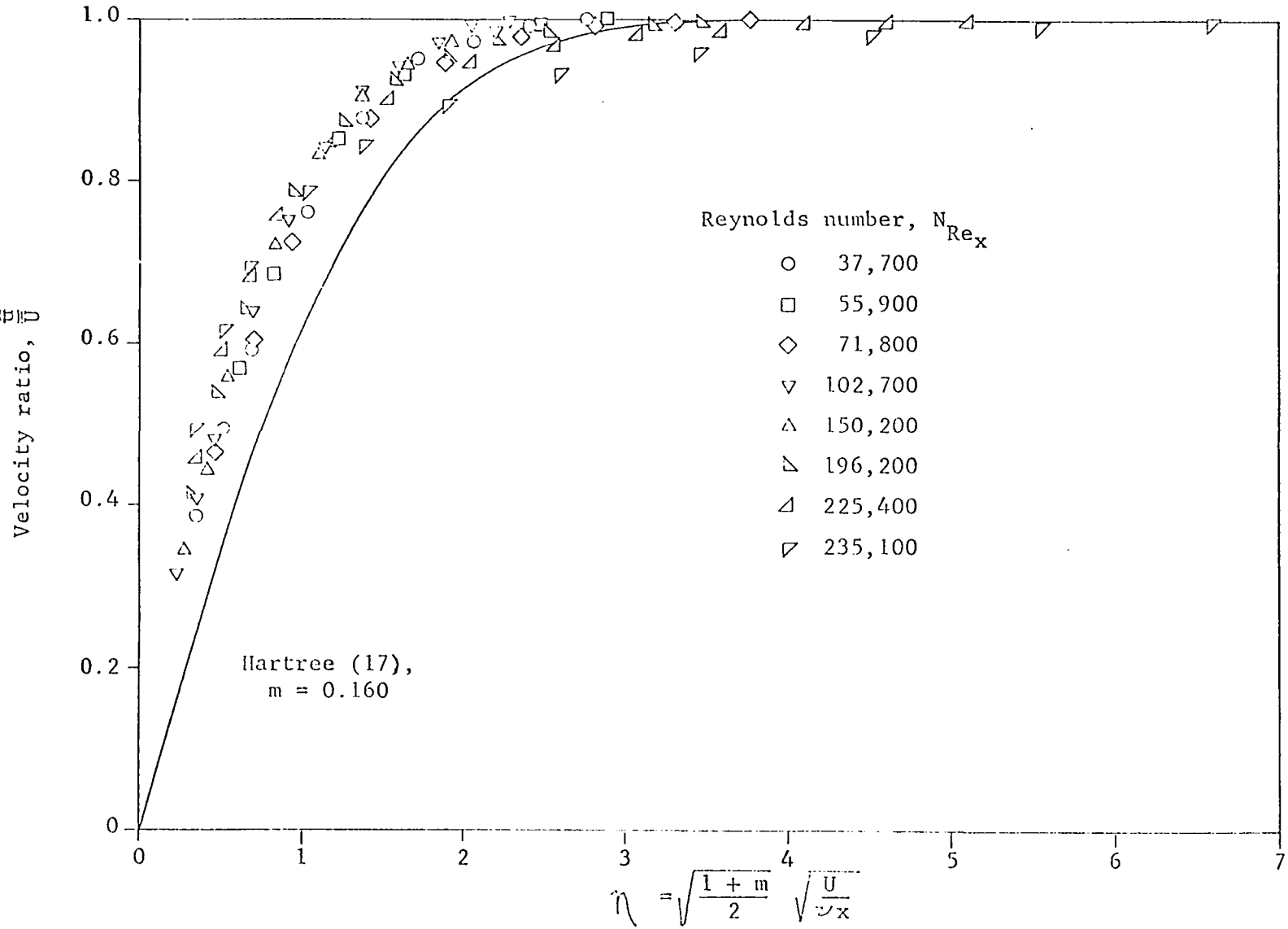
Velocity ratio, $\frac{u}{U}$
1.0
0.8
0.6
0.4
0.2
0
0
1
2
3
4
5
6
7
$\eta = \sqrt{\frac{1+m}{2}} \sqrt{\frac{U}{\nu x}}$
Reynolds number, N_{Re_x}
37,700
55,900
71,800
102,700
150,200
196,200
225,400
235,100
Hartree (17),
m = 0.160

Figure 30. Turbulent boundary layer profiles for high favorable pressure gradient with 0.090-inch grid

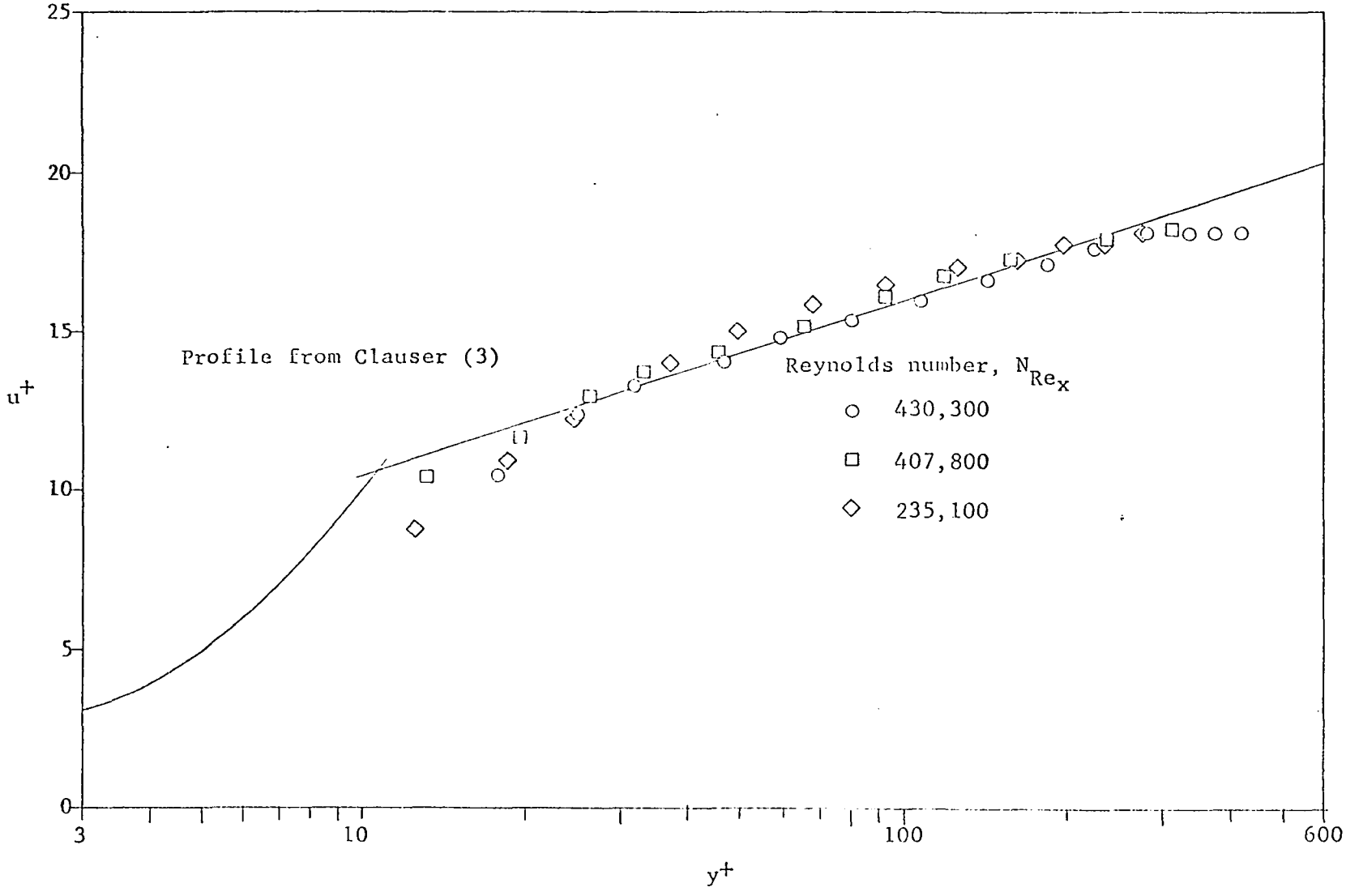
25
20
15
10
5
0
u+
3
10
100
600
y+
Profile from Clauser (3)
Reynolds number, N_{Re_x}
430,300
407,800
235,100

Figure 31. Heat transfer results for high favorable pressure gradient with 0.250-inch grid

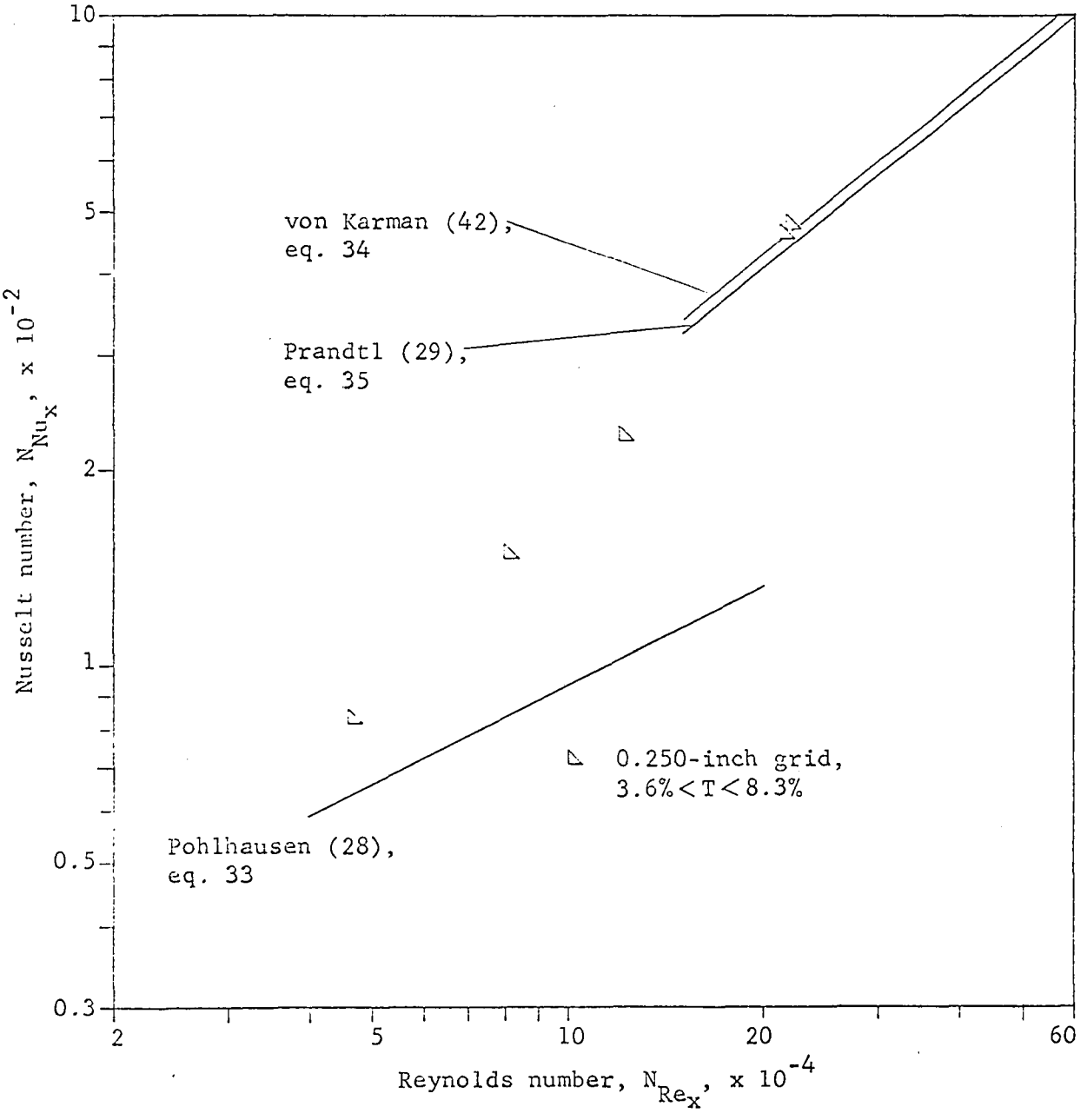
10
5
2
1
0.5
0.3
Nusselt number, N_{Nu_x}, x 10^{-2}
von Karman (42), eq. 34
Prandtl (29), eq. 35
Pohlhausen (28), eq. 33
0.250-inch grid, 3.6% < T < 8.3%
2
5
10
20
60
Reynolds number, N_{Re_x}, x 10^{-4}

Figure 32. Boundary layer profiles for high favorable pressure gradient with 0.250-inch grid

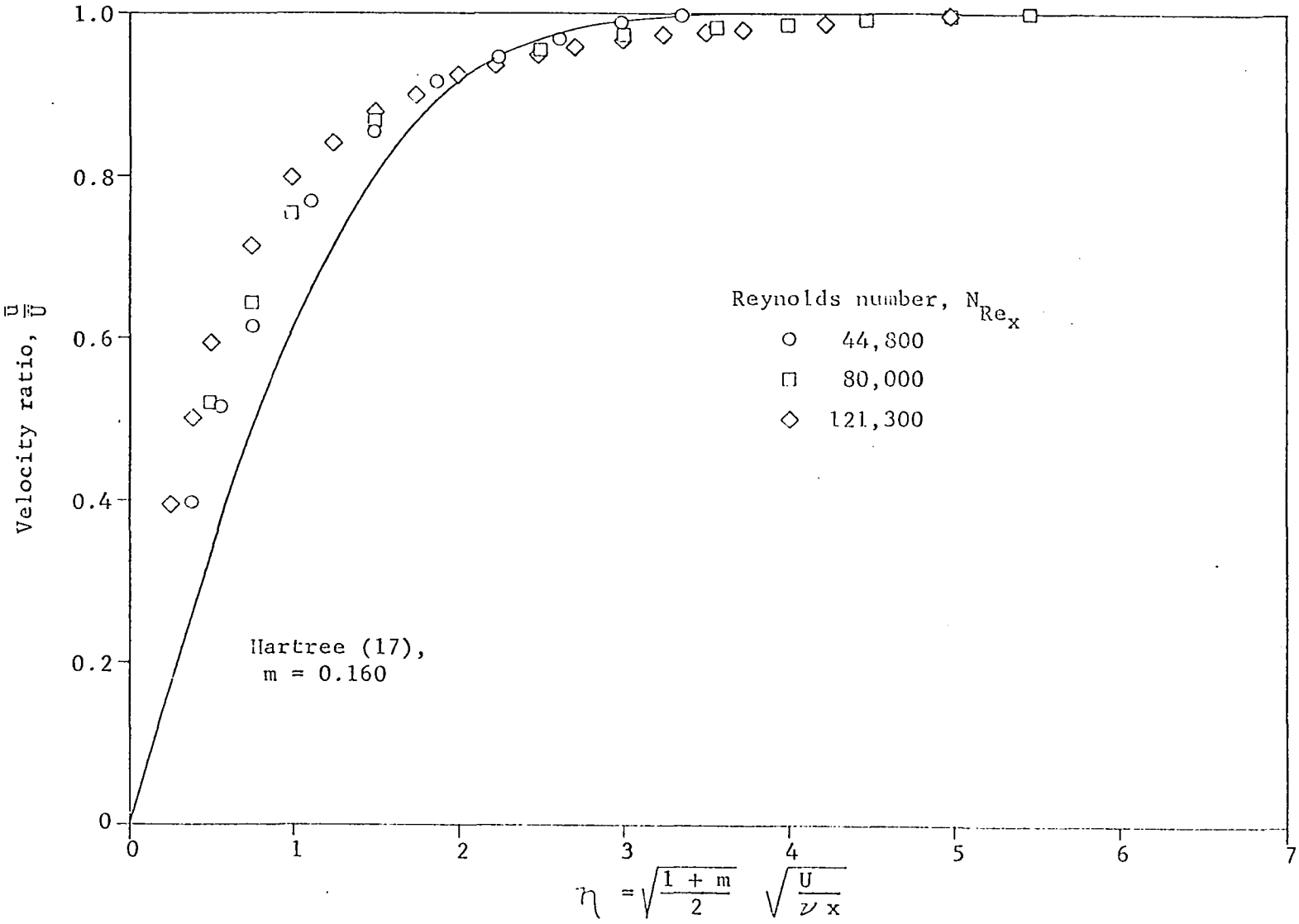
1.0
0.8
0.6
0.4
0.2
0
Velocity ratio, $\frac{\bar{u}}{\bar{U}}$
0
1
2
3
4
5
6
7
$\eta = \sqrt{\frac{1+m}{2}} \sqrt{\frac{U}{\nu x}}$
Reynolds number, N_{Re_x}
44,800
80,000
121,300
Hartree (17),
m = 0.160

121,300 the transition region is reached, but that the region is much larger than was found for lower free stream turbulence levels, and not so easily defined. The turbulent boundary layers in Figure 33 agree with the universal profile as has been the case for all turbulent profiles included in the work.

The changes of profile shape and lack of similarity are again evident in the curves. A comparison of these changes is made in Figure 34 where the flagged points represent the turbulence level generated by the 0.250 inch grid. The free stream turbulence levels found for the data presented here are from 3.64 to 8.20 per cent.

Discussion of the Results and Conclusions

The papers of Wang (43) and Edwards and Furber (9) and the results of this investigation agree on the effect of free stream turbulence intensity on the heat transfer from a flat plate with zero pressure gradient. In all of these researches, only a change of the position of transition from laminar to turbulent flow in the boundary layer takes place when the free stream turbulence intensity is increased.

The data obtained in this work do not agree with the results of Sugawara, *et al.* (37). The reasons for the disagreement are not fully apparent. Perhaps some difference between the data of Sugawara, *et al.* and that of this paper is due to the non-time-steady method of energy transfer measurement used in the former. If so, further investigation of

Figure 33. Turbulent boundary layer profiles for high favorable pressure gradient with 0.250-inch grid

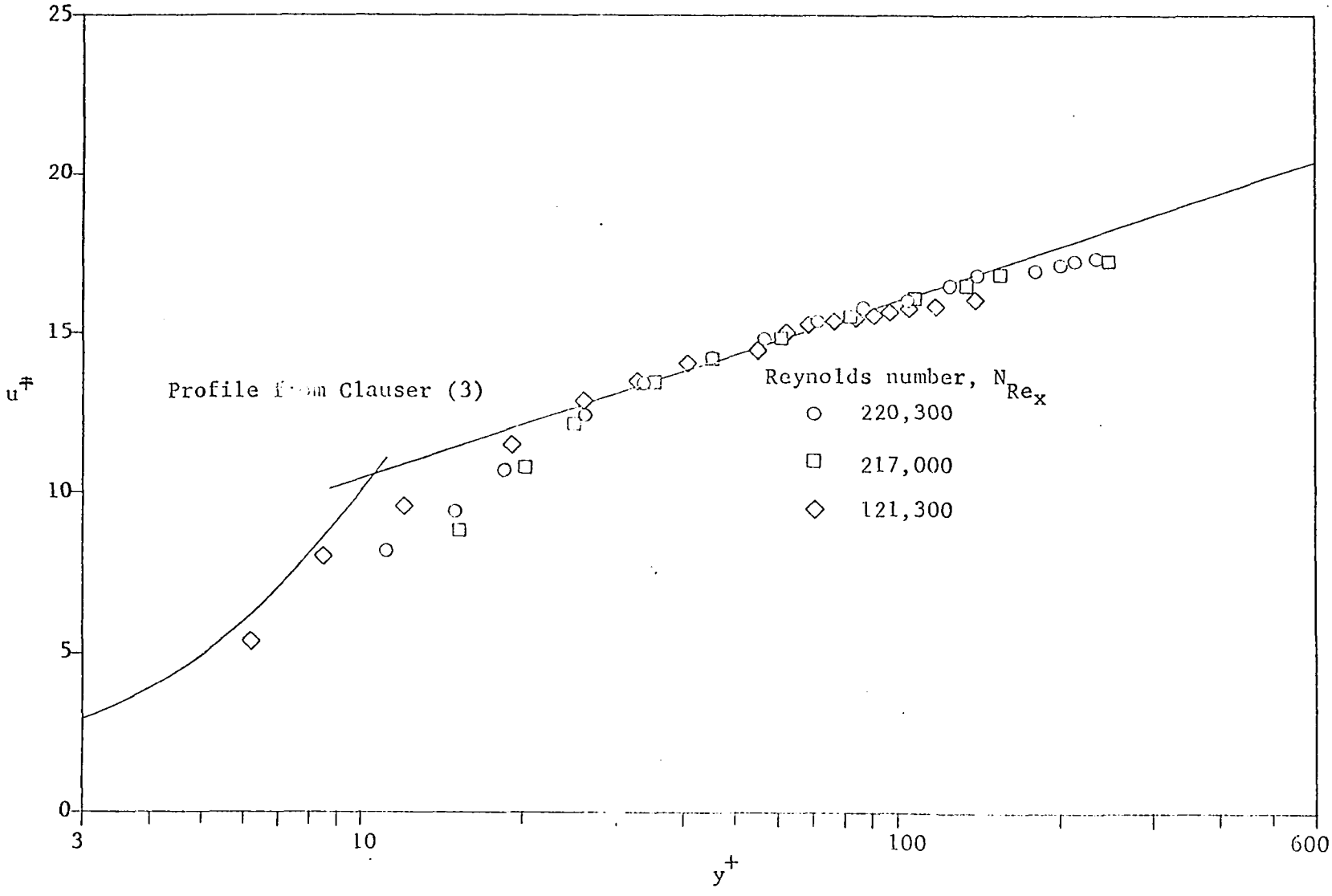
25
20
15
10
5
0
3
10
100
600
u^+
y^+
Profile from Clauser (3)
Reynolds number, N_{Re_x}
220,300
217,000
121,300

Figure 34. Comparison of boundary layer profiles for high favorable pressure gradient with 0.090- and 0.250-inch grids

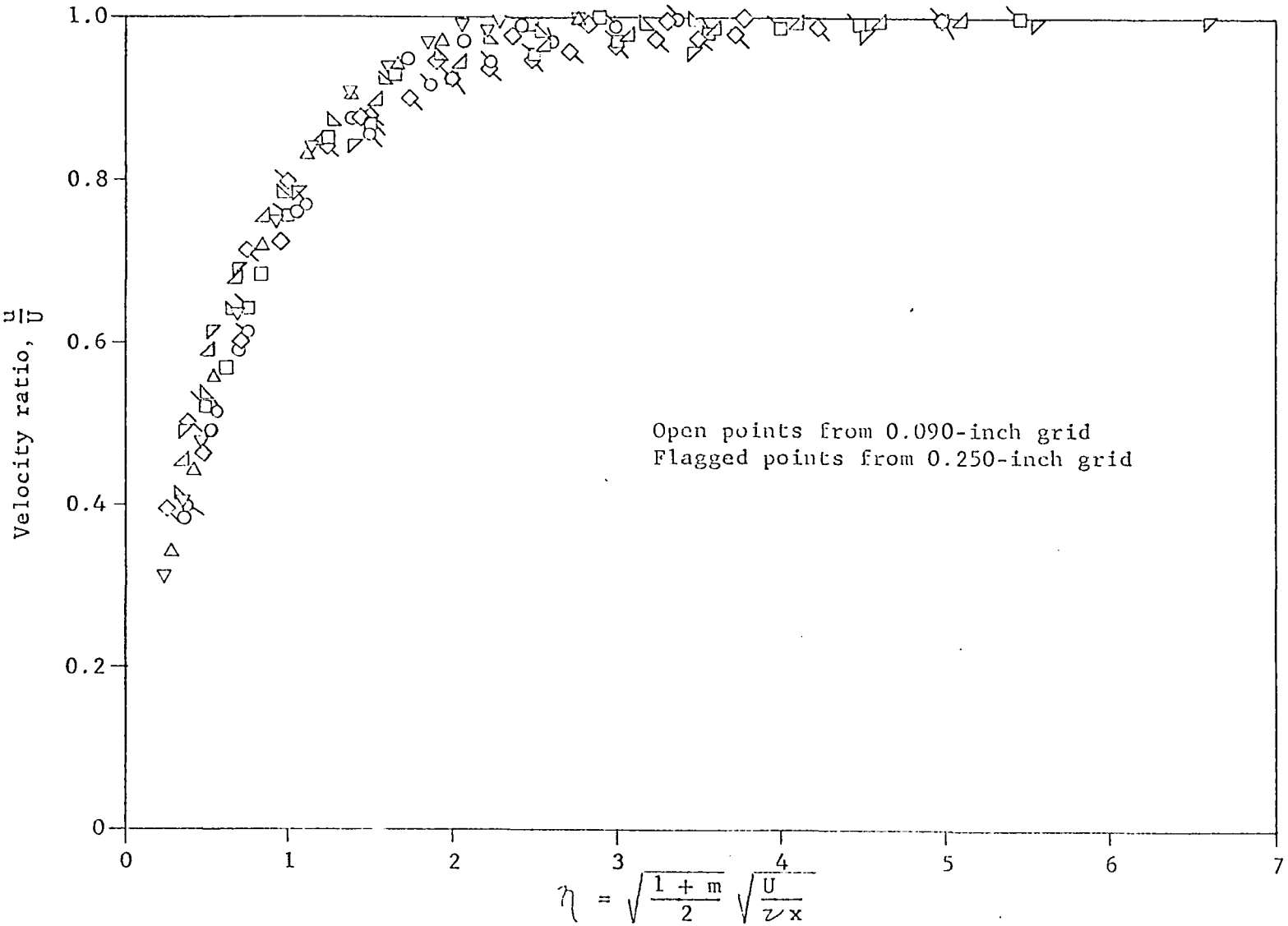
1.0
0.8
0.6
0.4
0.2
0
Velocity ratio, $\frac{u}{U}$
0
1
2
3
4
5
6
7
$\eta = \sqrt{\frac{1+m}{2}} \sqrt{\frac{U}{\nu x}}$
Open points from 0.090-inch grid
Flagged points from 0.250-inch grid

non-time-steady cooling on the laminar boundary layer is in order.

The data of Feiler and Yeager (12) were taken with a minimum free stream turbulence intensity which was much larger than the maximum turbulence intensity used in the zero pressure gradient portion of this work. In addition, the static pressure distribution along the plate surface is not given. For these reasons, no direct comparison can be made. It is interesting to note, however, that the slopes of the relations presented by Feiler and Yeager are different for heat transfer without a sound field present and for heat transfer with a sound field. Surprisingly, the slopes for data taken with a sound field are nearly the same as those found in this work, while the slopes of data taken without a sound field do not correspond with other results found in the literature.

Comparison of the present data with that taken on a flat plate with a pressure gradient by Wang (43) is also appropriate. Wang's points are plotted in Figure 35 along with lines representing data from this investigation. The pressure gradient used in Wang's work was not the same as either of those used in this work, based on a comparison of the data of this work with curves given by Wang. It is also probable that the pressure gradient used by Wang was one for which the expression for the free-stream velocity as a function of the distance from the leading edge was different than the function used here. Nevertheless, Figure 35 shows that Wang's data

Figure 35. Comparison of present data with that of Wang (43)

Numbers next to points represent per cent turbulence intensity found by Wang. Lines represent trends of data from both pressure gradients for this work.

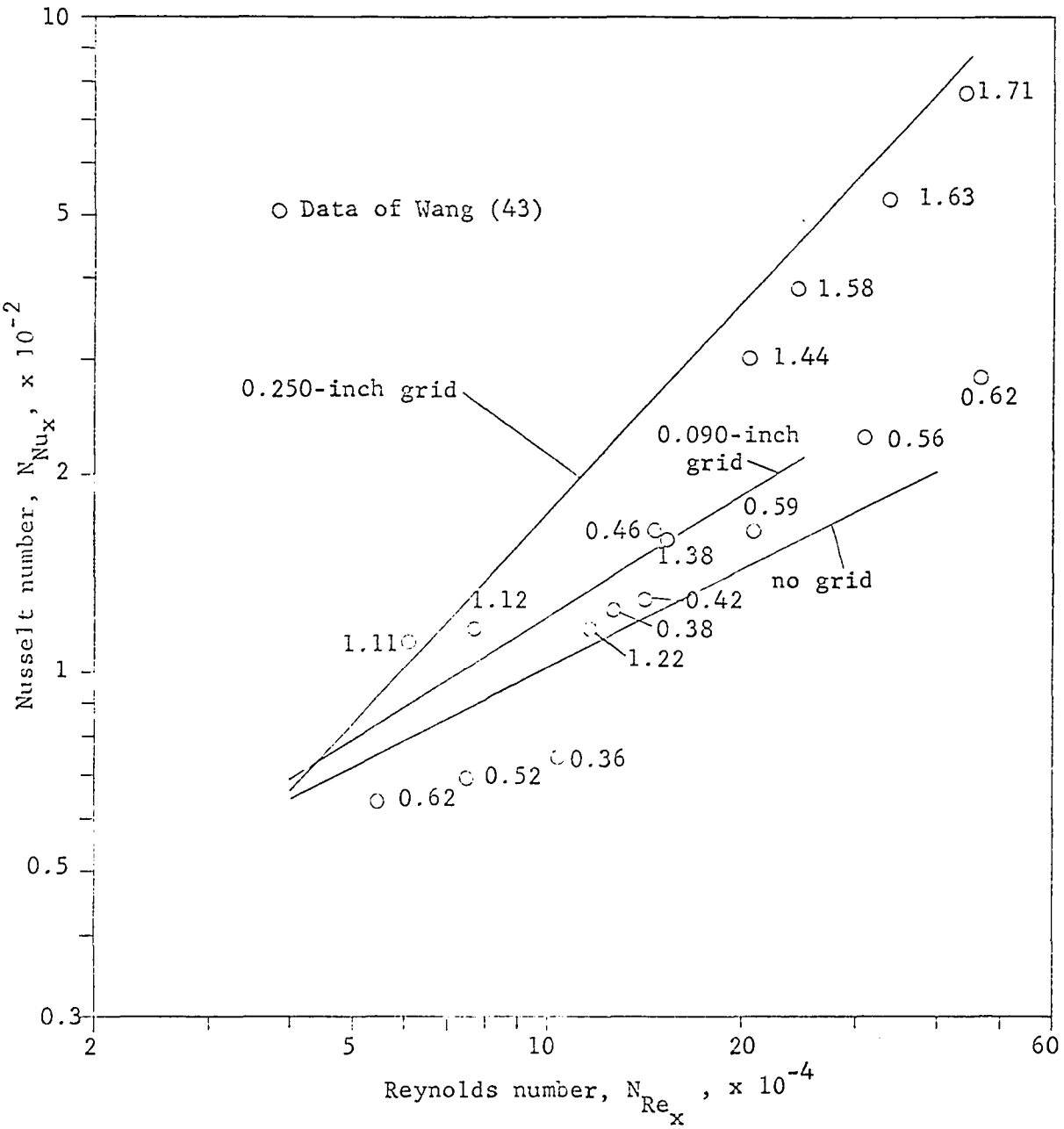
Data of Wang (43)
0.250-inch grid
0.090-inch grid
no grid
1.71
1.63
1.58
1.44
0.62
0.56
0.59
0.46
1.38
0.42
0.38
1.22
1.12
1.11
0.36
0.52
0.62
Nusselt number, N_{Nu_x}, x 10^{-2}
Reynolds number, N_{Re_x}, x 10^{-4}
10
5
2
1
0.5
0.3
2
5
10
20
60

generally follow the trends of the data from this work.

Wang used turbulence intensities in the ranges of 0.38 to 0.62 per cent and 1.12 to 1.71 per cent. In the higher turbulence range, for Reynolds numbers greater than 150,000, the points agree well in slope, but Wang's Nusselt numbers are about 20 per cent lower than the line representing this work. The points for Reynolds numbers below 150,000 are scattered, and do not agree.

Similarly, the points above a Reynolds number of 125,000 in the lower turbulence intensity range generally agree in slope, but have Nusselt numbers from 10 to 30 per cent lower. The points below a Reynolds number of 125,000 follow a line of lower slope than other points in this turbulence intensity range.

The above discussion shows that the work of Wang and the present data agree at least qualitatively. The greatest differences are in the magnitude of the Nusselt number increase.

One further comparison with published data can be made. A proposed theory on the transition of the laminar boundary layer in the presence of a pressure gradient has been published by van Driest and Blumer (41). From this theory, an equation can be derived which relates the free stream turbulence intensity, the Pohlhausen pressure gradient parameter $\bar{\Lambda}$, the Reynolds number based on the local boundary layer thickness and the local free stream velocity. Thus, for a flat

plate,

$$3.36(N_{Re_\delta})^2(T^2) + (1 - 0.0485\bar{\Lambda})N_{Re_\delta} - 9860 = 0 \qquad (40)$$

where Re_δ is the Reynolds number, $\bar{\Lambda}$ is the Pohlhausen parameter

$$\bar{\Lambda} = \frac{\delta^2}{\mu U}\frac{dp}{dx} \qquad (41)$$

and T is the free stream turbulence intensity. The equation is plotted in Figures 36 and 37 for the high and low pressure gradients respectively. The areas to the left and below the lines represent stable or laminar-flow conditions, while the areas above and to the right of the lines represent unstable or turbulent conditions. The two values of $\bar{\Lambda}$ shown bracket the range of experimental values of $\bar{\Lambda}$ found for all data in this work. It is interesting that the magnitude of $\bar{\Lambda}$ has little effect on the transition boundary layer Reynolds number except at very low turbulence intensities. The experimental points near the line representing transitional boundary layer Reynolds numbers shown on Figures 36 and 37 are labelled with their respective Reynolds numbers based on distance from the leading edge of the plate.

Both figures show no approach to the line representing the transition Reynolds number except for the point at a Reynolds number of 456,300 based on distance from the leading

Figure 36. Low pressure gradient data compared with the boundary-layer transition criterion of van Driest and Blumer (41)

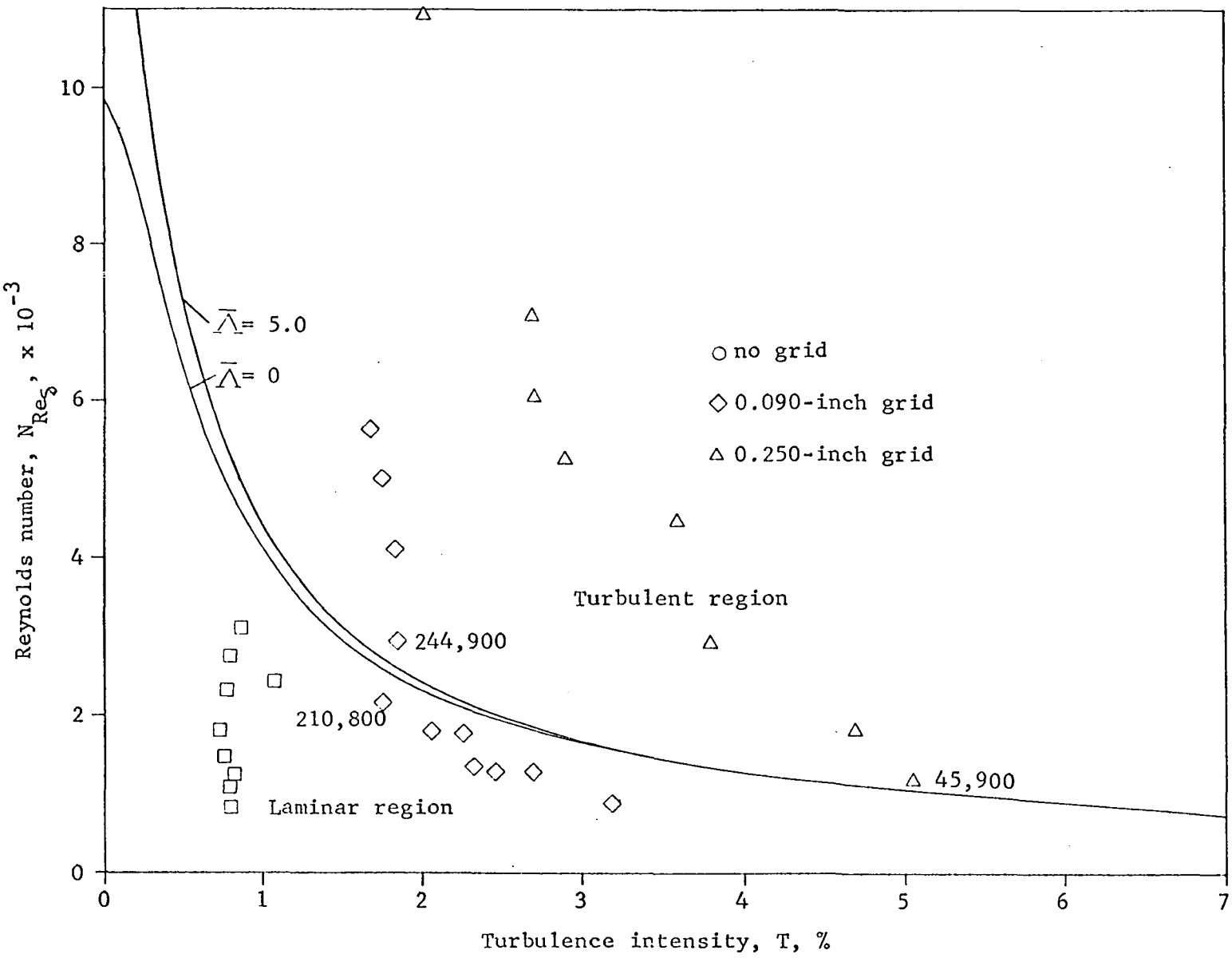
Reynolds number, N_{Re_δ}, x 10^{-3}
Turbulence intensity, T, %
$\bar{\Lambda}$= 5.0
$\bar{\Lambda}$= 0
○ no grid
◇ 0.090-inch grid
△ 0.250-inch grid
Turbulent region
Laminar region
244,900
210,800
45,900
0
1
2
3
4
5
6
7
0
2
4
6
8
10

Figure 37. High pressure gradient data compared with the boundary-layer transition of van Driest and Blumer (41)

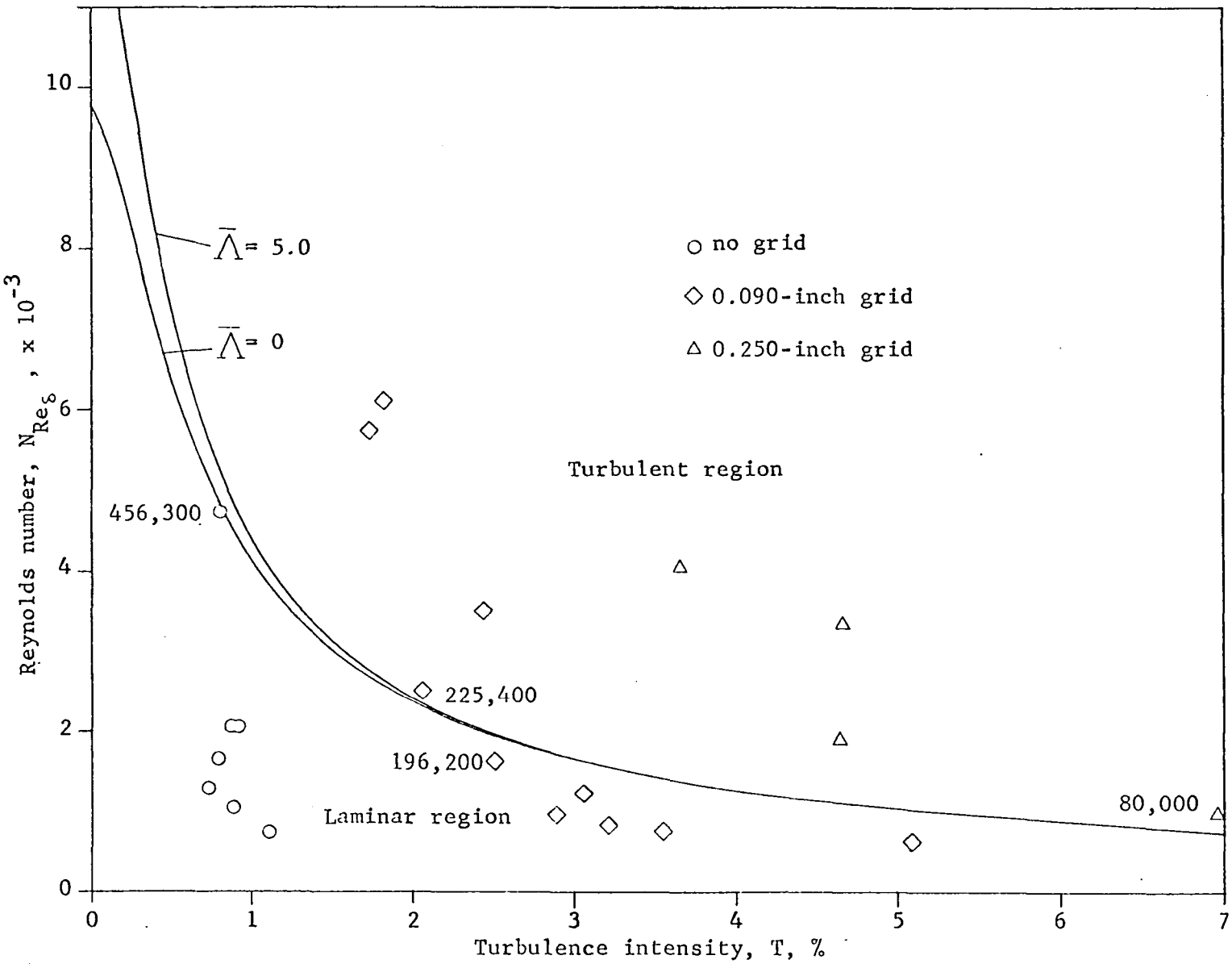
Reynolds number, N_{Re_ξ}, x 10^{-3}
Turbulence intensity, T, %
$\bar{\Lambda}$ = 5.0
$\bar{\Lambda}$ = 0
○ no grid
◇ 0.090-inch grid
△ 0.250-inch grid
Turbulent region
Laminar region
456,300
225,400
196,200
80,000
0
1
2
3
4
5
6
7
0
2
4
6
8
10

edge for the high pressure gradient with no grid. This point is on the line representing transition, and, comparing with the boundary layer profiles for that series of data, appears as the first turbulent point at the end of the transition.

The intermediate turbulence levels for both pressure gradients agree with the van Driest and Blumer equation also, with transition Reynolds numbers based on distance from the leading edge bracketing the line in both cases. Again, these correspond to the transition Reynolds numbers found from the boundary layer profile analysis.

The high turbulence level data in both cases have points which approach the recommended line from the turbulent side, thus indicating that the points were above the transition Reynolds number based on boundary layer thickness. This suggests that these points were at least in transition, if not turbulent. The heat transfer data for these points fall along the lines recommended for turbulent boundary layers and thus these results are to be expected according to van Driest and Blumer.

The transition criterion used above has an interesting further point that should be considered. In deriving their equation, van Driest and Blumer used an analysis which assumed that the scale of turbulence in the free stream was of the same order of magnitude as the boundary layer thickness. To check their theory against the present data, an estimation of the scale of turbulence used in this work is necessary. Since

no measurements of scale were made due to lack of equipment, the approximate eddy size may be estimated from the work of Dryden et al. (6) where data on the scale of turbulence downstream of grids is published. For all tests performed, the scale of turbulence varies from 0.125 inches up to 0.288 inches. Since these eddy sizes are easily of the order of magnitude of the boundary layer thicknesses involved, the comparison with van Driest and Blumer's theory is valid.

The previous analysis of the experimental results leads to several conclusions:

1. The new data presented in this thesis support the proponents of the theory that there is no effect of the free-stream turbulence intensity on heat transfer through a laminar boundary layer with zero pressure gradient. There is nothing in the present results that suggests changes other than moving the position of transition of the boundary layer for a change in free-stream turbulence intensity.

2. This work provides evidence that when a pressure gradient is imposed on the laminar boundary layer, and the free-stream turbulence intensity is raised, an increase in the Nusselt number will result, assuming the Reynolds number of the flow remains unchanged. Whether the boundary layer remains truly laminar during this process is shown to be doubtful. The boundary layer profiles indicate a change in shape due to the increase in free-stream turbulence, and they also show a loss of the similarity that existed prior to the

increase of turbulence intensity. The review of the turbulent boundary layer by Clauser (3) points out a similar process undergone by a laminar boundary layer in transition. Because the boundary layer equations for flow with a pressure gradient, including the fluctuating components of the velocity, have terms that resemble the Reynolds stresses of turbulent flow, it is reasonable to conclude that the flow is quasi-laminar, or in transition.

3. The data obtained in this study in the turbulent boundary layer range do not exhibit an increase in Nusselt number for any of the conditions tested. Although the range of testing in this region was limited, it appears that no increase is to be expected. This point of view is in concurrence with the general ideas of the wall layers of turbulent flow. Again referring to Clauser (3), it is found that the turbulent boundary layer shows little change in the velocity profile of the laminar sublayer and the inner wall layer with the imposition of a pressure gradient along the plate surface. Since the velocity distribution in this region is all-important in changing the temperature distribution, little change in the latter could be expected.

4. The velocity profiles for the boundary layers offer substantial support for the transition theory of van Driest and Blumer (39). Although they have compared their theory against the data of others taken on a body of revolution, the data of this work offer the first direct comparison for the

flat plate. In order to fully substantiate the theory of van Driest and Blumer, more work is needed in the very low turbulence area.

The conclusions stated above suggest further analytical and experimental investigations that may be based on the findings of this work. Some possible projects are:

1. An analytical and/or experimental study of the interaction of free-stream turbulence and a favorable pressure gradient to determine how the shape of the boundary layer profile changes with changes in free-stream turbulence and pressure gradient.

2. An analysis of heat transfer in a pressure gradient that includes the effect of scale or eddy size on the heat transfer coefficient from a flat plate.

3. An experimental investigation along the lines of paragraph 2, but including measurements of the Reynolds stresses in the boundary layer as the pressure gradient and the free-stream turbulence intensity are varied. These could then be compared with Reynolds stress terms found in the equations discussed in the analysis section of this thesis.

REFERENCES CITED

1. Baines, W. D. and Peterson, E. G. An investigation of flow through screens. American Society of Mechanical Engineers Transactions. 73: 467-480. 1951.

2. Clauser, F. H. Turbulent boundary layers in adverse pressure gradients. Journal of the Aeronautical Sciences. 21: 91-108. 1954.

3. Clauser, F. H. The turbulent boundary layer. In Dryden, H. L., Kuerti, G. and von Karman, T., eds. Advances in Applied Mechanics. 4: 1-51. New York, N. Y. Academic Press, Inc. 1956.

4. Drake, R. M. Investigation of point unit heat-transfer coefficients for laminar flow over an inclined flat plate. American Society of Mechanical Engineers Journal of Applied Mechanics Transactions. 16: 1-8. 1949.

5. Dryden, H. L. A review of the statistical theory of turbulence. Quarterly of Applied Mathematics. 1: 7-42. 1943.

6. Dryden, H. L., Schubauer, G. B., Mock, W. C. and Skramstad, H. K. Measurements of intensity and scale of wind-tunnel turbulence and their relation to the critical Reynolds numbers of spheres. U. S. National Advisory Committee for Aeronautics. Technical Report 581. 1937.

7. Eckert, E. R. G. Introduction to the transfer of heat and mass. New York, N. Y. McGraw-Hill Book Co., Inc. 1950.

8. Eckert, E. R. G. and Drake, R. M. Heat and mass transfer. New York, N. Y. McGraw-Hill Book Co., Inc. 1959.

9. Edwards, A. and Furber, B. N. The influence of free-stream turbulence on heat transfer by convection from an isolated region of a plane surface in parallel air flow. Institution of Mechanical Engineers Proceedings. 170: 941-954. 1956.

10. Fage, A. and Falkner, V. M. Relation between heat transfer and surface friction for laminar flow. Great Britain Aeronautical Research Council. Reports and Memorandum 1408. 1931.

11. Falkner, V. M. and Skan, S. W. Solutions of the boundary-layer equations. London, Edinburgh and Dublin Philosophical Magazine. Series 7. 12: 865-896. 1931.

12. Feiler, C. E. and Yeager, E. B. Effect of large-amplitude oscillations on heat transfer. U. S. National Aeronautics and Space Administration. Technical Report R-142. 1962.

13. Freiling, J., Eckert, R. E. and Westwater, J. W. Thermal conductivity of anisotropic materials. Industrial and Engineering Chemistry. 44: 906-910. 1952.

14. Gazley, C. Boundary layer stability and transition in subsonic and supersonic flow. Journal of the Aeronautical Sciences. 20: 19-28. 1953.

15. Giedt, W. H. Effect of turbulence level of incident air stream on local heat transfer and skin friction on a cylinder. Journal of the Aeronautical Sciences. 18: 725-730, 766. 1951.

16. Handbook of supersonic aerodynamics. Vol. 5. Sec. 15. Washington, D. C. U. S. Navy, Bureau of Ordnance. 1953.

17. Hartree, D. R. On an equation occurring in Falkner and Skan's approximate treatment of the equations of the boundary layer. Cambridge Philosophical Society Proceedings. 33, Part 2: 223-239. 1937.

18. Kestin, J. and Maeder, P. F. Influence of turbulence on transfer of heat from cylinders. U. S. National Advisory Committee for Aeronautics. Technical Note 4018. 1957.

19. Kestin, J., Maeder, P. F. and Sogin, H. H. The influence of turbulence on the transfer of heat to cylinders near the stagnation point. Zeitschrift fur Angewandte Mathematik und Physik. 12: 115-132. 1961.

20. King, L. V. On the convection of heat from small cylinders in a stream of fluid. Royal Society of London Philosophical Transactions. Series A, 214; 373-432. 1914.

21. Kline, S. J. and McClintock, F. A. Describing uncertainties in single-sample experiments. Mechanical Engineering. 75: 3-8. 1953.

22. Knudsen, J. G. and Katz, D. L. Fluid dynamics and heat transfer. New York, N. Y. McGraw-Hill Book Co., Inc. 1958.

23. Laurence, J. C. and Landes, L. G. Auxiliary equipment and techniques for adapting the constant-temperature hot-wire anemometer to specific problems in air-flow measurements. U. S. National Advisory Committee for Aeronautics. Technical Note 2843. 1952.

24. McAdams, W. H. Heat transmission. 3rd ed. New York, N. Y. McGraw-hill Book Co., Inc. 1954.

25. Mickelson, W. R. and Laurence, J. C. Measurement and analysis of turbulent flow containing periodic flow fluctuations. U. S. National Advisory Committee for Aeronautics. Research Memorandum E53F19. 1953.

26. Piercy, N. A. V. and Richardson, E. G. The turbulence in front of a body moving through a viscous fluid. London, Edinburgh and Dublin Philosophical Magazine. Series 7. 9: 1038-1041. 1930.

27. Piercy, N. A. V. and Richardson, E. G. The variation of velocity amplitude close to the surface of a cylinder moving through a viscous fluid. London, Edinburgh and Dublin Philosophical Magazine. Series 7. 6: 970-977. 1928.

28. Pohlhausen, E. Der Warmeaustauch zwischen festen Korpern und Flussigkeiten mit kleiner Reibung und kleiner Warmeleitung. Zeitschrift fur Angewandte Mathematik und Mechanik. 1: 115-121. 1921.

29. Prandtl, L. Bemerkung uber den Warmeubergang im Rohr. Physikalische Zeitung. 29: 487-489. 1928.

30. Reynolds, W. C., Kays, W. M. and Kline, S. J. Heat transfer in the turbulent incompressible boundary layer. I. Constant wall temperature. U. S. National Aeronautics and Space Administration. Technical Memorandum 12-1-58W. 1958.

31. Rubesin, M. W. The effect of an arbitrary surface-temperature variation along a flat plate on the convective heat transfer in an incompressible turbulent boundary layer. U. S. National Advisory Committee for Aeronautics. Technical Note 2345. 1951.

32. Sato, K. and Sage, B. H. Thermal transfer in turbulent gas streams - effect of turbulence on macroscopic transport from spheres. American Society of Mechanical Engineers Transactions. 80: 1380-1388. 1958.

33. Scesa, S. and Sauer, F. M. An experimental investigation of convective heat transfer to air from a flat plate with stepwise discontinuous surface temperature. American Society of Mechanical Engineers Transactions. 74: 1251-1255. 1952.

34. Schlichting, H. Boundary layer theory. 4th ed. New York, N. Y. McGraw-Hill Book Co., Inc. 1960.

35. Seban, R. A. The influence of free-stream turbulence on the local heat transfer from cylinders. American Society of Mechanical Engineers Transactions. Series C. Journal of Heat Transfer. 82: 101-107. 1960.

36. Short, W. W. and Sage, B. H. Temperature measurements in a spherical field: transfer coefficients and corrections for thermocouples in boundary flows. American Institute of Chemical Engineers Journal. 6: 163-167. 1960.

37. Sugawara, S., Sato, T., Komatsu, H. and Osaka, H. The effect of free-stream turbulence on heat transfer from a flat plate. U. S. National Advisory Committee for Aeronautics. Technical Memorandum 1441. 1958.

38. Taylor, G. I. Statistical theory of turbulence. Royal Society of London Proceedings. Series A. 151: 421-478. 1935.

39. Thrasher, L. W. and Binder, R. C. A practical application of uncertainty calculations to measured data. American Society of Mechanical Engineers Transactions. 79: 373-376. 1957.

40. van der Hegge Zijnen, B. G. Heat transfer from horizontal cylinders in a turbulent airflow. Applied Science Researches. Section A, 8: 205-223. 1958.

41. Van Driest, E. R. and Blumer, C. B. Boundary layer transition: free-stream turbulence and pressure gradient effects. American Institute of Aeronautics and Astronautics Journal. 1: 1303-1306. 1963.

42. von Karman, T. The analogy between fluid friction and heat transfer. American Society of Mechanical Engineers Transactions. 61: 705-710. 1939.

43. Wang, H. E. The influence of free-stream turbulence on the local coefficient of heat transfer from a flat plate. Xerox copy. Unpublished PhD. thesis. Providence, Rhode Island, Library, Brown University. 1959.

44. Young, A. D. and Maas, J. N. The behavior of a Pitot tube in a transverse total-pressure gradient. Great Britain Aeronautical Research Council. Reports and Memorandum 1770. 1936.

ACKNOWLEDGMENTS

The author would like to acknowledge the patience and understanding of the members of his graduate study committee, composed of Professor H. M. Black, Dr. Glenn Murphy, Professor S. J. Chamberlin, Dr. D. S. Martin, and Dr. G. K. Serovy.

This thesis was prepared under the direction of Dr. G. K. Serovy whose patience, understanding and sound counsel are profoundly appreciated.

The experimental work performed was done in the Iowa Engineering Experiment Station flow facility using equipment provided through a grant from the President's Permanent Objective Committee of the Alumni Achievement Fund. The author gratefully acknowledges the help of these organizations.

APPENDIX A

The following definitions of the terms turbulence intensity, scale of turbulence and spectrum of turbulence have been used in the text material.

Turbulence Intensity

The turbulence intensity for this work is defined as

$$T = \frac{\sqrt{\overline{U'^2}}}{\overline{U}} \tag{42}$$

where U' is the fluctuating component of the free-stream velocity and $\overline{U}$ is the time-average value of the free-stream velocity. In general, the definition of turbulence intensity should include the fluctuations in all three coordinate directions, but due to the implicitly assumed condition of isotropy of the free-stream fluctuations, the definition is that used above.

Scale of Turbulence

The scale of turbulence is defined for the references made to it in this work as

$$L = \int_0^\infty R_{xu'} dx \tag{43}$$

where the correlation coefficient $R_{xu'}$ is defined as

$$R_{xu'} = \frac{\overline{U'_A U'_B}}{\sqrt{\overline{U'_A}^2}\sqrt{\overline{U'_B}^2}} \qquad (44)$$

The scale of turbulence defined as above is sometimes known as the macro-scale or integral scale of turbulence and may be thought of as a measure of the eddy size in the flow. The velocity fluctuations U'_A and U'_B are measured at two points located on the x-axis and spaced a distance x apart.

APPENDIX B

The uncertainty in the Nusselt number is calculated from the final form of Equation 26, given below

$$w_N = \left[\left(\frac{x w_Q}{A k_a (t_s - t_f)}\right)^2 + \left(\frac{Q_n w_x}{A k_a (t_s - t_f)}\right)^2 + \left(\frac{Q_n x w_A}{A^2 k_a (t_s - t_f)}\right)^2 + \left(\frac{Q_n x w_t}{A k_a (t_s - t_f)^2}\right)^2\right]^{1/2} \qquad (45)$$

In using this equation to calculate the uncertainty, it was assumed that the value of thermal conductivity of the air was precise enough that any error in its magnitude had negligible effect on the resultant uncertainty in the Nusselt number.

Each of the uncertainty intervals in Equation 45 must be evaluated giving odds that the values for each variable will lie in the interval specified. The uncertainty intervals for the quantities used for computing the Nusselt number are given in Table 1.

Table 1. Values of uncertainty used for calculating the uncertainty in the Nusselt number

Variable	Uncertainty interval	Odds
x	± 0.02 in.	20 to 1
A	± 0.001 sq. ft.	20 to 1
$(t_s - t_f)$	± 0.5 F	20 to 1
Q_n	varies - see text	20 to 1

The uncertainty interval for Q_n is a function of the variables used to calculate Q_n and thus must be treated in a manner similar to that for finding N_{Nu_x}. The relation used to obtain Q_n was

$$Q_n = P - q_r - q_c \tag{19}$$

Substituting from Equations 20 and 21 for P, q_r and q_c,

$$Q_n = \frac{E^2}{R} - \epsilon\sigma A[T_s^4 - T_a^4] - \frac{k_p A(t_s - t_b)}{x_p} \tag{46}$$

The uncertainty in Q_n is then

$$w_Q = \left[\left(\frac{\partial Q_n}{\partial E} w_E\right)^2 + \left(\frac{\partial Q_n}{\partial R} w_R\right)^2 + \left(\frac{\partial Q_n}{\partial T_s} w_{T_s}\right)^2 + \left(\frac{\partial Q_n}{\partial T_a} w_{T_a}\right)^2 + \left(\frac{\partial Q_n}{\partial A} w_A\right)^2 + \left(\frac{\partial Q_n}{\partial (t_s - t_b)} w_{t_b}\right)^2 + \left(\frac{\partial Q_n}{\partial x_p} w_{x_p}\right)^2\right]^{1/2} \tag{47}$$

in which it has been assumed that k_p, σ, and ϵ all have small enough variations in their true values that the contribution of each and the total contribution of their aggregate uncertainty will be negligible.

It was not possible to obtain experimental values of the emissivity so values were taken from the technical literature. Unfortunately, experimenters do not agree on a single value of

emissivity, probably because of surface conditions or the like. As a result, values found in the literature varied from 0.05 to 0.15. Because this variation is not random, it cannot be included in the uncertainty analysis. It was assumed for the analysis that the value of emissivity was 0.10 and that the random variation in this assumption was small. This assumption means that errors in the value of Q_n may result. Calculations of Q_n with the maximum and minimum values of emissivity noted above show that under the worst possible conditions for this work, Q_n could vary by as much as 2.3 per cent. Interestingly enough, of all the experimenters quoted in relation to this work, only one (Wang, (41)) has used a correction for the radiant loss. The others have neglected it as unimportant. The uncertainty intervals for the variables used to calculate Q_n are given in Table 2.

Table 2. Values of uncertainty interval for variables used in calculating the net heat loss Q_n

Variable	Uncertainty interval	Odds
E	± 0.005 V	20 to 1
R	± 0.003 Ω	20 to 1
T_s	± 0.50 F	20 to 1
T_a	± 0.50 F	20 to 1
A	± 0.001 sq. ft.	20 to 1
$(t_s - t_b)$	± 0.25 F	20 to 1
x_p	± 0.01 in.	20 to 1

When the uncertainty intervals in Table 2 are used to calculate uncertainties in Q_n, it quickly becomes apparent that only two of the variables were of importance, the voltage reading E and the temperature difference $(t_s - t_b)$. Furthermore, when the resulting value of uncertainty in Q_n is used to calculate the uncertainty in the Nusselt number, it is found that this quantity is dependent to a large degree on the uncertainty in Q_n. Thus, measurements of Q_n are the critical point for meaningful data. Because of this dependence on the uncertainty in Q_n, uncertainties in other quantities which were not significant with respect to the uncertainty in Q_n were neglected. Results showing the maximum uncertainty for each set of data are given in Table 3.

The uncertainty in the Reynolds number was calculated from

$$w_R = \left[\left(\frac{x}{\nu} w_U\right)^2 + \left(\frac{U w_x}{\nu}\right)^2 + \left(\frac{-Ux}{\nu^2} w_\nu\right)^2\right]^{1/2} \qquad (48)$$

using the uncertainties listed in Table 4. The analysis showed that the uncertainty in the Reynolds number was dependent almost exclusively on the uncertainty in the velocity measurement. Because of the small dependence on the distance x and the kinematic viscosity ν, these variables were neglected in the final computations. The maximum uncertainty in The Reynolds number is tabulated in Table 3.

Table 3. Maximum uncertainties in Nusselt number, Reynolds number and turbulence intensity

Run	Maximum uncertainty in Nusselt number %	Maximum uncertainty in Reynolds number %	Maximum uncertainty in turbulence intensity %
Zero pressure gradient, no grid	± 4.96	± 2.41	± 16.8
Zero pressure gradient, 0.090 in. grid	± 5.23	± 2.56	± 8.2
Low pressure gradient, no grid	± 7.51	± 2.53	± 17.1
Low pressure gradient, 0.090 in. grid	± 4.68	± 2.23	± 9.5
Low pressure gradient, 0.250 in. grid	± 6.42	± 2.19	± 9.6
High pressure gradient, no grid	± 4.80	± 2.16	± 17.5
High pressure gradient, 0.090 in. grid	± 4.99	± 2.66	± 11.8
High pressure gradient, 0.250 in. grid	± 6.19	± 2.22	± 9.7

Table 4. Values of uncertainty used in the computation of uncertainty in the Reynolds number

Variable	Uncertainty interval	Odds
$\overline{U}$	$\pm$ 0.5 ft. per sec.	20 to 1
x	$\pm$ 0.02 in.	20 to 1

The uncertainty in the turbulence intensity was found from

$$w_T = \left[\left(\frac{4 w_{e'}}{\overline{e}_w \left[1 - \left(\frac{e_o}{\overline{e}_w} \right)^2 \right]} \right)^2 + \left(\frac{4 \sqrt{\overline{e'^2}} \left[1 - 3 \left(\frac{e_o}{\overline{e}_w} \right)^2 \right] w_{e_w}}{\overline{e}_w^2 \left[1 - \left(\frac{e_o}{\overline{e}_w} \right)^2 \right]^2} \right)^2 \right.$$

$$\left. + \left(\frac{8 e_o \sqrt{\overline{e'^2}}\, w_{e_o}}{\overline{e}_w^4 \left[1 - \left(\frac{e_o}{\overline{e}_w} \right)^2 \right]^2} \right)^2 \right]^{1/2} \qquad (49)$$

The uncertainties for the various quantities are listed in Table 5. Values of the uncertainty in the turbulence intensity are given in Table 3.

Table 5. Uncertainties for turbulence intensity calculation

Variable	Uncertainty interval	Odds
$\sqrt{\overline{e'^2}}$	$\pm$ 0.002 v	20 to 1
e_o	$\pm$ 0.05 v	20 to 1
$\overline{e_w}$	$\pm$ 0.05 v	20 to 1

APPENDIX C

Assembly Drawing of Plate

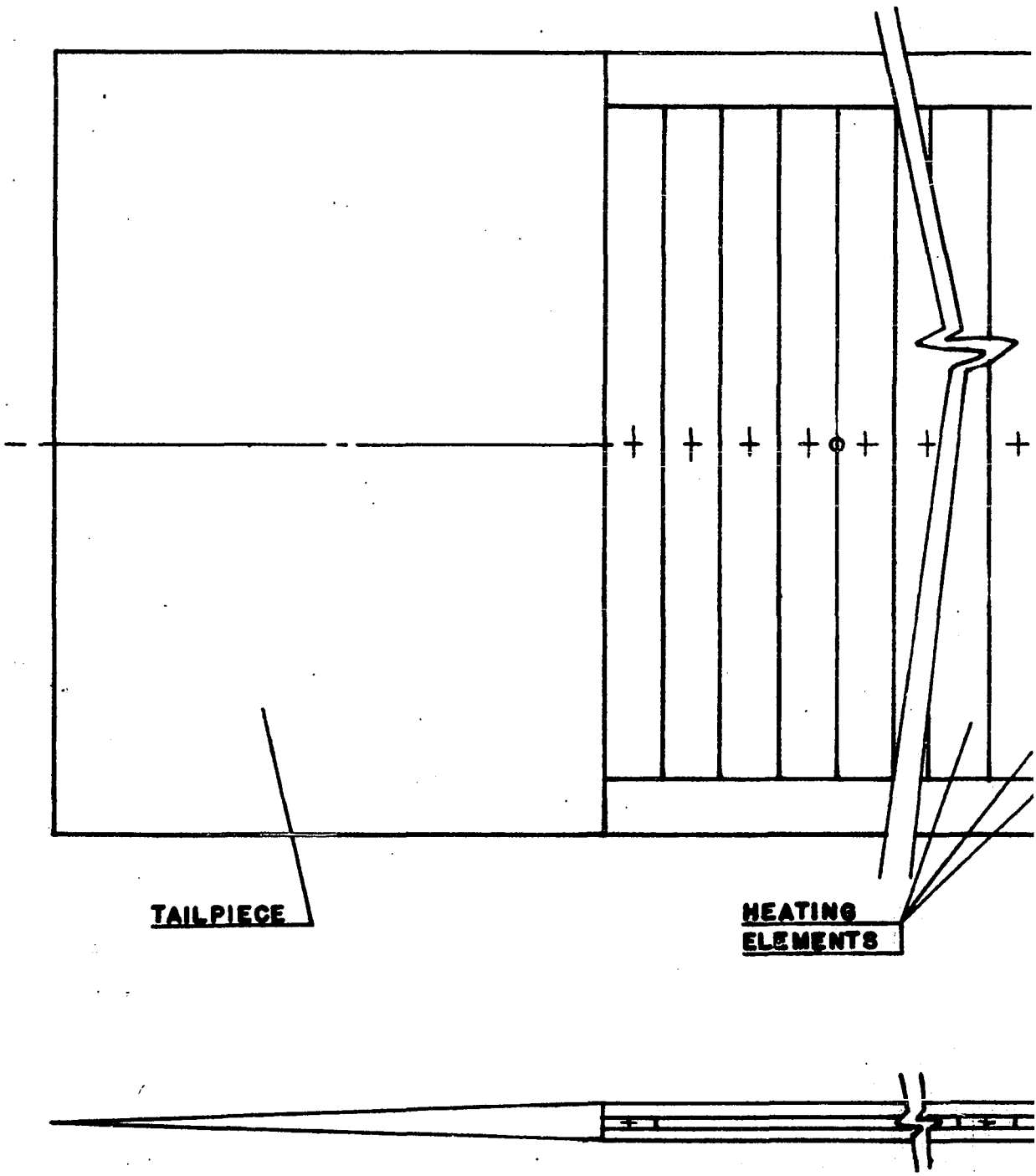

FIGURE 38. ASSEMBLY DRAWI

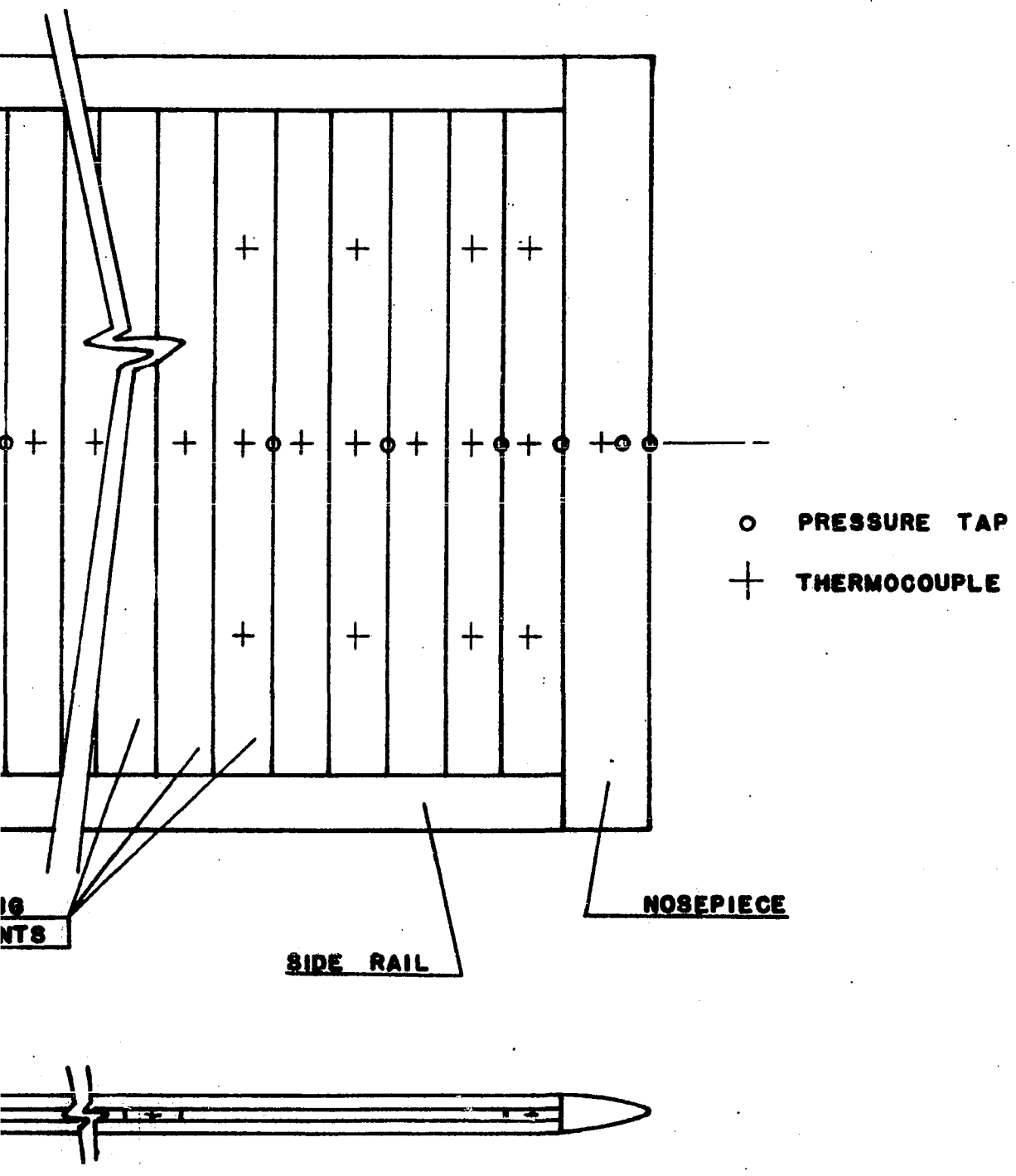

IBLY DRAWING OF PLATE

APPENDIX D

A set of sample heat transfer calculations is worked out below. The data are taken from the low pressure gradient series with the 0.090-inch grid installed:

Power input

$$P = \frac{E^2}{R} \text{ (conversion factor)}$$

$$= \frac{1.21}{0.308} (3.413)$$

$$= 13.43 \text{ Btu/hr}$$

Radiation loss

$$q_r = A(T_s^4 - T_a^4)$$

$$= (0.174 \times 10^{-8})(0.10)(0.0833)\left[(556)^4 - (541.6)^4\right]$$

$$= 0.136 \text{ Btu/hr}$$

Conduction loss

$$q_c = \frac{k_p A}{x_p} (t_s - t_b)$$

$$= \frac{(0.143)(0.0833)(12)(1.48)}{(0.1405)}$$

$$= 1.51 \text{ Btu/hr}$$

Net loss by convection

$$Q_n = P - q_r - q_c$$

$$= 13.43 - 0.136 - 1.51$$

$$= 11.78 \text{ Btu/hr}$$

Nusselt number

$$N_{Nu_x} = \frac{Q_n x}{A(t_s - t_f)k_a}$$

$$= \frac{11.78(0.891)}{0.0833(14.4)(0.0154)}$$

$$= 568$$

Correction for unheated starting length (turbulent region)

$$N_{Nu_x, \text{ corrected}} = N_{Nu_x}\left[1 - \left(\frac{x}{x_o}\right)^{39/40}\right]^{-7/39}$$

$$= 568(0.969)$$

$$= 550$$

Reynolds number

$$N_{Re_x} = \frac{\rho U x}{\nu}$$

$$= \frac{(0.07013)(58.9)(0.891)}{125.5 \times 10^{-7}}$$

$$= 293{,}100$$